WDL-TR4725
10 November 1971

ENGINEERING EXPERIMENTAL PROGRAM ON THE EFFECTS OF NEAR-SPACE RADIATION ON LITHIUM-DOPED SOLAR CELLS

FINAL REPORT

Prepared for

JET PROPULSION LABORATORY
CALIFORNIA INSTITUTE OF TECHNOLOGY
Pasadena, California

JPL Contract 952585

PHILCO Ford

Philco-Ford Corporation
Western Development Laboratories Division
Palo Alto, California 94303

PHILCO Ford
Philco-Ford Corporation
Western Development Laboratories Division

WDL Technical Report 4725
10 November 1971

ENGINEERING EXPERIMENTAL PROGRAM ON THE EFFECTS OF NEAR-SPACE RADIATION ON LITHIUM-DOPED SOLAR CELLS

FINAL REPORT

Prepared for

JET PROPULSION LABORATORY
CALIFORNIA INSTITUTE OF TECHNOLOGY
Pasadena, California

JPL Contract 952585

This work was performed for the Jet Propulsion Laboratory, California Institute of Technology, as sponsored by the National Aeronautics and Space Administration under Contract NAS7-100.

PHILCO-FORD CORPORATION
WDL Division
Palo Alto, California

PHILCO
Philco-Ford Corporation
Western Development Laboratories Division

ABSTRACT

PHILCO-FORD WDL-TR4725
ENGINEERING EXPERIMENTAL
PROGRAM ON THE EFFECTS OF
NEAR-SPACE RADIATION AND
LITHIUM-DOPED SOLAR CELLS
FINAL REPORT
10 November 1971

UNCLASSIFIED
JPL Contract 952585
95 Pages

This report presents the results of a contract to experimentally evaluate the real-time degradation characteristics of lithium-diffused silicon solar cells. A strontium-90 radioisotope was used for simulation of a typical earth-orbital electron environment. The experiment was performed in an ion pump vacuum chamber with samples maintained at -50°, +20°, +50°, and +80°C. Samples were illuminated during the 6-month exposure run with solar cell I-V characteristics measured periodically in situ. This 6-month exposure corresponded to a 1 MeV equivalent fluence of approximately 10^{14} electrons/cm^2. Several types of lithium cells were irradiated and compared directly with conventional N/P cells. The best lithium cells compared favorably with N/P cells, particularly at the higher test temperatures. With a slight improvement of initial performance characteristics, lithium cells appear feasible for 5 to 10 year missions at synchronous altitude. Based on the reported results and those of other irradiation experiments, lithium cells would appear to be superior to N/P cells in proton-dominated earth-orbital environments. Another important conclusion of the effort was that illuminated/loaded cells degrade more rapidly than do dark/unloaded cells. The irradiation experiment provided data of high quality with a high degree of confidence because of the experimental and statistical analysis techniques utilized.

FOREWORD

The information presented in this report was generated during the performance of JPL Contract 952585. This contract was performed in the Power, Control, and Materials Technology Department of Philco-Ford Corporation's Western Development Laboratories. The department, as well as this contractual effort, was managed by D. L. Reynard. Individual contributors to this effort were: H. E. Pollard, D. C. Briggs, D. G. Peterson, and D. R. Spratling.

Technical monitoring and support at JPL were received from Dr. E. C. deWys, Dr. J. M. Weingart, and Mr. R. Patterson. Their enthusiastic support and important technical contributions are gratefully acknowledged.

DISCLAIMER

This report contains information prepared by Philco-Ford Corporation under JPL Contract 952585. Its content is not necessarily endorsed by the Jet Propulsion Laboratory of the California Institute of Technology, or by the National Aeronautics and Space Administration.

TABLE OF CONTENTS

TABLE OF CONTENTS (Cont)

LIST OF ILLUSTRATIONS

LIST OF ILLUSTRATIONS (Cont)

LIST OF ILLUSTRATIONS (Cont)

LIST OF TABLES

SUMMARY

This report summarizes the results of a contract to experimentally evaluate the real-time degradation characteristics of lithium-diffused silicon solar cells. Lithium solar cells recover spontaneously from radiation-induced displacement damage and are therefore of potential value to future spacecraft programs. Their temporal performance characteristics are intrinsically dependent upon the rate at which damage is introduced (as well as upon lithium concentration and cell temperature), and hence it can be hypothesized that accelerated irradiation experiments may yield questionable results. This program compares the net degradation characteristics of various types of lithium cells with those of conventional N/P solar cells. A radioisotope source was used to provide an electron spectrum corresponding to that in near-earth orbits.

The program consisted of three phases: design and fabrication of experimental equipment, a 6-month exposure run, and a brief period of analysis followed by preparation of the final report. An earlier report, WDL-TR4213, described the experimental approach and the design of the experimental equipment. The present report concentrates on experimental results and conclusions. In its original configuration, the contract included an electron accelerator irradiation of lithium and N/P cells and a comparative analysis of the results from both accelerated and real-time tests. This portion of the program was deleted from the contract with the intent that it would be performed at JPL.

The samples consist of seven basic types of lithium cells obtained from two manufacturers. These are compared with each other and with three types of conventional N/P cells. Sample temperatures are: -50°, +20°, +50°, and +80°C. The 6-month exposure (corresponding to a 1 MeV equivalent fluence of approximately 10^{14} electrons/cm^2) was performed in a vacuum chamber employing a VacIon pumping system. All cells (with the exception of one type) were illuminated and loaded during the exposure. Periodic performance measurements were made with the cells in the chamber using a Spectrolab X-25 Mark II solar simulator.

The data produced during the experiment was of high quality because of the experimental techniques used and the careful methods of performance measurement. The results were therefore analyzed with a level of confidence considerably higher than in previous

real-time efforts or in those using electron accelerators. With the exception of nine temporary warmup periods of the -50°C sample block, all experimental equipment operated perfectly during the 6-month exposure period.

In general, the lithium cells demonstrated performance characteristics better than expected in the electron environment in that they are roughly equivalent to N/P cells at normal operating temperatures. The better lithium cells showed virtually no additional recovery after the irradiation was completed. This fact, coupled with the observation that the damage rate experienced was six times that expected in a synchronous equatorial orbit, indicates that the lithium content of the cells was higher than optimal for these conditions. It may thus be argued that the lithium cells could possibly be better optimized for the synchronous orbit case, permitting a higher initial (and final) power output. One can therefore conclude that present-day lithium cells are marginally feasible for synchronous orbit missions, but that the performance of lithium cells might exceed that of N/P cells with further development.

It was observed that both lithium and N/P cells appear to degrade more rapidly in the illuminated and loaded condition than in the dark and unloaded condition (4 to 5 percent difference in 6 months). From this observation, it follows that, for accurate results, future irradiation experiments should be conducted with the illuminated and loaded condition or should empirically compensate for the expected difference.

SECTION 1

INTRODUCTION

1.1 BACKGROUND AND OBJECTIVES

Silicon solar cells diffused with lithium spontaneously recover from radiation-induced damage. This recovery phenomenon primarily depends on temperature and the amount of lithium in the material (Ref. 1). Furthermore, the rate of recovery is independent of the damage rate (Ref. 2). Irradiation experiments with lithium cells typically involve the use of a Van de Graaff accelerator (at flux rates as much as five orders of magnitude higher than those expected in space) and a post-irradiation period of observation of the annealing phenomena (Refs. 3, 4). Because of these differences in damage rate, a direct observation of net damage required conducting an experimental program in which lithium cells were irradiated at a rate representative of a typical space environment.

Several years ago, it was observed that strontium-90 (Sr-90) possessed spectral characteristics that closely approximated the trapped electron spectrum in earth-orbital situations. Furthermore, the electron flux rate emitted by Sr-90 was such that small amounts of the isotope could be conveniently used to irradiate a fairly large sample area at typical earth-orbit average rates. Early experiments (Ref. 5) used Sr-90 to evaluate the thermal/optical properties of spacecraft thermal control materials, optical surfaces, and conventional solar cell/cover composites. Sr-90 therefore appeared attractive for the irradiation of lithium solar cells at real-time rates so that time-dependent uncertainties would be eliminated. It was realized that Sr-90 produces a realistic spectrum of electrons (with respect to near-earth electron spectra) which could conceivably yield results different from those obtained with a monoenergetic source of electrons.

NASA's Goddard Space Flight Center sponsored two programs in 1967-68 for the Sr-90 irradiation of lithium solar cells. These programs (Refs. 6, 7), performed by Philco-Ford and Lockheed-Georgia, provided the first real-time degradation data for lithium cells as well as the first direct comparison of different lithium cell types. While many qualitative conclusions

(Ref. 8) were reached as a result of these programs, the data produced were less than desirable for several reasons. Sample characteristics (manufacturing processes, materials, etc.) were not adequately defined or recorded. For the most part, only one sample of each cell type was irradiated at each temperature. Diffusion pump vacuum systems were used with the attendant uncertainty of contamination effects. Solar cell characteristics measurements were made primarily with tungsten light sources employing questionable calibration techniques.

The program described in this report had the general objective of updating knowledge of lithium cell degradation characteristics with a substantial improvement of experimental techniques over those of previous efforts. Specifically, the objectives of the program were to:

a. Evaluate lithium cells which represent the most recent state of development of such cells.

b. Expose these cells to a 6-month period of Sr-90 irradiation in a combined vacuum-temperature-illumination environment.

c. Simulate typical earth-orbital average flux rate and electron spectrum irradiation.

d. Irradiate cells over a range of typical operating temperatures.

e. Use high quality solar simulator for all cell measurements.

f. Use ion pump vacuum system for the environmental chamber.

1.2 TECHNICAL APPROACH

To meet the stated objectives, the following technical approach was formulated jointly by JPL and Philco-Ford:

a. Review past lithium cell developments with the assistance of the cell manufacturers. Select only the best-performing cells for this experiment.

b. Construct an experimental sample matrix which efficiently permits direct comparison among various cell types of interest.

c. Design the experimental chamber and the arrangement of associated equipment such that experimental uncertainty and error are minimized.

d. Design a semiautomatic data acquisition system providing the best compromise between data accuracy and acquisition speed.

e. Use standard statistical analysis techniques to determine significance of results.

This approach was incorporated into the contract Statement of Work and formed the basis for the detailed program requirements described later.

1.3 SIGNIFICANCE OF RESULTS

This experimental program, recently completed, is judged to have been highly successful in terms of meeting its stated objectives and requirements and in providing the first statistically significant real-time test data of lithium solar cells. Further, the quality of the data and the design and analysis methods employed have resulted in a high degree of confidence in the results and in the subsequent conclusions.

This report summarizes the experimental results and conclusions of the program. The report also provides a brief description of the experimental equipment. A more complete description of this equipment is provided in an earlier report (Ref. 9).

It should be initially noted that all graphs in this report having an abscissa of time and/or an ordinate of maximum power (P_{max}) are plotted on identical scale dimensions. Thus, one can turn from one graph to another without confusing scale changes.

SECTION 2

EXPERIMENTAL APPROACH

2.1 PROGRAM REQUIREMENTS

Several detailed requirements were established for the program, based upon the previously mentioned objectives. Other requirements were specifically mentioned in the contract or were self-imposed on the basis of experience. The detailed program requirements are listed below:

a. Use a Philco-Ford-owned vacuum chamber, pumping system, and radioisotope source, appropriately modified to meet all requirements.

b. Irradiate at least 100 solar cells in the environmental chamber (four cells of each type under each set of test conditions).

c. Maintain uniform electron flux and illumination within typical standards of acceptance (±20% for electron flux, ±5% for illumination for 1 x 2 cm cell) and at levels comparable to earth-orbital conditions. (An illumination intensity uniformity of approximately ±2% was obtained.)

d. Use solar simulator for all cell measurements -- all measurements to be in situ.

e. Design and use semiautomatic data acquisition system to increase data collection accuracy and efficiency.

f. Subject the reduced data to typical statistical analyses.

g. Maintain cell temperatures at -50°, 20°, 50°, and 80°C. (These represent a typical range of operating temperatures, that is, +20° to +80°C, and a temperature where lithium atom mobility is extremely low, that is, -50°C.)

h. Illuminate all cells (with the exception of one group) during the exposure and load them to a point near the maximum power point. (One group is to be kept shaded during the irradiation and left in the open-circuit condition.)

These requirements were used as constraints or goals in arriving at the configuration of the experimental equipment. In effect, they constituted a challenge in terms of designing a chamber and facility which best met all requirements with a minimum amount of compromise.

2.2 EXPERIMENTAL SAMPLE MATRIX AND SELECTION CRITERIA

It was established that the program should evaluate only those types of lithium cells that would be most immediately suitable for spacecraft use. Thus, only cells developed by the two commercial solar cell suppliers, Centralab and Heliotek, were considered. Both companies were briefed on the intent of this program and were asked to recommend lithium cell types for such an evaluation. Based partly upon their recommendations and partly upon Philco-Ford proposals to JPL, the basic comparisons to be performed in the program were developed and are shown in Table 2-1. Tradeoffs considered in formulating these comparisons were: number of cells per type, number of cell types, number of temperatures, and available sample area within the chamber.

A direct comparison of lithium and N-on-P cells was made primarily at +20°C. Additional comparative data was obtained at -50° and +80°C. The comparison between lithium cells made from crucible-grown silicon and those made from float-zone refined silicon is fundamental to the program and was therefore made at all four sample temperatures.

At the time that the experimental sample matrix was established, it was thought that appreciable differences in embrittlement characteristics would be observed in cells with junctions formed from a BBr_3 diffusion as compared to BCl_3. It was subsequently discovered that little or no observable difference could be detected in the two types of cells (Ref. 10). Thus, the two types of boron diffusion represented in this experiment are variations of the basic BCl_3 process normally used for P-on-N cell manufacture. The difference between the two types is in terms of boron "tack-on" time which is discussed further in a later section.

Another comparison involved bare vs covered lithium cells. It was thought that surface characteristics might be of importance in lithium cell performance degradation (Ref. 11).

TABLE 2-1

SAMPLE COMPARISONS

Comparison		Temperature (°C)
Bare Lithium Cells	Bare N/P Cells	+20
Crucible Lithium Cells (425-90-60) (450-20-0)	Float Zone Lithium Cells (425-90-120) (350-90-60) (2 Boron Diffusions)	-50, +20, +50, +80
Boron Diffusion 1 (Float Zone)	Boron Diffusion 2 (Float Zone)	-50, +20, +80
Bare Lithium Cells (Cruc 425-90-60)	Integral Covered Lithium Cells (Cruc 425-90-60)	+20
Illuminated and Loaded (Lithium Cells and N/P Cells)	Dark and Unloaded (Lithium Cells and N/P Cells)	+20
Heliotek Lithium Cells (Crucible and Float Zone)	Centralab Lithium Cells (Crucible and Float Zone)	-50, +20, +80

Notes:

1. Numbers such as 425-90-60 refer to the lithium diffusion characteristics diffusion temperature - diffusion time - redistribution time. Temperatures are in °C, and times in minutes.

2. Boron Diffusion 1 refers to an 8-minute preheat time, a 5-minute boron "tack-on" time, and an 8-minute boron diffusion time. This is commonly referred to as 8-5-8 boron diffusion. Boron Diffusion 2 refers to 8-8-8 boron diffusion characteristics.

A direct comparison has thus been provided to permit an observation of any gross differences due to covering the cells.

The effect of injection level upon observable damage in silicon solar cells was considered potentially important in the early phases of lithium cell development (Ref. 12). It was felt that the observed radiation damage (as measured in terms of power degradation) would be different depending on illumination level. This program had an objective of demonstrating the effect (if any) of illumination on solar cell damage. The advantages offered by this program in this regard as compared to earlier real-time irradiation programs are primarily those of better sample size statistics and the employment of improved experimental techniques.

The selected experimental sample matrix is presented in Table 2-2. While it was impossible to completely fill the matrix because of chamber limitations, a substantial amount of comparative data for a large number of cell types was obtained over a variety of test conditions. In the final sample configuration, 128 cells were irradiated in the chamber. This number was significantly higher than required by the original matrix called for in the contract. Current 10-ohm-cm N-on-P cells from both manufacturers are included, as are 1964 N-on-P cells from a batch used in earlier irradiation programs. It is thus possible to relate the results of this experiment with those of earlier definitive efforts.

2.3 EXPERIMENTAL EQUIPMENT ARRANGEMENT AND MEASUREMENT PHILOSOPHY

Considerable thought was given to the design and arrangement of the experimental equipment in terms of meeting the aforementioned requirements and objectives. It was clear that a different approach (from earlier real-time irradiation experiments) was necessary in order to increase the credibility and significance of the experimental results. Several design approaches were conceived and discussed with JPL personnel. The selected approach represented several iterations of the original concept and resulted in an experimental system which met the prestated desires at a minimum cost.

The requirement for in situ solar cell measurements dictated the necessity for a chamber window of sufficient size to permit uniform illumination of all samples. Because of the nominal illumination area of 13 inches diameter of the X-25 solar simulator, the projected

TABLE 2-2

EXPERIMENTAL SAMPLE MATRIX

Type	Diffusion Characteristics	Mfg	Cell Code	Radioisotope/Vacuum						1-MeV Accelerator
				Illuminated and Loaded					Dark and Unloaded	
				-50°C	+20°C	+50°C	+80°C	+20°C	+20°C	+20°C
				A	B	C	D	E	F	
Lithium P/N Crucible	425-90-60	Hel	A	4	4	4	4		4	4
	425-90-60	Cen	B	4	4		4			4
	425-20-0	Cen	C	4	4		4			4
	425-90-120 1-mil Cover	Hel	D		4					4
Lithium P/N Float Zone	425-90-120	Hel	E	4	4	4	4		4	4
	350-90-60	Hel	F	4	4		4			4
	Boron No. 1 425-90-120	Cen	G	4	4		4			4
	Boron No. 2 425-90-120	Cen	H	4	4		4			4
10Ω-cm N/P	Current	Cen	I	4				4	4	4
	Current	Hel	J				4	4		
	1964	Hof	K					4		

Notes:

1. Numbers such as 425-90-60 refer to the lithium diffusion characteristics diffusion temperature - diffusion time - redistribution time. Temperatures are in °C, and times in minutes.

2. Boron Diffusion 1 refers to an 8-minute preheat time, a 5-minute boron "tack-on" time, and an 8-minute boron diffusion time. This is commonly referred to as 8-5-8 boron diffusion. Boron Diffusion 2 refers to 8-8-8 boron diffusion characteristics.

3. The 1-MeV accelerator cells were sent to JPL for irradiation. The results of this irradiation are not presented in this report.

4. Cell code used in other tables: first letter indicates cell type; second letter indicates environmental conditions.

sample area was constrained to 12 inches in diameter. The chamber itself was designed with a 14 inch diameter.

It was necessary to translate (or rotate) either the simulator or the vacuum chamber to permit standardization and monitoring of the simulator output characteristics. The selected approach was to laterally translate the simulator (and beam) from a standardization fixture to the chamber window (see Figure 3-1). It was decided initially that the simulator would only be used for solar cell measurements and that a lower cost light source would be used for cell illumination between measurement periods.

It was essential that the electron flux (and spectrum) be as uniform as possible over the entire sample area. Since the available radioisotope source was a small cylindrical tube (approximately 1 inch in length), the samples were arranged spherically around the source center as if it were a point source. The samples were mounted in groups (according to temperature) on flat plates whose centroids were equidistant from the source center. Thus, the cells were uniformly irradiated with electrons, but were in groups at different angles of incidence with the light source.

It was decided that cell performance measurements should be made in a manner as accurate and repeatable as possible. This requirement led to the use of four-wire leads to each cell. The proven method of using an x-y plotter with extreme care given to plotter calibration and paper alignment was selected as the basic data acquisition procedure. A semi-automated cell switching system was employed as a means of reducing the time required for data acquisition and to reduce the potential for human error.

SECTION 3

EXPERIMENTAL EQUIPMENT DESCRIPTION AND PERFORMANCE

3.1 RADIATION FACILITY

The Philco-Ford Radiation Facility was established to provide a location where advanced research involving the use of radioisotopes can be safely conducted and where radioactive sources can be safely stored. The Radiation Facility contains the irradiation chamber with the vacuum system and the illumination systems. All ancillary electronic equipment used for performance measurements and environmental control is located in an adjacent room. The principal items of equipment in the Radiation Facility are arranged as shown in Figure 3-1. Lead shielding surrounds the cylindrical portion of the test chamber to reduce the dose rate at any position 1 foot from the chamber walls to less than 18 mr/hr. Lead sheets line the walls of the Radiation Facility adjacent to the exposure chambers to reduce the radiation level outside the facility to less than 0.2 mr/hr.

A Spectrolab X-25 Mark II Solar Simulator is positioned on a platform attached with linear bearings to cylindrical rails accurately positioned in the floor. When data are to be taken, the simulator is aligned with the calibration panel and standardized, then immediately repositioned in front of the chamber window for data acquisition.

3.2 CHAMBER DESIGN

The irradiation of the solar cells is conducted in an evacuated chamber. The selected chamber design is a stainless steel cylinder with a diameter of 14 inches and a length of 22 inches as shown in Figure 3-2. The solar cells are attached to thermal control blocks, which are in turn attached to a flange providing closure to one end of the cylinder. A flanged window provides closure at the other end. The vacuum pumping system is located beneath the chamber and is attached to the lower side of the horizontally oriented cylinder. Two access ports are also located in the side of the cylinder, one being used for the insertion of the isotope and the other a spare.

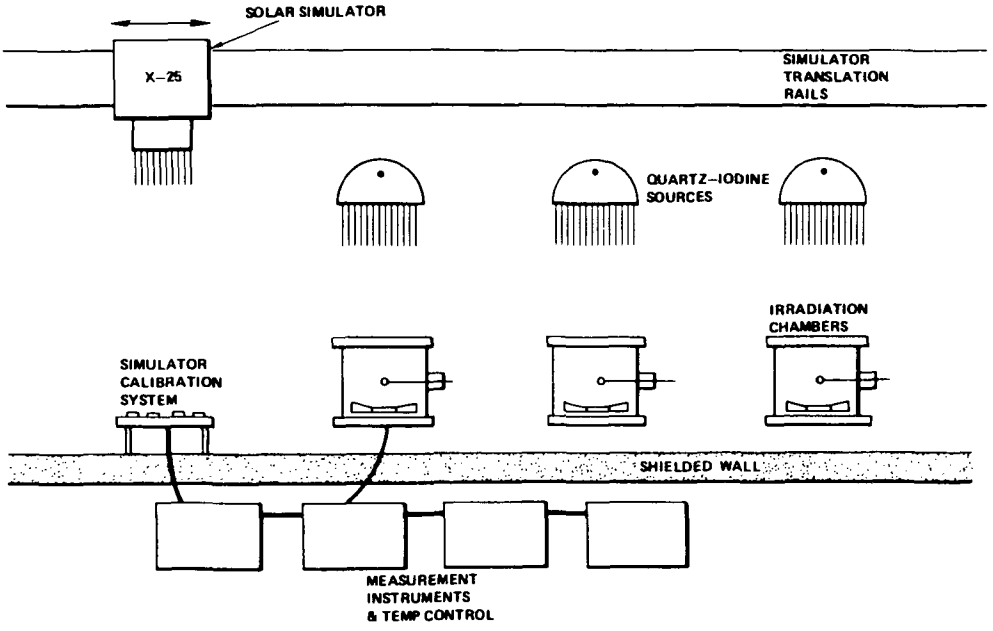

Figure 3-1 Philco-Ford Radiation Facility

The window permitting illumination of the solar cells is Corning 7940 fused silica (optical grade), 15 inches in diameter and 1 inch thick. The plane surfaces of the window were specified to be parallel within 1 minute of angle to minimize distortion of the solar simulator illumination. The window is mounted in a flange allowing a 13.5-inch-diameter clear opening. The high-purity fused silica was specified so that color center formation and the resulting decrease in transmission are minimized.

The solar cells are located at the end of the cylinder opposite the window as shown in Figure 3-3. There are six groups of cells, one group at each of the following test conditions: -50°C, 20°C dark, 20°C (two groups), 50°C, and 80°C. The 20°, 50°, and 80°C groups are mounted on temperature control blocks using a water-cooled heat sink. The -50°C block is attached to a liquid nitrogen (LN_2)-cooled heat sink. The surface of each block is at an angle such that the central cell on the block is normal to a line from the isotope center and 8 inches from the isotope center. The cells are consequently located at angles as high as 27° from normal to the illumination. This is well within the range of demonstrated cosine dependence (Ref. 13). All data presented in this report are corrected to normal incidence. The water-cooled heat sink and the LN_2-cooled heat sink are attached to the door of the chamber. The door seals the chamber using a Viton O-ring.

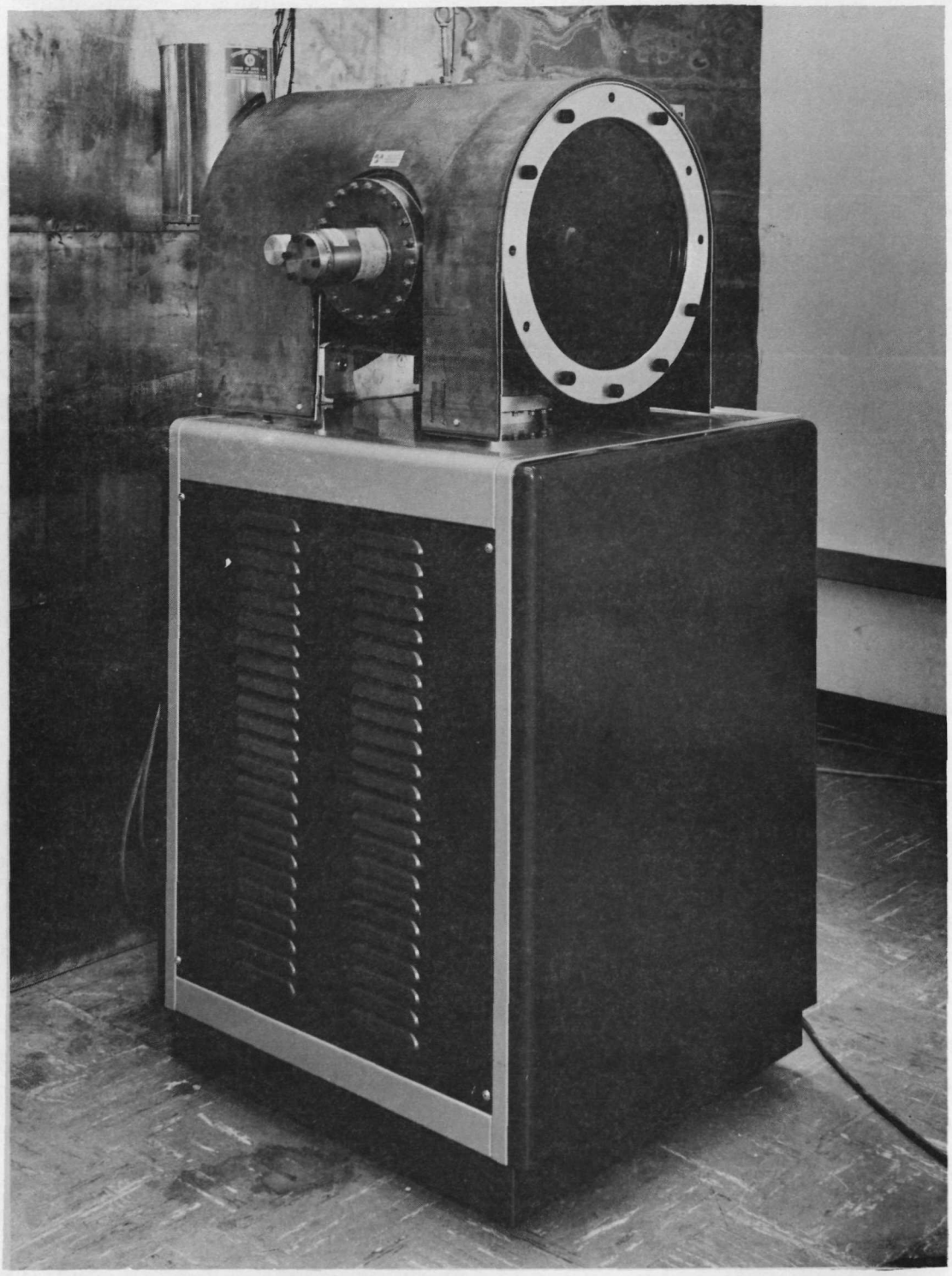

70.05.292-2

Figure 3-2 Irradiation Chamber and Vacuum System

A shade is attached to one of the 20°C blocks to prevent cell illumination other than when performance is being measured. The shade is made of an aluminum frame hinged to the block. The frame is covered with 0.00025 inch aluminized mylar, which permits the electron spectrum to pass through essentially unaltered. The shade can be opened or closed by actuating a rod through a push-pull feedthrough located on the chamber door.

3.3 VACUUM SYSTEM

The vacuum system is located directly beneath the irradiation chamber and connected to it through a 6-inch opening. A Varian 140-liter/second ion pump provides primary pumping with a normal operating pressure of 10^{-6} torr or lower. The ion pump was selected because of its long-term operating reliability and inherent cleanliness.

The vacuum system and chamber are fabricated from stainless steel tubing and utilize metal-to-metal seals. The resulting vacuum system has an outgassing rate of the inner walls of less than 2×10^{-9} torr liter/sec/cm^2. The vacuum system is contained in a standard electronic rack, 38 inches high, with the irradiation chamber mounted just above the top surface of the rack. The electronics equipment to operate the vacuum system is contained in another rack which is located a safe distance from the irradiation chamber.

The vacuum system operated satisfactorily during the period of irradiation and during subsequent annealing observations. The mean value of the chamber pressure over the entire period was 2.5×10^{-6} mmHg. Minimum chamber pressure was 4×10^{-7} mmHg; maximum pressure was 9×10^{-6} mmHg. Upon completion of the irradiation and annealing periods, the chamber was opened and a visual inspection of the test samples was performed. It was found that a light coat of an oily appearing film had deposited on the entire exposed surface of the -50°C sample block. It was determined that the presence of film contributed about 3% loss to the observed short-circuit current of the -50°C cells. No other cells or surfaces within the chamber showed any sign of deposition.

3.4 TEMPERATURE CONTROL SYSTEM

Each cell mounting plate is combined with a heater and thermal resistance block. The thermal resistance blocks were designed such that, under one-sun illumination, the desired

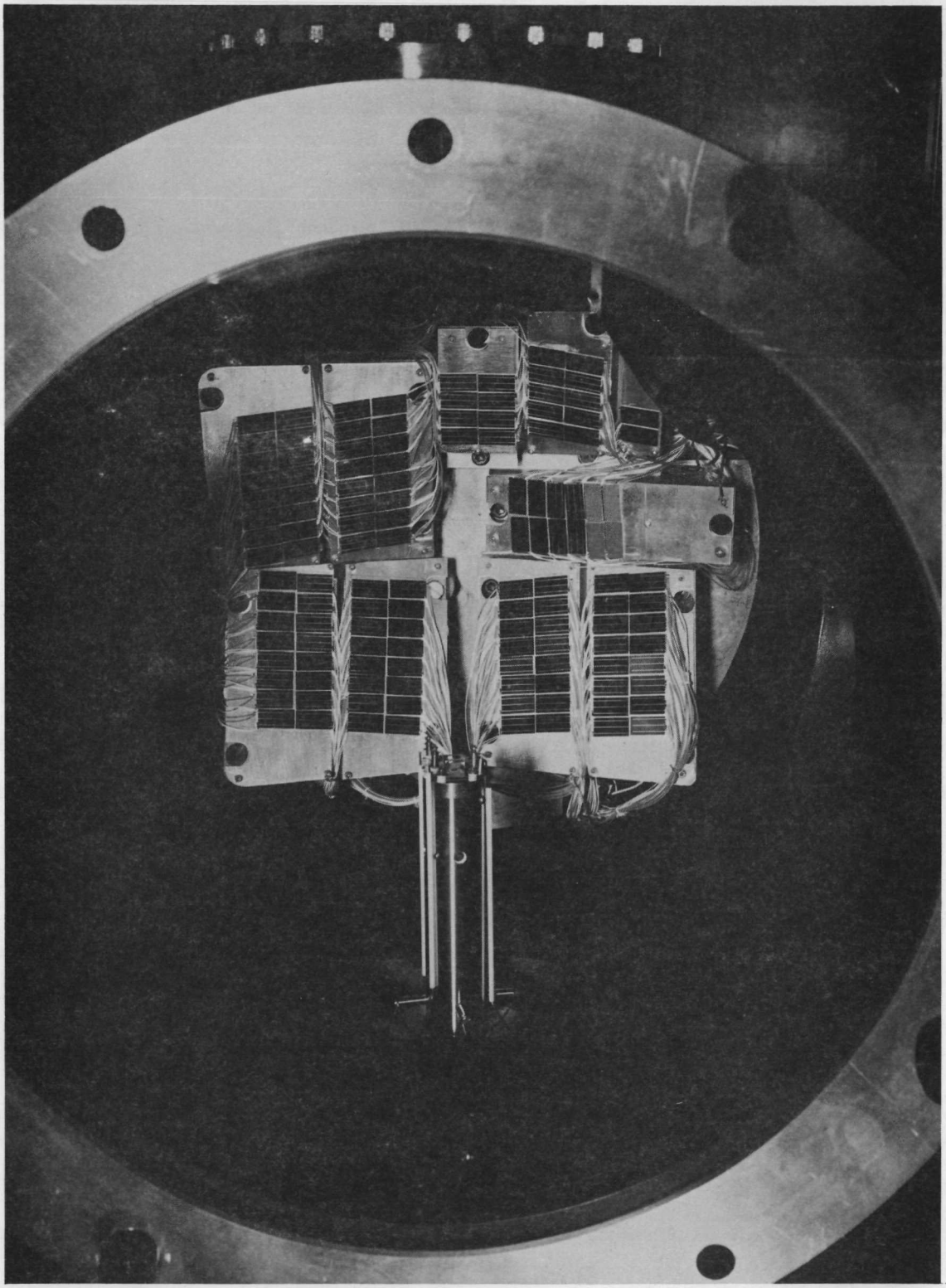

70.04.208-1

Figure 3-3 Solar Cell Samples Installed in Chamber

sample temperature is maintained with a minimum of additional heat from the heaters. The blocks are mounted to a heat sink, cooled by water for the 20°, 50°, and 80°C blocks, and to a heat sink cooled by LN_2 for the -50°C block. The heaters used are cartridge types, 200 watts, 3/8 inch in diameter, and are inserted in the center of each sample block. The cells are mounted to aluminum plates which are in turn attached to the temperature control blocks. Dow Corning Sylgard 184, typically used as a cover glass adhesive, was selected to affix the cells to the plate. To assure adequate heat transfer, the adhesive was filled with zinc oxide to increase thermal conductance. Based on calculations, it is felt that cell temperature and sample block temperature are essentially the same.

Two thermocouples are located on each sample block and another thermocouple on the surface of each solar cell plate. One of the thermocouples from each block is connected to a temperature controller and the other two continuously record on a 12-point strip-chart recorder. A potentiometer was used to assure that the temperatures indicated on both the controller and recorder were accurate. Since the controllers are of the on-off relay type, a Variac is located in each heater circuit and adjusted to the minimum voltage while maintaining positive control.

The temperature control system for the +20°, +50°, and +80°C sample blocks operated completely satisfactory. Temperatures were recorded continually throughout the exposure period. Actual mean operating temperatures and temperature ranges for these blocks are indicated in Table 3-1.

TABLE 3-1

SAMPLE BLOCK TEMPERATURES

Sample Block	Temperature (°C)			
	Nominal	Mean	Maximum	Minimum
B	+20	21.1	23.3	19.4
C	+50	49.9	50.5	49.4
D	+80	80.1	80.6	79.5
E	+20	23.9	24.4	22.2
F	+20 (Dark)	23.7	23.9	22.2

The -50°C sample block temperature was controlled with a liquid nitrogen system. Despite extensive checkout procedures, there were nine periods of temporary failure for this system. The extent of these failures, both in terms of temperature and time, is shown in the temperature - time history plot of Figure 3-4. The result of these brief warmup periods can be observed in the annealing characteristics of the lithium cells, most prominently with float zone cells.

3.5 RADIOISOTOPE SOURCE

3.5.1 Isotope Characteristics

Sr-90 was selected for simulation of the trapped electron environment because the smoothed composite spectrum of Sr-90 and its daughter, Y-90, closely approximates the spectrum of the trapped electron belt to approximately 2 MeV. Thus, Sr-90 serves as a close approximation to the natural environment at those altitudes where the electron species are dominant in terms of producing solar cell damage. This tends to be valid for most orbital altitudes with the exception of those from approximately 1500 to 3000 nautical miles (nmi) where the trapped high-energy proton belt is more effective in producing solar cell damage than are trapped electrons. Even in this region, proton damage can be empirically equated to 1-MeV electron damage, and the net damage can be hypothetically attributed entirely to electrons with a spectrum which is also similar to the Sr-90/Y-90 spectrum. The radioisotope spectrum is shown in comparison with the 18,000 nmi trapped electron spectrum in Figure 3-5. Curves for other orbital altitudes have an equivalent degree of similarity.

Figure 3-6 indicates the anticipated range of electron fluxes as a function of orbital altitude. Measured data are shown for a period of relative solar quiet (1964) and calculated for a period of relatively high solar activity (1968). The increase in electron flux rate in the 6000 to 12,000 nmi range during the 1968 period is due to a compression of the trapped electron belt at these altitudes because of the influence of higher solar activity on the fringes of the earth's magnetosphere. The peak 1500 to 1800 nmi is primarily due to the artificial electron belt formed as a result of the Starfish nuclear detonation in 1962. The magnitude of this peak is thought to be decaying exponentially back toward a natural trapped electron environment (Ref. 14).

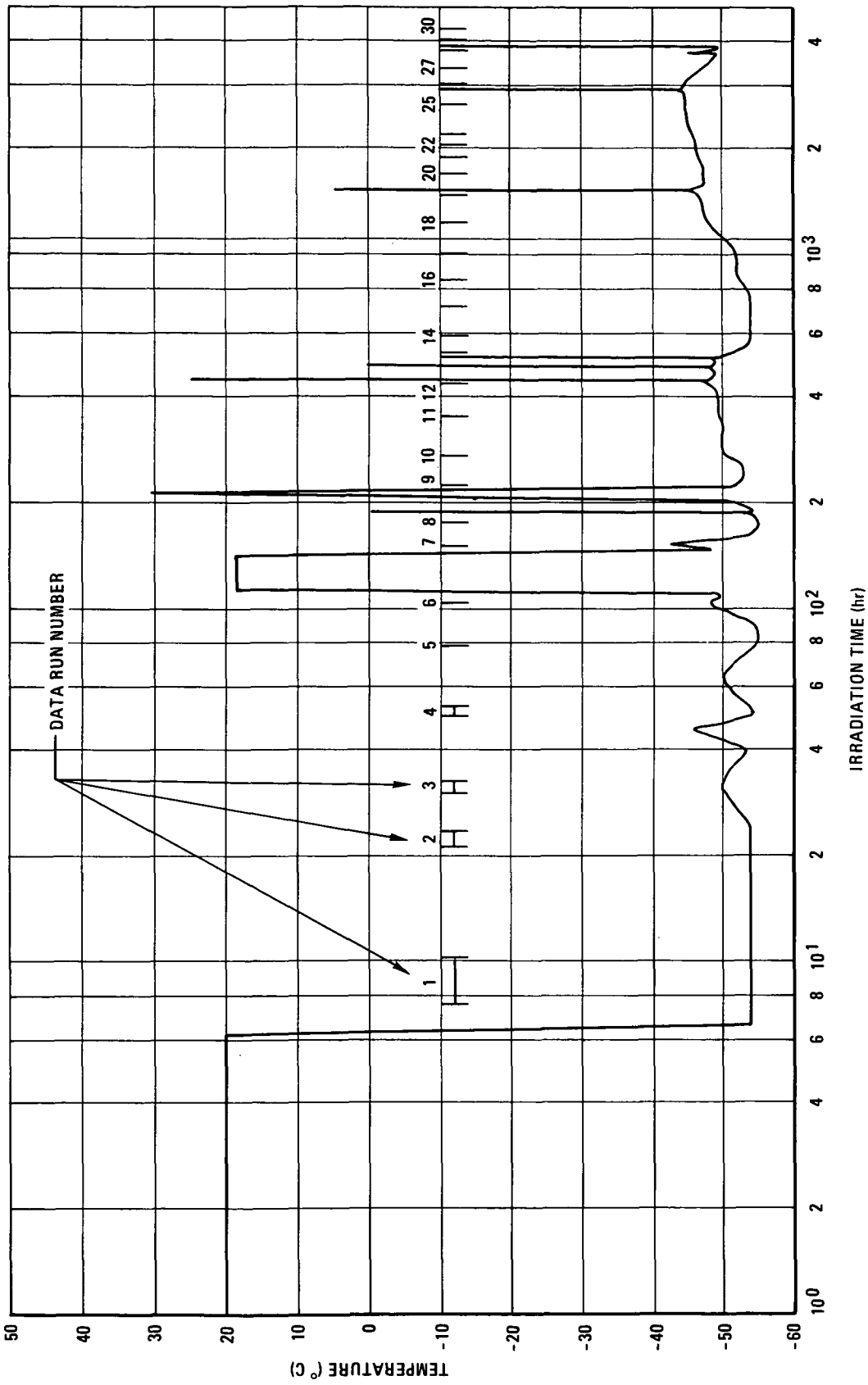

Figure 3-4 Temperature History of -50° Cell Block

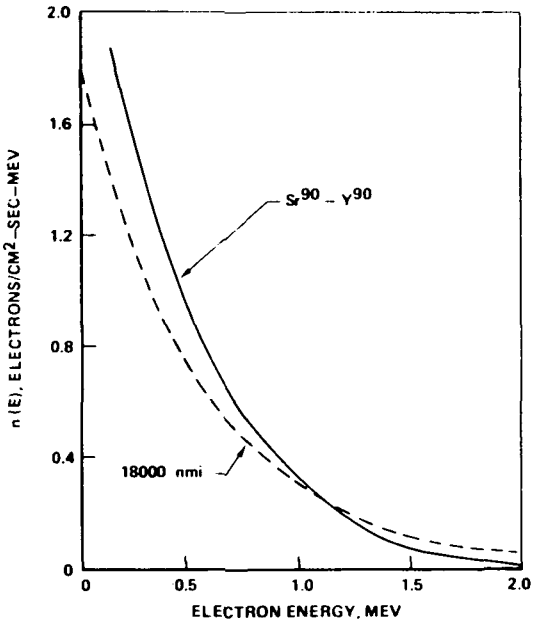

Figure 3-5 Isotope Characteristics

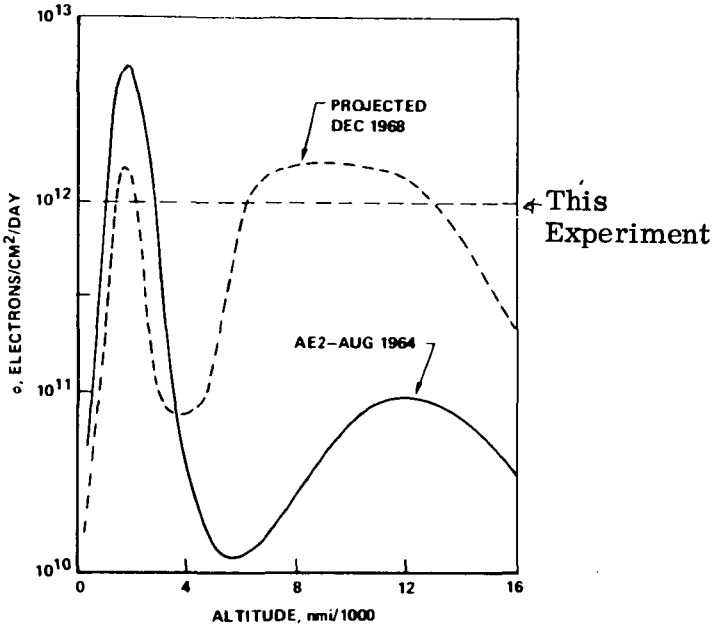

Figure 3-6 Trapped Electron Environment

3.5.2 Source Packaging

The source geometry was selected as an optimum shape consistent with ease of packaging and desired spectral characteristics. The isotope rod and canister are shown in Figure 3-8. The canister serves as a shielded container to house the isotope rod during storage and transportation. The canister is mated to the chamber for irradiation purposes, and the rod is then inserted into the chamber after the lead-filled door is opened.

The cylindrical container geometry provides acceptable uniformity of flux and spectrum over the sample area. A sample dipole calculation of monoenergetic flux emanating from a line source with the same geometry yields a maximum difference of approximately 1.3% between the normal point and a point on the extreme edge of the sample area.

In addition to the line source flux calculations, a more complex calculation was performed to evaluate the variation of electron spectra at various sample positions. Referring to Figure 3-7, it is seen that the path length through solid material of an electron emanating from the differential isotope element designated as point A is different for a sample location at the source "equator" (0°) from that at a sample location at "latitude 60°." This difference is due to isotope "self-shielding" and is manifested in a difference at the low energy end of the spectrum. Most of this spectral effect occurs at energies lower than the threshold energy

for displacement damage in n-type silicon. However, it is estimated that this effect would result in differences in short-circuit current degradation of 3% or less (for N/P cells). The actual effect observed will be much less than 3% because of scattering from the chamber walls and source container which tends to smooth the lower end of any incident spectrum.

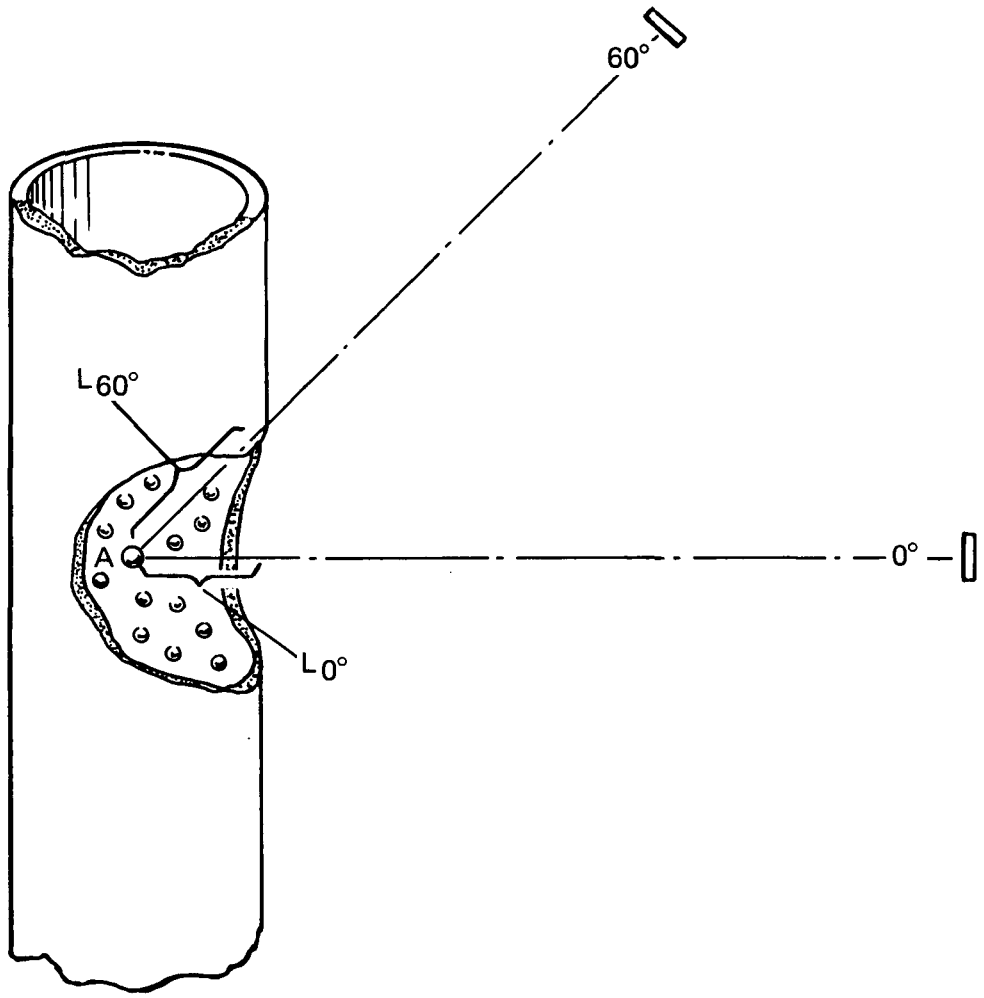

Figure 3-7 Pictorial Representation of Electron Path Length Difference

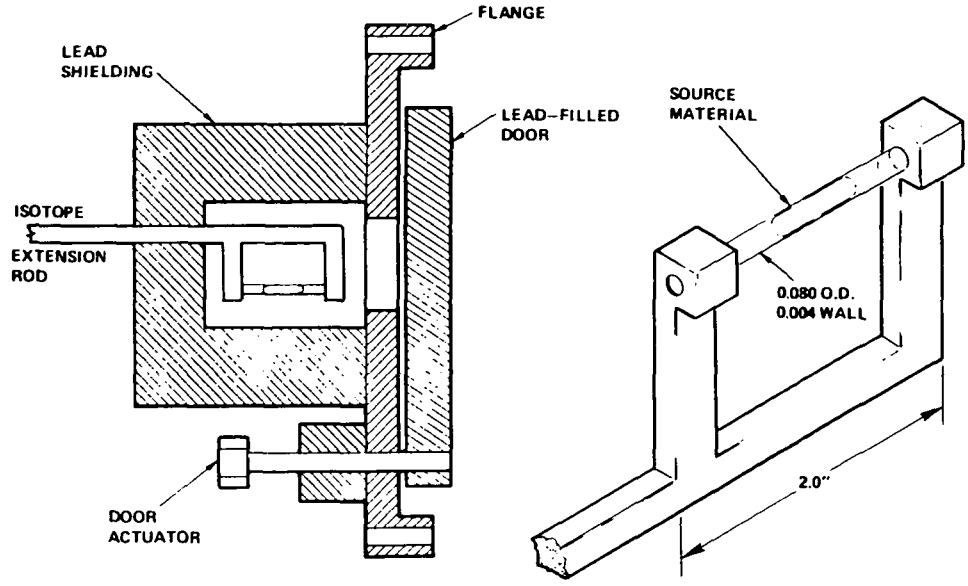

Figure 3-8 Isotope Rod and Canister

3.5.3 Flux Equivalence

The intent of this experimental program was to irradiate solar cells at a rate which would produce degradation in a conventional N/P cell equivalent to that caused by 1-MeV electrons at approximately 10^{12} electrons/cm^2/day. Using cell type K (irradiated in several earlier 1-MeV accelerator experiments) as a dosimeter, the 6-month 1-MeV equivalent fluence is judged to be 1.2×10^{14} electrons/cm^2. This corresponds to a 1-MeV electron flux of 7×10^{11} electrons/cm^2/day.

Comsat Laboratories (Ref. 15) estimates that the mean 1-MeV equivalent flux in synchronous orbit (for N/P cells with a 12-mil cover) is $4\text{-}8 \times 10^{13}$ electrons/cm^2/year. Thus, this 6-month exposure was equivalent to about 3 years at synchronous altitude. The irradiation rate was therefore about six times that expected at synchronous altitude. Since the lithium cells irradiated had essentially no post-irradiation annealing and if the rate was indeed six times higher than required, it follows that the cell annealing rate was considerably higher than that required at synchronous altitude. An optimized lithium cell for synchronous altitude would probably require a lower lithium concentration than those of the cells included in this experiment.

3.5.4 Flux Uniformity

Dosimetry measurements were made in the test chamber using 23 thermoluminescent dosimeters (TLDs) at various locations. These dosimeters indicated a flux variation of ±15% over the sample area. This value is not directly applicable to that for solar cells because of the effect of the energy threshold for displacement damage in silicon. A ±15% variation of flux as measured by TLD's would correspond to a much lower variation in terms of solar cell damage. Each of the solar cell samples within a given group was compared with the others within the group for any apparent correlation with flux rate variation. No such correlation was observed. It was therefore concluded that there was no significant variation of flux over the sample area so far as solar cell damage was concerned.

Calculations of electron spectra and flux support the position that the irradiation rates are uniform from the standpoint of solar cell damage. There are no indications, either analytical or physical, of any characteristic that would tend to adversely affect flux uniformity.

3.6 ILLUMINATION SYSTEMS

Two illumination systems were used for this program. One is a high-quality solar simulator and the other a general-purpose quartz-iodide illuminator. The Spectrolab X-25 Mark II Solar Simulator with close spectral filtering to match air mass zero solar characteristics was used for all electrical performance measurements. When cell measurements were not being made, the cells were loaded near the maximum power point and were illuminated at one-sun equivalent intensity with the quartz-iodide source. This source consists of a Colortran 1000-W lamp with a parabolic reflector. With the selected approach to illumination, the solar simulator was not subjected to long-term operation.

Calibration and standardization of the solar simulator were required for the correlation of I-V data over the long duration of the test. To facilitate standardization, a fixture was designed and fabricated which incorporates solar cells to measure the primary characteristics of the light beam. The intensity, uniformity, and spectral content of the simulator beam were checked before every data cycle. The standardization procedure is described further in detail in Appendix A.

The intensity of the quartz-iodide tungsten source was adjusted using a standard cell referred to as the "chamber intensity monitor." This monitor consisted of a 10 Ω-cm N/P silicon solar cell in a typical sealed "standard solar cell" enclosure. The cell was mounted on the rear flange of the vacuum chamber adjacent to a 2-inch-diameter window. Light from the light sources thus passed through the large front window, then through the smaller rear window, and then onto the standard cell.

The intensity of the solar simulator was adjusted using a standardization fixture mounted next to the vacuum chamber in the same plane as the experiment samples (Figure 3-9). The simulator, mounted on a linear bearing table, was adjusted for intensity, analyzed spectrally, analyzed for uniformity, then translated to illuminate the cells within the chamber.

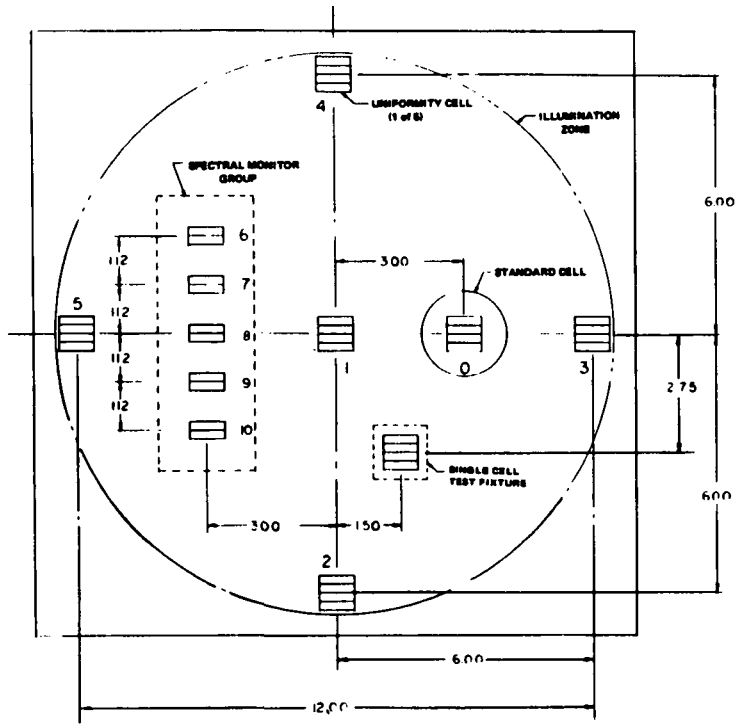

Figure 3-9 Simulator Standardization Fixture Layout

A secondary standard, calibrated to a JPL secondary balloon standard, was mounted to the fixture in a location identified as "standard cell." Blue and red Wratten filters, similar to those utilized at JPL in other programs, were used in conjunction with this standard cell to provide a measure of blue and red content of the simulator output as a function of time. Another fixture, identified as "spectral monitor group," was used for additional spectral content measures. This fixture incorporated solar cells as detectors employing bandpass

filters over various portions of the light source spectral output. Data from these standards are presented in Appendix A.

The secondary standard cell identified in the previous paragraph was used for all simulator intensity adjustments. After the intensity was adjusted to produce the desired short-circuit current from this cell, data were taken to check the spectral characteristics and uniformity of the simulator. These data clearly indicate a significant shift in the simulator output from blue to red. Cell measurements with the blue Wratten filter decreased 3.3% during the 6-month exposure period. Red filter readings increased 3.3%. Red/blue ratio increased 6.3%.

As shown in Appendix A, unfiltered uniformity monitor output (five cells) increased from zero to 1.6% during the 6-month period. The output of the chamber intensity monitor on the rear of the chamber (with light passing through two windows) increased 1.3%. These factors indicate that the secondary standard cell was apparently more blue-sensitive than the uniformity and chamber intensity monitor.

Transmission measurements were not performed on either front or rear chamber windows. From the chamber intensity monitor readings, however, it appears fairly certain that any spectral transmission changes in either window produced negligible effects in cell output.

3.7 DATA ACQUISITION SYSTEM

The solar cell performance was determined by measuring the I-V curve of each cell using the data acquisition system. This system consists of: (1) four-wire cell leads, (2) automatic cell switching system, (3) Spectrolab D-550 electronic load unit, (4) Mosley x-y recorder, and (5) precision voltmeter and ammeter. This apparatus, coupled with high-quality solar simulation and well-defined standardization procedures, produces data with an optimum degree of accuracy and repeatability. A further description of the arrangement of this equipment and the procedures for its use are included in Appendix B.

A four-wire connection to each solar cell was used to obtain accurate I-V data, particularly near the maximum power point. Two leads were used for current measurement and two for voltage measurement.

The degradation characteristics of the cells were determined by sequentially acquiring accurate I-V measurements. The cells were initially measured as received under one-sun illumination at 28°C. Three cells of each group were also measured at 20°, 30°, and 40°C to determine the temperature coefficients of their I-V characteristics. The cells were again measured after installation in the irradiation chamber and before the isotope was installed. The initial chamber measurements were made at vacuum and temperature test conditions and are therefore used as the baseline measurements. Measurements of the reverse illuminated characteristics and dark forward/reverse characteristics were made, prior to test initiation and three times during the exposure.

Extra cell samples were used as test controls to determine the effect, if any, of maintaining the solar cells at +20° and 80°C for 6 months. These cells were measured periodically and stored in the vacuum oven for the remainder of the time.

The data acquisition system, described further in Appendix B and in WDL Report TR-4213A, operated satisfactorily and provided data of high quality throughout the exposure period. No equipment breakdowns or performance degradations were observed.

SECTION 4

SAMPLE DESCRIPTIONS

4.1 CELL DESCRIPTION AND INVENTORY

Descriptive information was provided by the cell manufacturers. This information is summarized in Table 4-1. Lithium cells of both crucible-grown and float-zone-refined silicon were manufactured by both cell manufacturers. The particular configurations delivered were selected by both manufacturers as the most promising types available in early 1970.

It should be noted that the Centralab float zone cells are actually made from Monex (Monsanto) material. It is also important to note the BCl_3 diffusion characteristics provided by Centralab. For their lithium cells, all BCl_3 diffusions were performed at 1050°C with preheat - tack-on - diffusion times of 8-5-8 minutes with the exception of cell type G. Cell type G had an 8 minute tack-on time, presumably resulting in a higher boron surface concentration and a steeper concentration gradient.

The sample cell inventory is shown in Table 4-2. It was necessary to order additional Centralab cells to replace those damaged (through contact failure) during assembly. The cells indicated as 20° and 80°C Vacuum Storage were kept under those conditions for approximately 7 months as unirradiated control cells. Their electrical properties were again measured for a determination of changes during storage. The 20°C vacuum storage cells were sent to JPL at the end of the 7-month storage period to be incorporated into 1-MeV irradiation experiments.

4.2 INITIAL ELECTRICAL CHARACTERISTICS

The electrical characteristics of all delivered cells were measured as the cells were received. These characteristics (at 23°C) are summarized in Table 4-3. Maximum power characteristics are shown graphically in chart form in Figure 4-1. 95% confidence limits are shown for the cell quantities noted.

TABLE 4-1

SOLAR CELL DESCRIPTIONS

Cell Code	Cell Description			Mfr Date	Silicon Resistivity (Ω-cm)	Slice Orientation	Dopant	Silicon Mfr	BCl_3 Diff. Char.	Lithium Concentration (atoms/cm^3)		
	Silicon Type	Cell Mfr	Lithium Diff. Char.							Front	Peak	Rear
A	Crucible	HEL	425-90-60	1-70	15-25	100	As	HEL		7×10^{16}	1.3×10^{17}	2×10^{16}
B	Crucible	CENT	425-90-60	2-70	~50	111	As	CENT	1050°C 8-5-8			
C	Crucible	CENT	425-20-0	2-70	~50	111	As	CENT	1050°C 8-5-8			
D	Crucible	HEL	425-90-60 (covered)	1-70	15-25	100	As	HEL		7×10^{16}	1.3×10^{17}	2×10^{16}
E	Float Zone	HEL	425-90-120	1-70	16-24	111	P	TI		8×10^{16}		6×10^{16}
F	Float Zone	HEL	350-90-60	1-70	16-24	111	P	TI		5×10^{16}		2×10^{16}
G	FZ (Monex)	CENT	425-90-120	2-70	~40	111	P	Monsanto	1050°C 8-8-8			
H	FZ (Monex)	CENT	425-90-120	2-70	~40	111	P	Monsanto	1050°C 8-5-8			
I	N/P	CENT		2-70	~10		B	CENT				
J	N/P	HEL		1-70	~10		B	HEL				
K	N/P	HOFF		64	~10		B	HOFF				

Notes:

1. 425-90-60, etc, refers to lithium diffusion characteristics (diffusion temperature in °C, diffusion time in minutes, redistribution time in minutes).
2. Type D had a 1-mil integral cover. All other types were bare.
3. 8-5-8, etc, refers to boron diffusion characteristics (preheat time in minutes, "tack-on" time, diffusion time).

TABLE 4-2

CELL INVENTORY

	Cell Code	A	B	C	D	E	F	G	H	I	J	K
Availability	Vendor*	H	C	C	H	H	H	C	C	C	H	O
	Quantity Purchased	30	20	20	12	30	20	20	20	20	10	-
	Number Damaged in Assembly	0	8	3	0	1	0	4	8	0	0	0
	Supplemental Cells Obtained	0	4	4	0	0	0	3	4	0	0	8
	Total Obtained	30	24	24	12	30	20	23	24	20	10	5
Usage	Number in Chamber	20	12	12	4	20	12	12	12	12	8	4
	20°C/Vacuum Storage for 1-MeV Exposure**	4	4	4	4	4	4	4	4	4	2	4
	80°C/Vacuum Storage	4	0	4	4	4	4	3	0	4	0	0
	Spares, 20°C/Vacuum Storage	2	0	1	0	1	0	0	0	0	0	0

* Vendors:

H - Heliotek
C - Centralab
O - Old Hoffman

** Sent to JPL for 1-MeV irradiation.

TABLE 4-3

CELL INITIAL CHARACTERISTICS (measured at 23°C and 140 mW/cm^2)

Cell Description				No. of Cells	I_{sc} (mA)		V_{oc} (V)		I_{MP} (mA)		V_{MP} (V)		P_{max} (mW)		CPF	
Code	Type	Mfr*	Lithium Diff. Char.		Mean	% Dev.	Mean	% Dev.	Mean	% Dev.	Mean	% Dev.	Mean	% Dev.	Mean	% Dev.
A	Cruc.	H	425-90-60	30	61.2	3.43	0.585	1.28	55.8	3.30	0.481	1.35	26.82	4.43	0.749	1.17
B	"	C	425-90-60	24	67.0	1.49	0.604	0.71	61.1	1.60	0.493	1.14	30.12	2.24	0.745	0.16
C	"	C	425-20-0	24	70.1	1.63	0.611	1.36	63.4	5.34	0.499	3.41	31.66	7.95	0.739	6.50
D	"	H	425-90-60 (1-mil cover	12	62.9	4.08	0.592	0.96	56.6	3.07	0.453	2.83	25.61	3.50	0.689	4.02
E	FZ	H	425-90-120	30	62.5	2.14	0.558	0.91	57.2	2.02	0.453	0.99	25.92	2.54	0.743	0.94
F	"	H	350-90-60	20	67.8	2.33	0.554	0.67	61.2	1.90	0.447	1.19	27.37	2.06	0.729	1.25
G	"	C	425-90-120 (8-8-8)	23	60.3	2.38	0.554	0.86	54.6	2.48	0.425	2.07	23.23	3.17	0.704	2.34
H	"	C	425-90-120 (8-5-8)	24	62.8	3.82	0.569	1.05	57.0	3.83	0.455	2.15	25.97	4.13	0.727	1.94
I	N/P	C		20	69.4	1.29	0.554	0.90	63.8	1.12	0.449	1.29	28.65	1.65	0.745	0.87
J	"	H		10	67.6	1.25	0.551	0.36	61.6	1.01	0.448	1.25	27.61	1.73	0.741	1.39
K	"	O		8	71.2	1.79	0.543	0.44	64.4	1.92	0.443	1.92	27.85	1.72	0.720	1.94

*Manufacturers are: H - Heliotek; C - Centralab; O - Old Hoffman.

Notes:

1. 425-90-60, etc, refers to lithium diffusion characteristics (diffusion temperature in °C, diffusion time in minutes, redistribution time in minutes).
2. Type D had a 1-mil integral cover. All other types were bare.
3. 8-5-8, etc, refers to boron diffusion characteristics (preheat time in minutes, "tack-on" time, diffusion time).
4. $CPF = P_{max}/V_{oc} \times I_{sc}$.
5. $\%\ \text{Deviation} = \frac{\text{one standard deviation}}{\text{mean}} \times 100$.

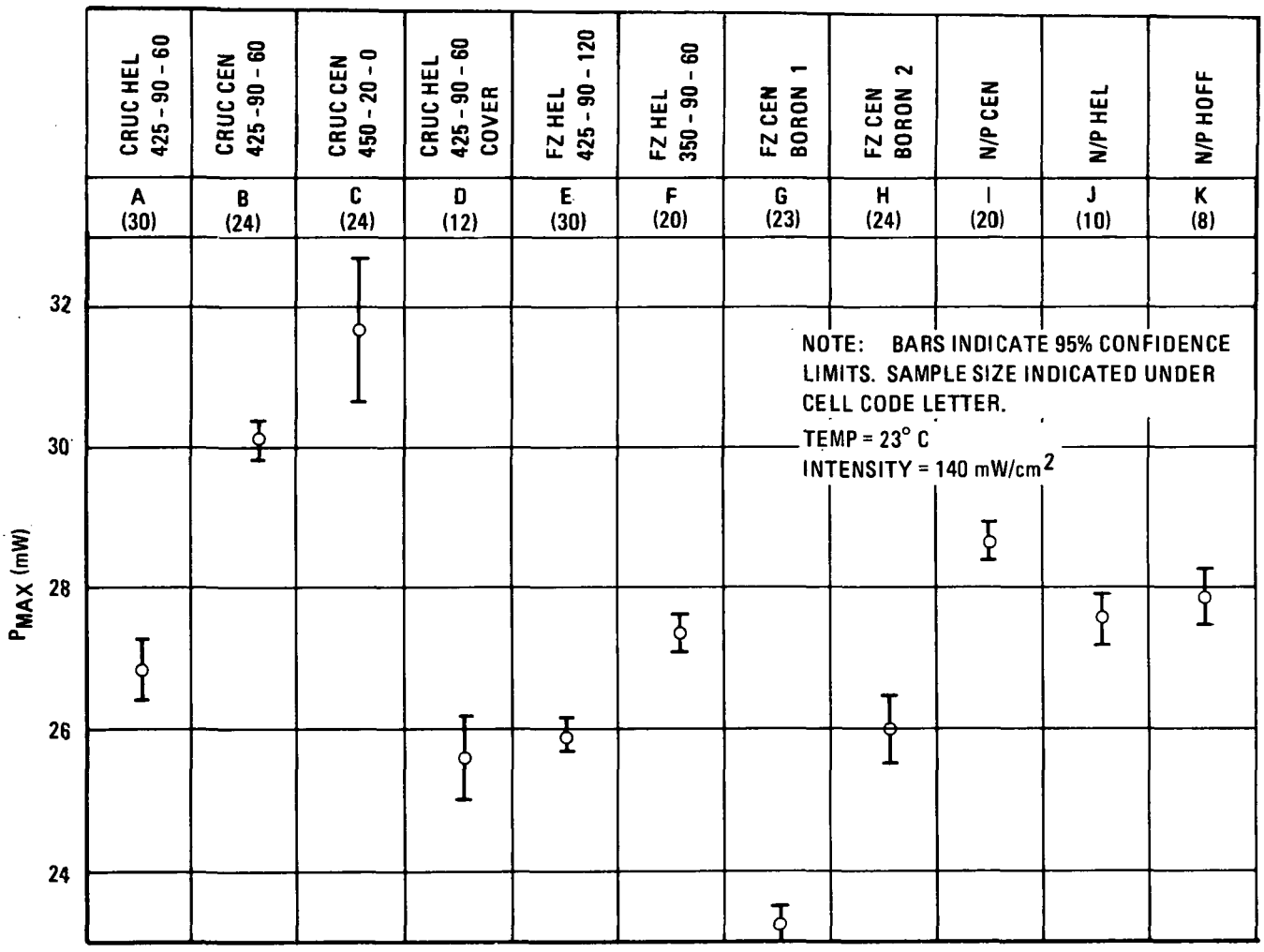

Figure 4-1 Initial Maximum Power Characteristics

As can be seen, the lithium cell distributions are of the same magnitude as the N/P cells. Investigations of performance data on the entire lot of cells manufactured (from which the cells delivered to WDL were selected) have indicated that the lot variances were not substantially greater than for the smaller groups delivered to WDL.

It is interesting to compare the performance characteristics of the 1970 lithium cells used in this experimental program to those of the 1967 lithium cells used in the earlier irradiation program performed for GSFC. Comparative data are presented in Table 4-4. It is seen that a considerable improvement has been made in terms of maximum power and curve power factors. The other significant improvement is that of narrower distributions (lower standard deviation) of the cell parameters. From these data, it is apparent that the cell production processes are better understood and controlled with the newer cells.

4.3 TEMPERATURE COEFFICIENT DATA

Temperature coefficients were calculated based on measurements at +20°, +30°, and +40°C. Measurements were restricted to this narrow temperature range in order to minimize potential damage to the lithium cells by prolonged exposure to higher temperatures. Mean temperature coefficients are presented in Table 4-5.

These data are presented graphically in Figure 4-2 along with 95% confidence limits. The limits are relatively wide because the data are based on a sample size of three. There is no apparent significant difference between lithium and N/P cell temperature coefficients for maximum power for the two cell types. This is a reportedly typical difference for P/N and N/P cells (Ref. 16). Relatively, the P/N cells will gain some advantage over the N/P cells at the higher operating temperatures. This fact is considered important in interpreting the degraded performance data in the following section.

4.4 DIODE CHARACTERISTICS DATA

Diode characteristics (ie, dark and illuminated, forward and reverse) were measured on all 128 cells irradiated in the chamber. These data have not as yet been reduced or analyzed.

TABLE 4-4

COMPARISON OF 1970 LITHIUM CELLS WITH 1967 LITHIUM CELLS

Cell Type	Year	I_{sc}		V_{oc}		P_{max}		CPF	
		Range of Means (mA)	% Dev.	Range of Means (mV)	% Dev.	Range of Means (mW)	% Dev.	Range of Means	% Dev.
Crucible Lithium Cells	1967	60.8-66.9	4.5-6.9	528-584	7.2-9.6	22.6-24.9	14.6-34.1	0.637-0.719	4.3-28.8
	1970	61.2-70.1	1.5-3.4	585-611	0.7-1.4	26.8-31.7	2.2- 8.0	0.739-0.749	0.2- 6.5
Float Zone Lithium Cells	1967	57.0-60.0	1.4-4.2	564-568	2.1-5.8	21.5-22.2	14.0-31.5	0.654-0.665	11.9-27.5
	1970	60.3-67.8	2.1-3.8	554-569	0.7-1.1	23.2-27.4	2.1- 4.1	0.704-0.743	0.9- 2.3
N/P Cells (Used in each experiment	1967	71.7	2.7	543	0.7	24.8	15.3	0.647	5.9
	1970	67.6-69.4	1.3	551-554	0.4-0.9	27.6-28.7	1.7	0.741-0.745	0.9- 1.4

Note: $\%\ \text{Deviation} = \frac{\text{one standard deviation}}{\text{mean}} \times 100.$

TABLE 4-5

MEAN TEMPERATURE COEFFICIENTS
(Sample Size = 3)

Cell Code	Temperature Coefficient		
	P_{max} (mW/°C)	I_{sc} (mA/°C)	V_{oc} (mV/°C)
A	-0.090	0.0684	-2.10
B	-0.125	0.0600	-1.80
C	-0.118	0.0816	-1.94
D	-0.065	0.0534	-2.13
E	-0.098	0.0750	-2.04
F	-0.105	0.0816	-1.98
G	-0.097	0.0650	-2.48
H	-0.105	0.0650	-2.04
I	-0.153	0.0380	-2.28
J	-0.147	0	-2.07
K	-0.133	0.0380	-2.04

Note: Intensity = 140 mW/cm^2; temperature range = 20 - 40°C.

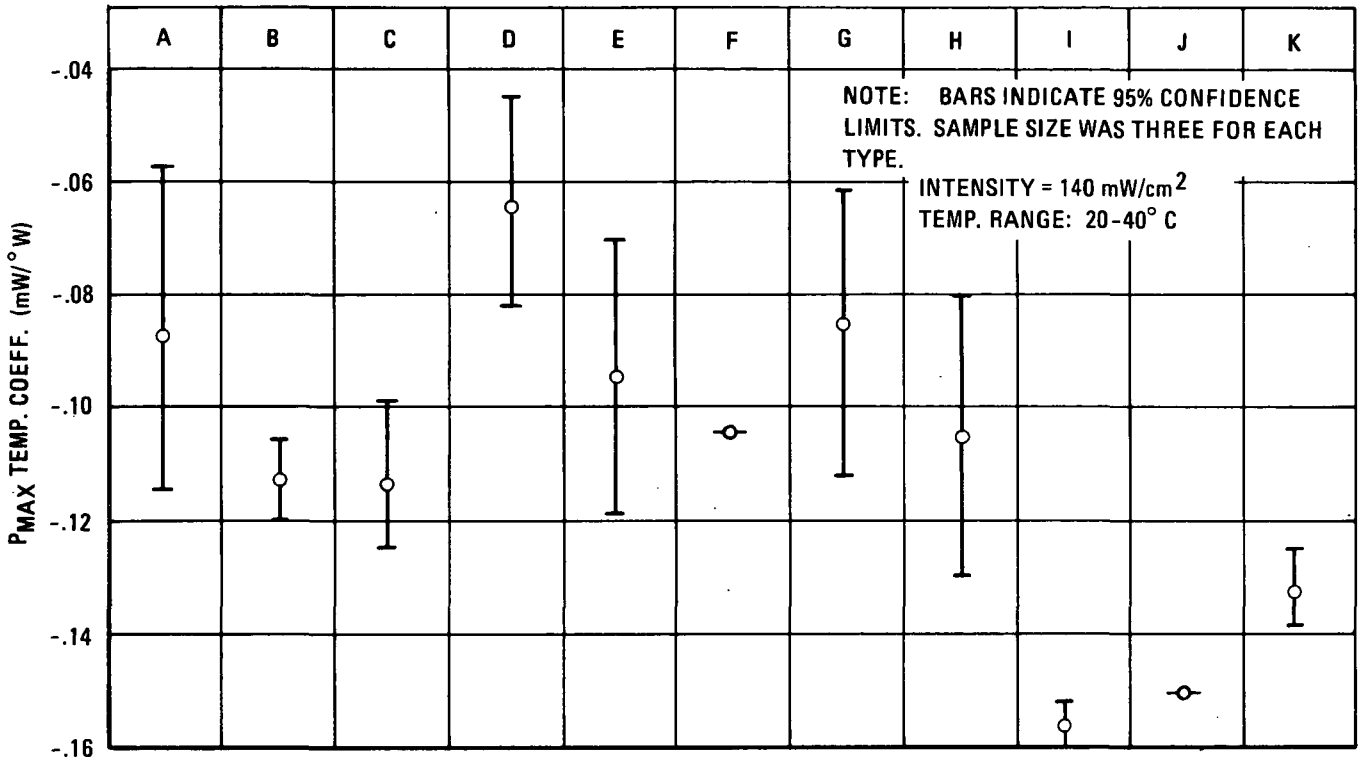

Figure 4-2 Temperature Coefficient Characteristics

SECTION 5

RESULTS

5.1 GENERAL

The data produced during this experimental program is uniquely characterized by virtue of its quantity and its quality. Over 6000 individually plotted I-V curves were produced through the course of the effort. Because of this vast amount of raw data and because of contractual funding limitations, it was not possible to completely analyze the data to maximize the extraction of useful or explanatory information. Thus the report summarizes the overall program results with emphasis on their most significant aspects such as maximum power characteristics. Short-circuit current and open-circuit voltage characteristics are treated in a relatively incomplete fashion.

The quality of the data is high compared to earlier similar experimental efforts because of improved physical design and layout of the experimental apparatus and the techniques used for data acquisition. Statistical analysis of data and a low degree of experimental error have resulted in high confidence in the observed results.

It is important to briefly review the treatment of the raw data before examining the results. As explained earlier, all experimental sample solar cells were mounted on blocks whose surfaces were not perpendicular to the light source/sample line. All data (i.e., maximum power and short-circuit current) are therefore corrected to normal incidence using a cosine factor. No temperature corrections are applied (see actual temperatures listed in Table 3-1). No attempt is made to relate irradiation time with an equivalent 1-MeV fluence. No corrections are made for electron flux uniformity or illumination source uniformity.

Also to be noted at the outset are certain results and information which have a bearing on the interpretation of the data presented in this section. These are: radiation source uniformity, lithium cell storage stability, and post-irradiation annealing characteristics.

From the standpoint of solar cell damage, the electron flux rate is judged to be constant over the entire sample surface based on spectrum calculations. It is important to note that non-irradiated samples were stable over the period of the irradiation. Further, virtually no post-irradiation annealing was observed in any of the lithium cells after the radiation source was removed. These characteristics are discussed in greater detail in later sections. They are mentioned at this point, however, because of their importance in understanding the radiation degradation phenomena being presented.

5.2 SIX-MONTH IRRADIATION RESULTS

5.2.1 Tabularized End-of-Run Data

The results of the 6-month irradiation are presented in Table 5-1 in the form of initial (immediately prior to irradiation) data and final (after 180 days) data. Both sets were taken at the specified test temperature.

The maximum power (P_{max}), short-circuit current (I_{sc}), and open-circuit voltage (V_{oc}) degradation data of Table 5-1 present little in the way of unexpected results. The curve power factor (CPF) data (maximum power divided by the product of short-circuit current and open-circuit voltage) are somewhat surprising, however. Firstly, the CPF degradation for N/P cells ranged from 0 to 6%. This apparently contradicts earlier results where no such degradation was observed. The lithium cells, on the other hand, show a CPF degradation as high as 5% (cell group FD) to a CPF improvement as high as 7% (group GA).

5.2.2 Statistical Analyses

The data presented in Table 5-1 were analyzed statistically to determine the extent, if any, of significant difference in post-irradiation maximum power of various sample combinations. This analysis was performed by way of direct two-way comparisons.

TABLE 5-1

TABULARIZED INITIAL AND END-OF-RUN RESULTS

Cell Type	Cell Code	T (°C)	P_{max} (mW)			I_{sc} (mA)			V_{oc} (volts)			CPF		
			Initial	Final	Relative	Initial	Final	Relative	Initial	Final	Relative	Initial	Final	Relative
Hel Crucible 425-90-60	AA	-50	31.7	22.4	0.706	54.4	40.2	0.739	0.751	0.713	0.949	0.776	0.781	1.0064
	AB	+20	26.9	21.8	0.810	61.5	52.5	0.854	0.599	0.553	0.923	0.730	0.751	1.028
	AC	+50	23.6	21.9	0.928	61.6	59.5	0.966	0.533	0.514	0.964	0.719	0.716	0.996
	AD	+80	21.1	19.7	0.934	65.2	62.5	0.958	0.472	0.455	0.964	0.686	0.692	1.009
	AF	+20	28.7	24.4	0.850	65.0	58.7	0.903	0.597	0.558	0.934	0.740	0.745	1.0067
Cen Crucible 425-90-60	BA	-50	37.3	23.3	0.625	60.5	40.2	0.664	0.771	0.712	0.923	0.799	0.814	1.019
	BB	+20	30.7	22.3	0.726	68.1	53.3	0.783	0.609	0.551	0.905	0.740	0.759	1.026
	BD	+80	23.3	19.8	0.850	69.2	62.7	0.906	0.495	0.463	0.935	0.680	0.682	1.003
Cen Crucible 450-20-0	CA	-50	38.8	23.3	0.601	63.3	41.4	0.654	0.773	0.706	0.913	0.793	0.803	1.013
	CB	+20	31.7	22.1	0.697	68.8	52.8	0.767	0.618	0.541	0.875	0.745	0.774	1.039
	CD	+80	24.4	20.6	0.844	72.3	66.1	0.914	0.501	0.456	0.910	0.673	0.683	1.010
Hel Crucible 425-90-60 (1-mil cover)	DB	+20	26.7	20.6	0.772	63.8	52.4	0.821	0.597	0.552	0.925	0.701	0.712	1.016
Hel Float Zone 425-90-120	EA	-50	32.2	21.8	0.677	56.4	39.8	0.706	0.737	0.701	0.951	0.774	0.781	1.009
	EB	+20	26.5	23.4	0.883	62.9	56.9	0.904	0.567	0.558	0.984	0.743	0.737	0.992
	EC	+50	23.2	21.6	0.931	63.5	61.2	0.964	0.509	0.492	0.967	0.717	0.717	0
	ED	+80	18.8	16.6	0.883	63.6	61.2	0.962	0.433	0.402	0.928	0.682	0.675	0.989
	EF	+20	26.4	24.7	0.936	63.2	60.7	0.960	0.563	0.551	0.979	0.742	0.738	0.995
Hel Float Zone 350-90-60	FA	-50	33.4	22.4	0.671	57.5	41.0	0.713	0.720	0.689	0.957	0.807	0.793	0.983
	FB	+20	27.4	19.7	0.719	67.2	54.6	0.813	0.559	0.508	0.909	0.729	0.710	0.974
	FD	+80	20.1	15.9	0.791	71.3	64.9	0.910	0.435	0.397	0.913	0.648	0.617	0.952
Cen Float Zone Boron 1	GA	-50	27.7	20.5	0.740	53.8	39.1	0.727	0.720	0.685	0.951	0.715	0.765	1.070
	GB	+20	23.7	21.6	0.911	59.3	55.1	0.929	0.554	0.545	0.984	0.721	0.719	0.997
	GD	+80	17.7	15.7	0.887	63.7	60.4	0.948	0.422	0.400	0.948	0.658	0.649	0.986
Cen Float Zone Boron 2	HA	-50	34.3	20.4	0.595	58.7	36.6	0.624	0.746	0.695	0.932	0.783	0.802	1.024
	HB	+20	26.2	23.9	0.912	62.5	58.3	0.933	0.577	0.564	0.977	0.726	0.727	1.001
	HD	+80	19.4	17.1	0.881	65.0	61.4	0.945	0.447	0.422	0.944	0.667	0.660	0.989
Cen 10Ω-cm N/P	IA	-50	37.5	30.0	0.800	64.2	54.7	0.852	0.724	0.721	0.996	0.807	0.761	0.943
	IE	+20	29.6	24.9	0.841	69.0	62.8	0.910	0.569	0.538	0.946	0.754	0.737	0.977
	IF	+20	29.6	26.4	0.892	71.8	67.7	0.943	0.558	0.536	0.961	0.739	0.727	0.984
Hel 10Ω-cm N/P	JD	+80	19.8	17.6	0.889	70.8	67.1	0.948	0.429	0.404	0.942	0.652	0.649	0.995
	JE	+20	28.3	24.5	0.866	67.4	61.2	0.908	0.565	0.539	0.954	0.743	0.743	0
Hof 10Ω-cm N/P	KE	+20	26.7	22.2	0.831	66.1	58.7	0.888	0.558	0.530	0.949	0.724	0.713	0.985

Notes:
1. All data represent means of values for four cells. For entire group characteristics, refer to Table 4-3.
2. Cell Code: 1st letter indicates cell type, 2nd letter indicates test condition. Refer to Experimental Sample Matrix.
3. All data have been corrected to normal incidence, 140 mV/cm^2 values. No other corrections were applied.
4. "Initial" refers to values immediately prior to irradiation.
5. "Final" refers to values after 180 days of irradiation.

PHILCO
Philco-Ford Corporation
Western Development Laboratories Division

Table 5-2 presents the results of this analysis, which used the following procedure:

a. Test "t" statistic assumption of equal variances using F statistic.

b. Test for difference between power outputs using "t" statistics at 2.5% level of significance.

c. If differences existed, estimate magnitude of difference at the 2.5% level of significance. This magnitude, which can be called δ_{crit}, has the following significance: It is the maximum amount by which $\bar{x}_1$ and $\bar{x}_2$ can be assumed to be different at the 2.5% level of significance. (See Appendix D for details.)

Both absolute and relative degraded maximum power figures were subjected to the statistical tests. It is important to realize that certain assumptions are implied in the use of either relative or absolute degradation data. These are:

a. Absolute

1. Samples represent production population exactly (both mean and variance).
2. There is little or no chance of improving initial performance characteristics.

b. Relative

1. Comparable types can be made with identical initial characteristics (identical means).
2. Poorer types can be improved.
3. Improved types will have identical variances.

It is not advisable to use either type of degradation data without considering these assumptions. The use of absolute data appears much more reasonable, however, in selecting one type of cell over another. The entire question depends on the abilities of the cell manufacturer to produce cells duplicating those included in the test. This risk is present in any purchase of solar cells, particularly after a production line has been shut down for a period.

TABLE 5-2

RESULTS OF SIGNIFICANT DIFFERENCE TESTS

Cell Codes	Common Factors	Pertinent Comparison	Post-Irradiation Absolute Maximum Power							Final Relative Maximum Power (P_{max}/Initial P_{max})						
1/2		1/2	$\bar{x}_1$	$\bar{x}_2$	s_1	s_2	F-test ($s_1 = s_2$) $F_{0.01}$	Significant Difference (2.5% level)	% δ $\alpha = 0.025$	$\bar{x}_1$	$\bar{x}_2$	s_1	s_2	F-test ($s_1 = s_2$) $F_{0.01}$	Significant Difference (2.5% level)	% δ $\alpha = 0.025$
AB/AC	Hel Cruc 425-90-60	20°/50°	21.86	21.88	0.61	0.59	Yes	No	--	0.811	0.928	0.308	0.033	Yes	Yes	11.4
AB/AF	Hel Cruc 425-90-60, 20°	Light/Dark	21.86	24.34	0.61	0.42	Yes	Yes	7.6	0.811	0.847	0.308	1.24	Yes	Yes	0.265
AC/AD	Hel Cruc 425-90-60	50°/80°	21.88	19.65	0.59	0.51	Yes	Yes	7.0	0.928	0.933	0.033	0.185	Yes	No	--
EB/EC	Hel FZ 425-90-120	20°/50°	23.47	21.64	0.88	0.67	Yes	Yes	3.4	0.886	0.936	0.078	0.338	Yes	Yes	3.3
EB/ED	Hel FZ 425-90-120	20°/80°	23.47	16.54	0.88	0.72	Yes	Yes	29.0	0.886	0.880	0.078	0.220	Yes	No	--
EB/EF	Hel FZ 425-90-120, 20°	Light/Dark	23.47	24.76	0.88	0.25	Yes	Yes	1.7	0.886	0.936	0.078	0.162	Yes	Yes	3.8
EC/ED	Hel FZ 425-90-120	50°/80°	21.64	16.54	0.67	0.72	Yes	Yes	22.0	0.936	0.880	0.338	0.220	Yes	Yes	3.6
GB/GD	Cen FZ 425-90-120, 8-8-8	20°/80°	21.63	15.66	0.84	0.34	Yes	Yes	28.0	0.911	0.885	0.103	0.008	Yes	Yes	1.8
HB/HD	Cen FZ 425-90-120, 8-5-8	20°/80°	23.83	17.17	1.18	0.92	Yes	Yes	25.0	0.909	0.889	0.210	0.026	Yes	Yes	0.57
IA/IE	Cen 10Ω-cm N/P	-50°/20°	30.07	24.97	0.49	0.26	Yes	Yes	16.0	0.802	0.844	0.384	0.058	Yes	Yes	2.6
IE/IF	Cen 10Ω-cm N/P, 20°	Light/Dark	24.97	26.50	0.26	0.83	Yes	Yes	1.7	0.844	0.896	0.058	0.178	Yes	Yes	4.3
JD/JE	Hel 10Ω-cm N/P	80°/20°	16.60	24.45	0.40	0.10	Yes	Yes	36.0	0.889	0.863	0.328	0.116	Yes	Yes	0.62
AB/DB	Hel Cruc 425-90-60, 20°	Uncovered/Covered	21.86	20.58	0.61	1.49	Yes	Yes	1.3	0.811	0.772	0.308	0.477	Yes	Yes	1.5
AB/EB	Hel 425-90-60, 20°	Cruc/FZ	21.86	23.47	0.61	0.88	Yes	Yes	2.5	0.811	0.886	0.308	0.078	Yes	Yes	6.5
AB/JE	20°	Hel Cruc 425-90-60/Hel N/P	21.86	24.45	0.61	0.10	No	Yes	8.6	0.811	0.863	0.308	0.116	Yes	Yes	3.8
AC/EC	50°	Hel Cruc 425-90-60/Hel FZ 425-90-120	21.88	21.64	0.59	0.67	Yes	No	--	0.928	0.936	0.033	0.338	Yes	No	--
AD/BD	Cruc 425-90-60, 80°	Hel/Cen	19.65	19.83	0.51	0.22	Yes	No	--	0.933	0.851	0.185	0.061	Yes	Yes	7.2
AD/ED	80°	Hel Cruc 425-90-60/Hel FZ 425-90-120	19.65	16.54	0.51	0.72	Yes	Yes	13.0	0.933	0.880	0.185	0.220	Yes	Yes	3.6
AD/JD	80°	Hel Cruc 425-90-60/Hel N/P	19.65	17.60	0.51	0.40	Yes	Yes	7.6	0.933	0.889	0.185	0.328	Yes	Yes	2.4
AF/EF	20° Dark	Hel Cruc 425-90-60/Hel FZ 425-90-120	24.34	24.76	0.42	0.25	Yes	Yes	0.22	0.847	0.936	1.24	0.162	Yes	Yes	5.9
AF/IF	20° Dark	Hel Cruc 425-90-60/Cen N/P	24.34	26.50	0.42	0.83	Yes	Yes	4.9	0.847	0.896	1.24	0.178	Yes	Yes	1.4
BD/CD	80°	Cen Cruc 425-90-60/Cen Cruc 425-20-0	19.83	20.55	0.22	0.62	Yes	Yes	1.8	0.851	0.842	0.061	0.198	Yes	No	--
EB/JE	20°	Hel FZ 425-90-120/Hel N/P	23.47	24.45	0.88	0.10	No	Yes	0.50	0.886	0.863	0.078	0.116	Yes	Yes	1.1
ED/JD	80°	Hel FZ 425-90-120/Hel N/P	16.54	17.60	0.72	0.40	Yes	Yes	1.5	0.880	0.889	0.220	0.328	Yes	No	--
EF/IF	20° Dark	Hel FZ 425-90-120/Cen N/P	24.76	26.50	0.25	0.83	Yes	Yes	3.5	0.936	0.896	0.162	0.178	Yes	Yes	2.4
GB/HB	Cen FZ 425-90-120, 20°	8-8-8/8-5-8	21.63	23.83	0.84	1.18	Yes	Yes	3.5	0.911	0.909	0.103	0.210	Yes	No	--
GB/JE	20°	Cen FZ 425-90-120, 8-8-8/Hel N/P	21.63	24.45	0.84	0.10	No	Yes	8.6	0.911	0.863	0.103	0.116	Yes	Yes	3.8
GD/ED	80°	Cen FZ 425-90-120, 8-8-8/Hel FZ 425-90-120	15.66	16.54	0.34	0.72	Yes	Yes	0.66	0.885	0.880	0.008	0.220	Yes	No	--
GD/HD	Cen FZ 425-90-120, 80°	8-8-8/8-5-8	15.66	17.17	0.34	0.92	Yes	Yes	3.4	0.885	0.889	0.008	0.026	Yes	No	--
IE/JE	20°	Cen N/P / Hel N/P	24.97	24.45	0.26	0.10	Yes	Yes	1.0	0.844	0.863	0.058	0.116	Yes	Yes	0.73
JE/KE	20°	Hel N/P / Hof N/P	24.45	22.19	0.10	0.27	Yes	Yes	8.5	0.863	0.833	0.116	0.244	Yes	Yes	2.1

Note: Refer to Appendix D for explanation of δ. $\%\delta = \frac{2\delta}{\bar{x}_1 - \bar{x}_2} \cdot 100$.

5.3 MAXIMUM POWER VS TIME

5.3.1 Regression Curves

Figures 5-1 through 5-9 present maximum power data (corrected to normal incidence) as a function of time. Each figure represents a particular cell type and presents the data for that type at all temperatures at which it was irradiated. The curves are hand-fitted to pass through each data point. The data points are not shown for the sake of avoiding a cluttered appearance. Individual data points are provided, however, in Appendix C.

Initial (before irradiation) data for each cell group are presented along the ordinate. Referring to Figures 5-1, 5-2, and 5-3, it is interesting to note the small amount of degradation in the +50 and +80°C groups for cell type A (Hel Cruc 425-90-60) as compared to the +80°C data for types B (Cen Cruc 425-90-60) and C (Cen Cruc 450-20-0).

In Figures 5-4, 5-5, 5-6, and 5-7, note the small amount of degradation of the +20°, +50°, and +80°C groups for cell types E (Hel FZ 425-90-120), G (Cen FZ Boron 1), and H (Cen FZ Boron 2) compared to cell type F (Hel FZ 350-90-60). Particular note should be taken of the +20°C data of type E (Hel FZ 425-90-120) compared to type A (Hel Cruc 425-90-60). It is seen that the float zone cell appears to degrade less on a relative basis than does the crucible cell.

5.3.2 Correlation Analysis

An analysis of the correlation characteristics was performed on the data for two cell groups. These groups were selected as a typically good (low scatter) cell type and a typically poor (high scatter) type.

The "bow-tie" formula for confidence limit calculation was applied to these data, resulting in the limits shown in Figure 5-10 by the lines on either side of the least squares fitted curves. As seen in the figure, confidence in the combined data is significantly increased over that for individual points because of the relationship with adjacent data points.

Correlation coefficients were calculated for each group shown in Figure 5-10. These coefficients were 0.985 for group IE and 0.943 for group GB. From these calculations, it

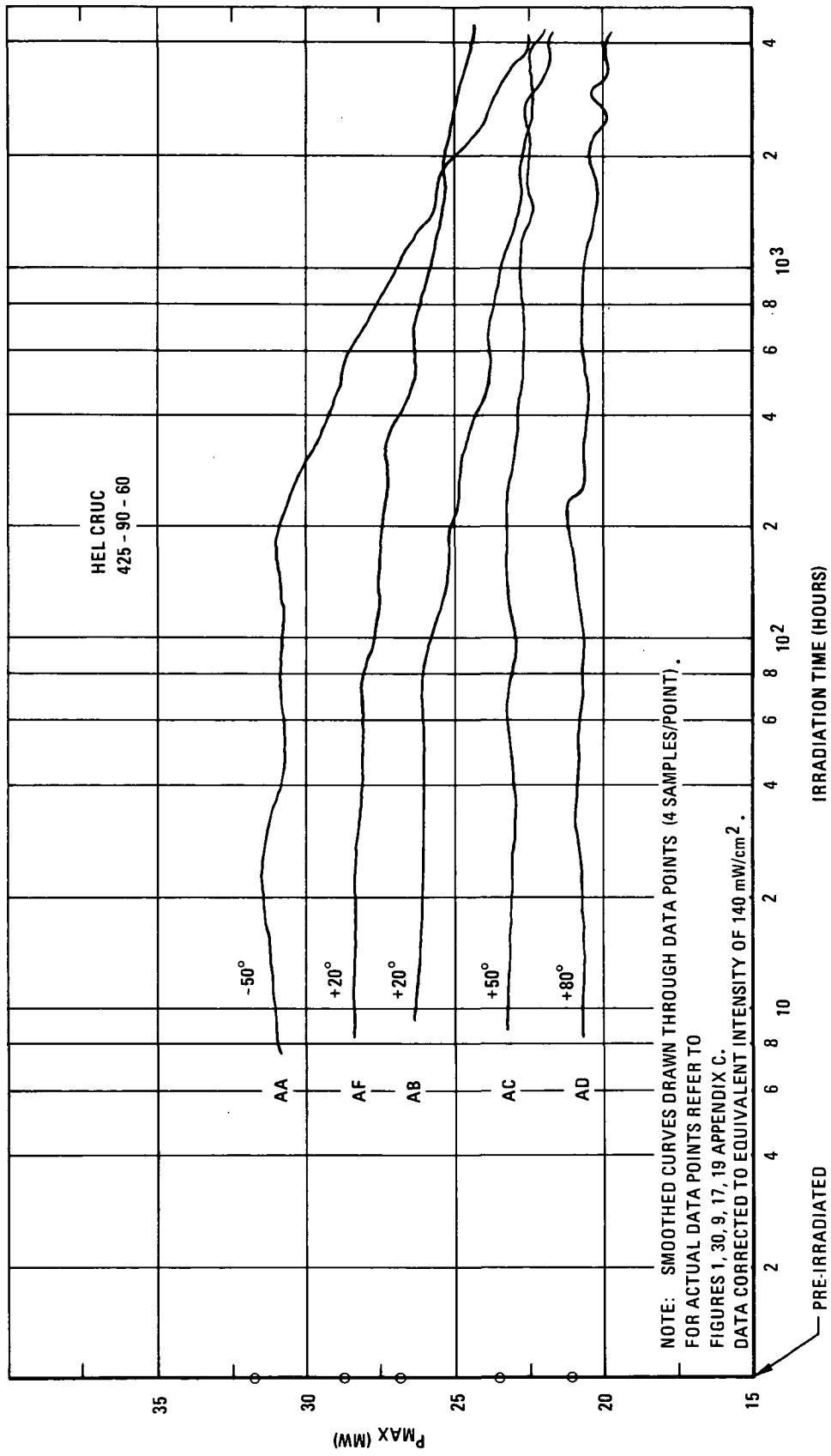

Figure 5-1 Heliotek Crucible Cell Comparisons at -50°, +20°, +50°, and +80°C

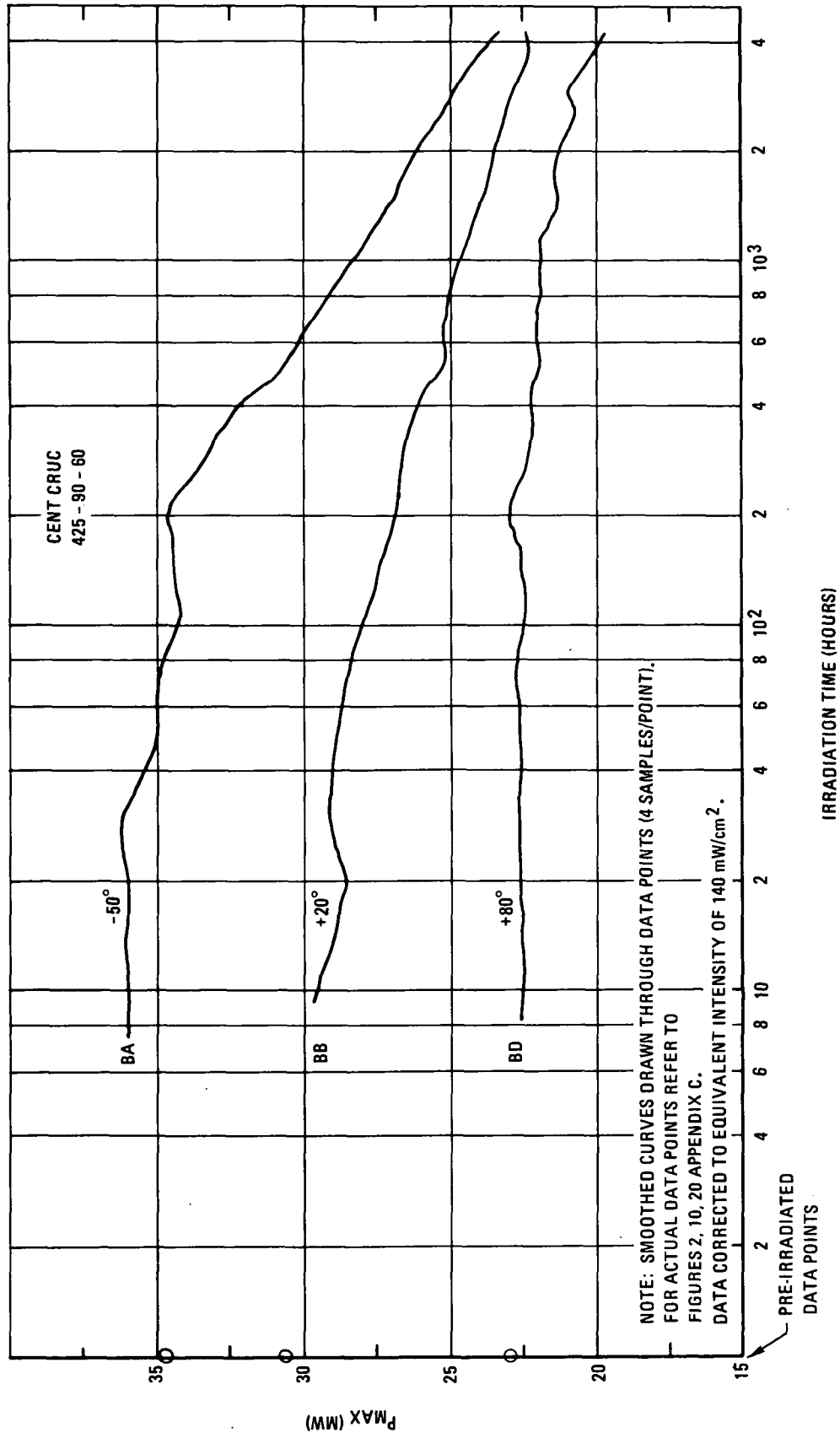

Figure 5-2 Centralab Crucible Cell Comparisons at -50°, +20°, and +80°C

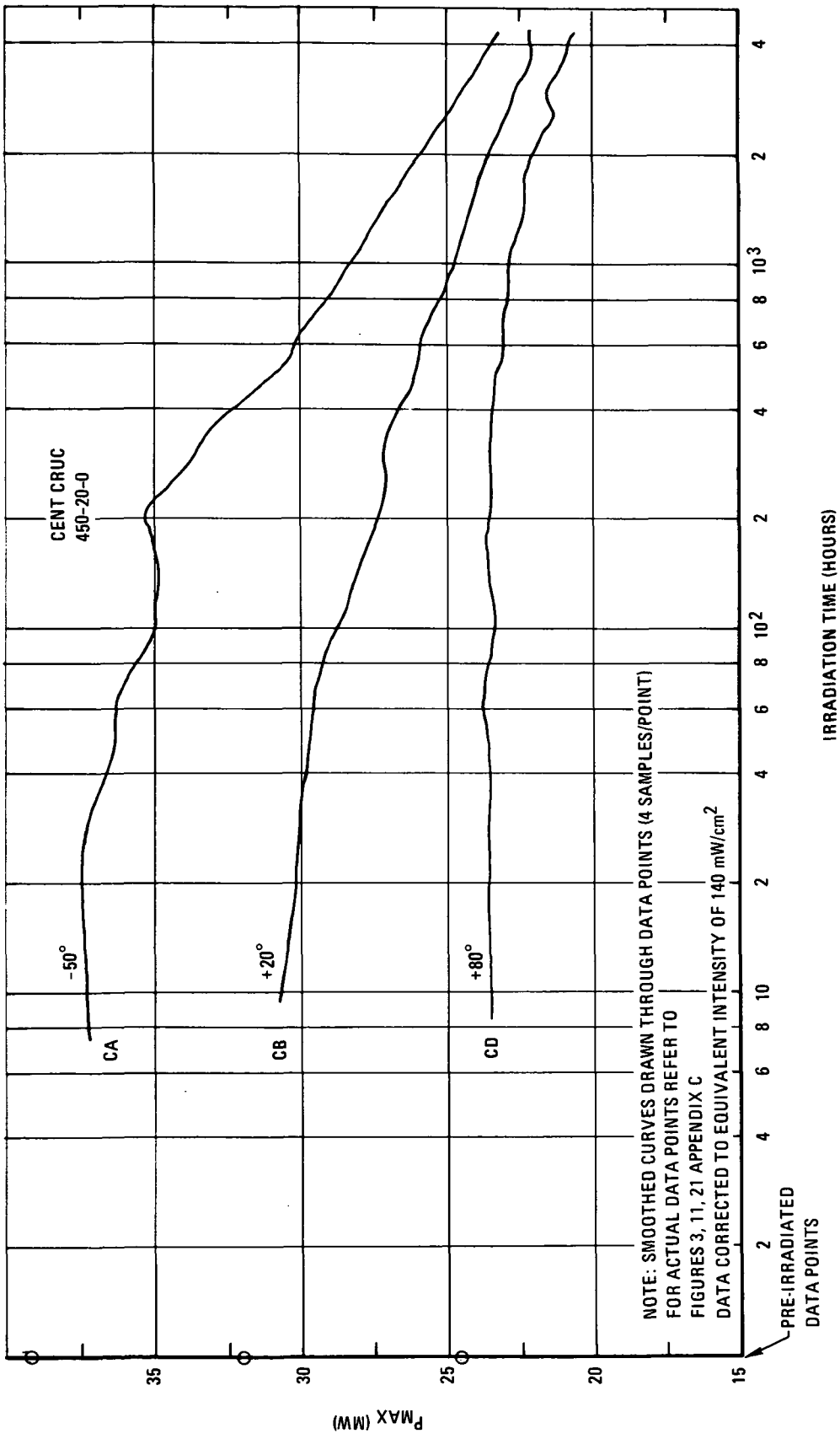

Figure 5-3 Centralab Crucible Cell Comparisons at -50°, +20°, and +80°C

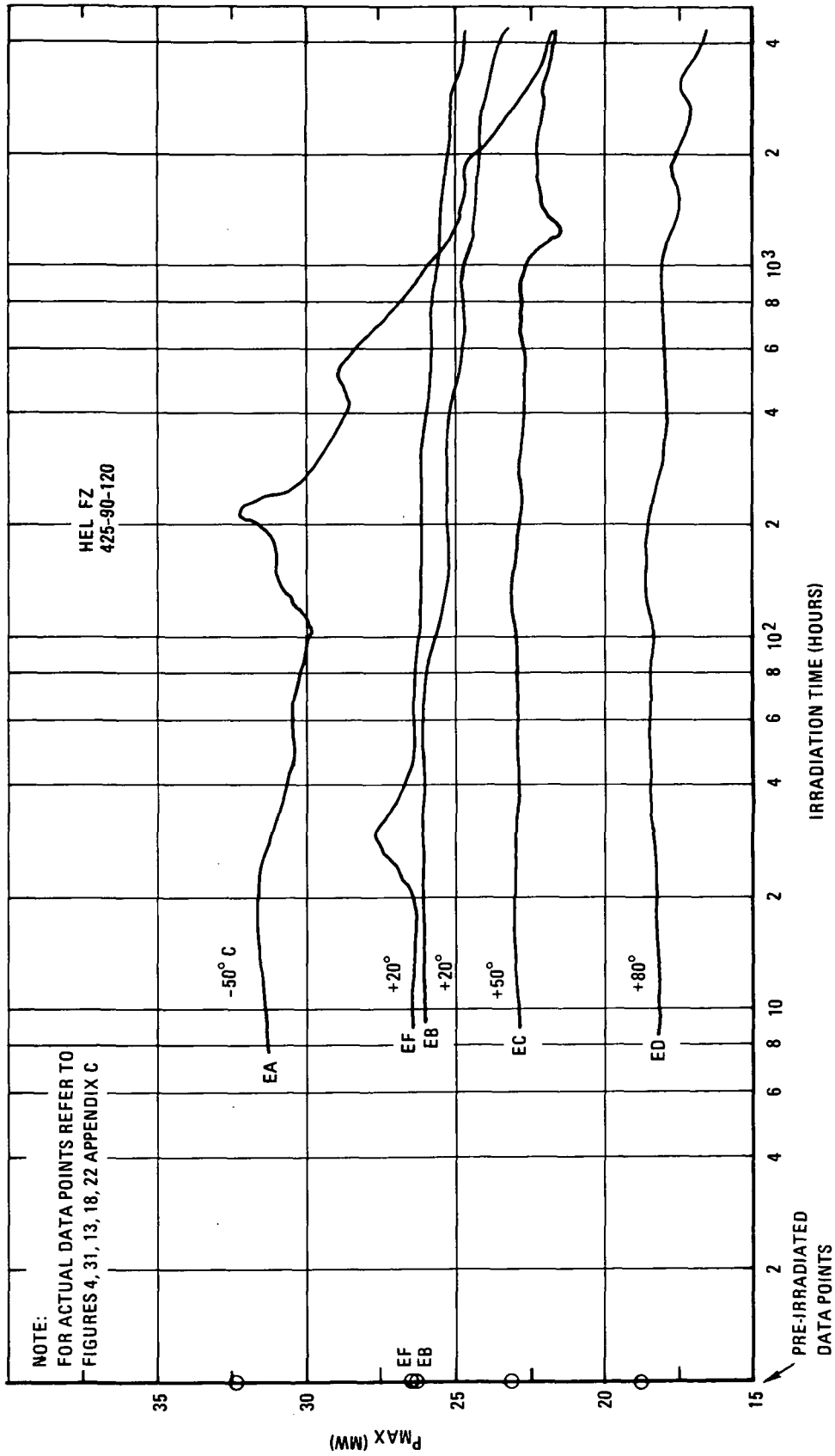

Figure 5-4 Heliotek Float Zone Cell Comparisons at -50°, +20°, +50°, and +80°C

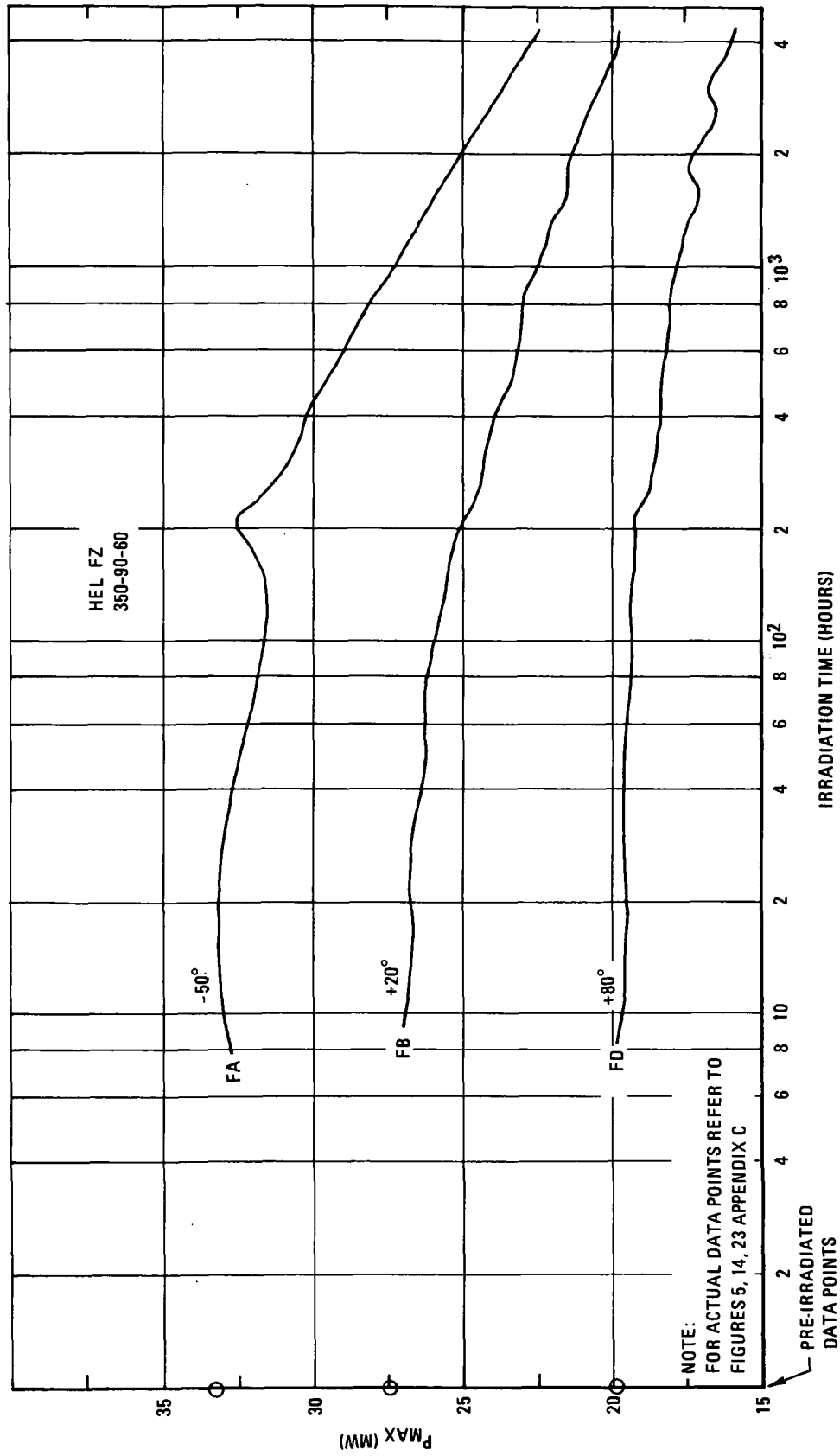

Figure 5-5 Heliotek Float Zone Cell Comparisons at -50°, +20°, and +80°C

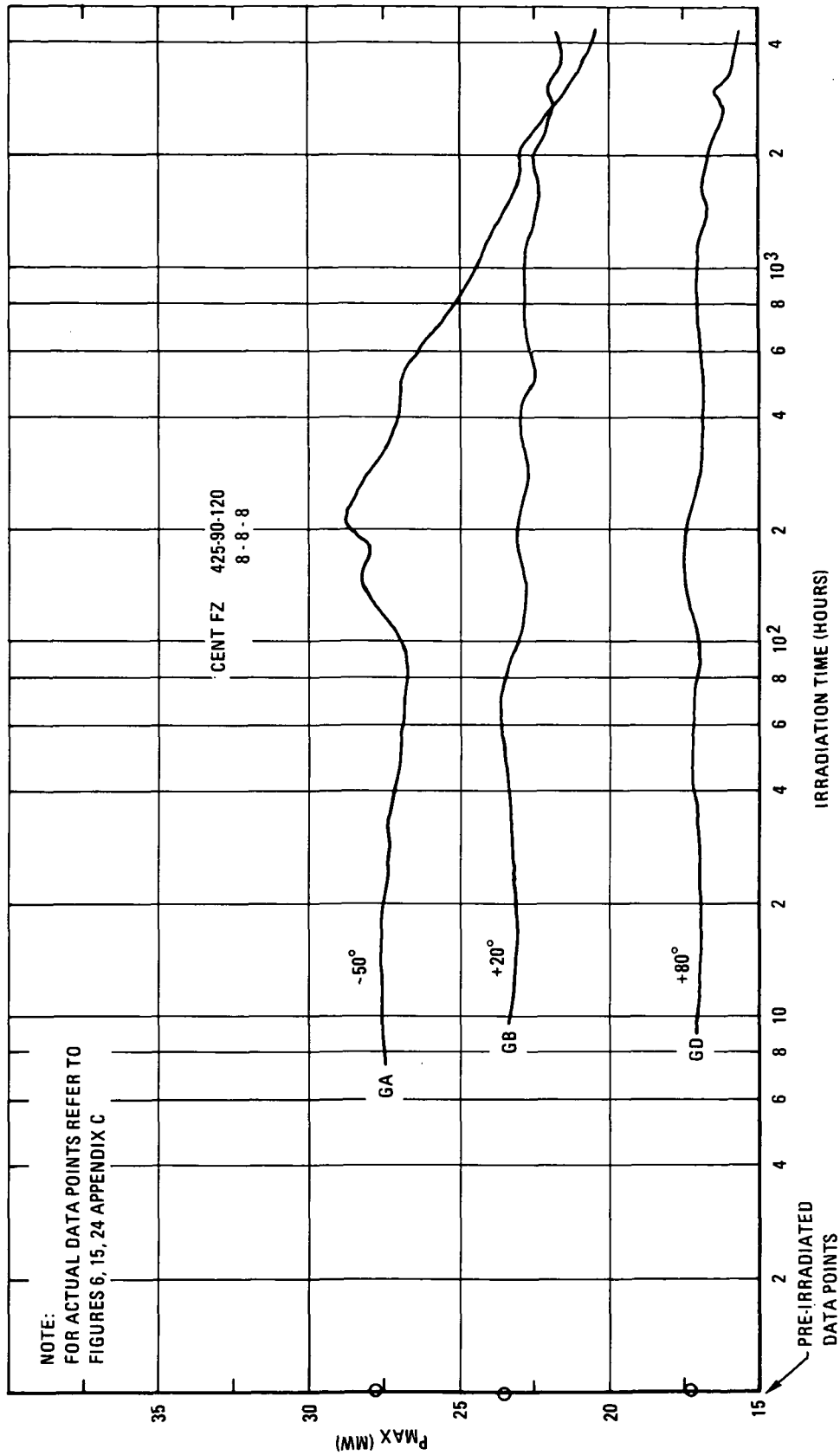

Figure 5-6 Centralab Float Zone Cell Comparisons at -50° and +80°C

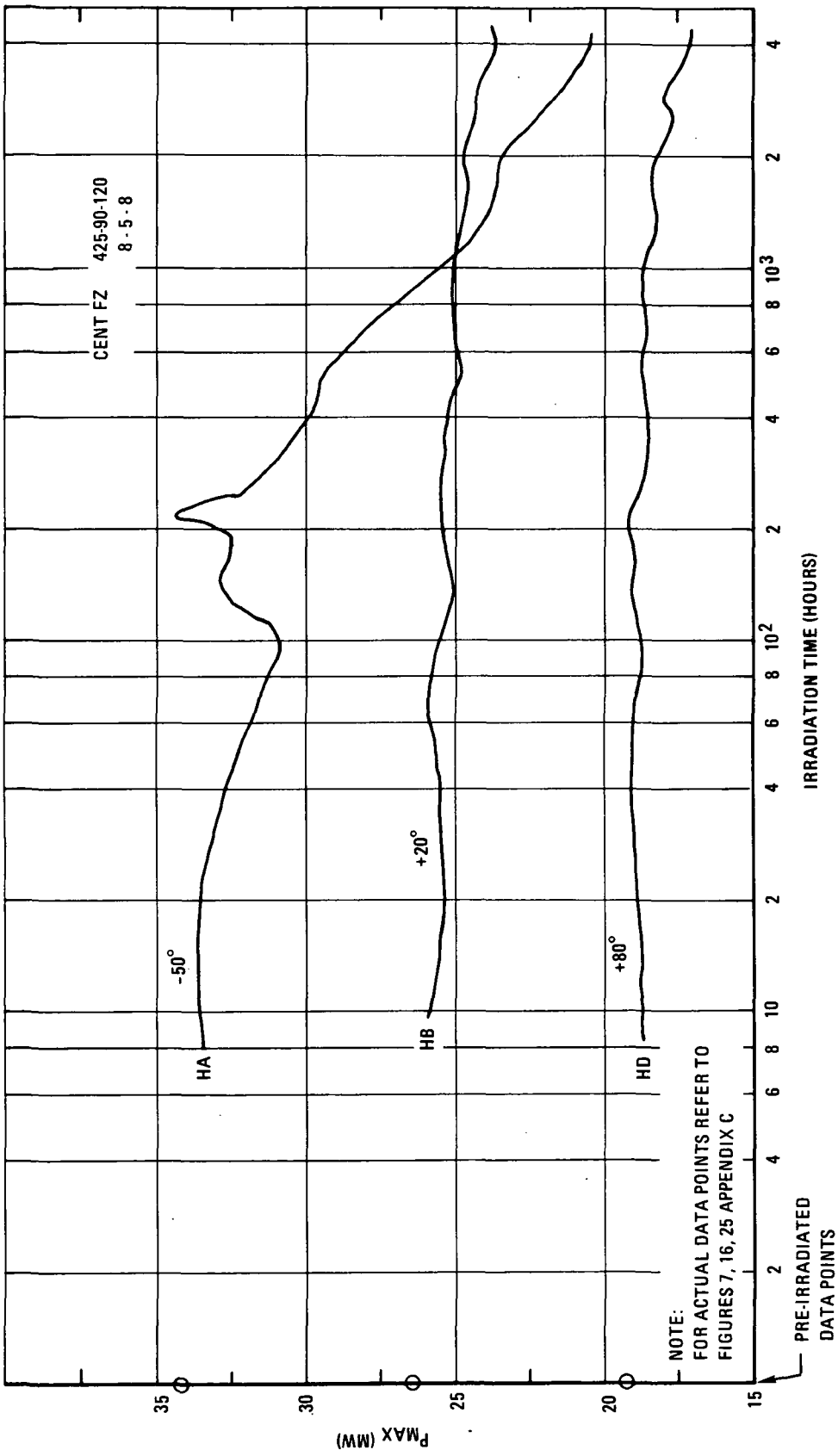

Figure 5-7 Centralab Float Zone Cell Comparisons at -50°, +20°, and 80°C

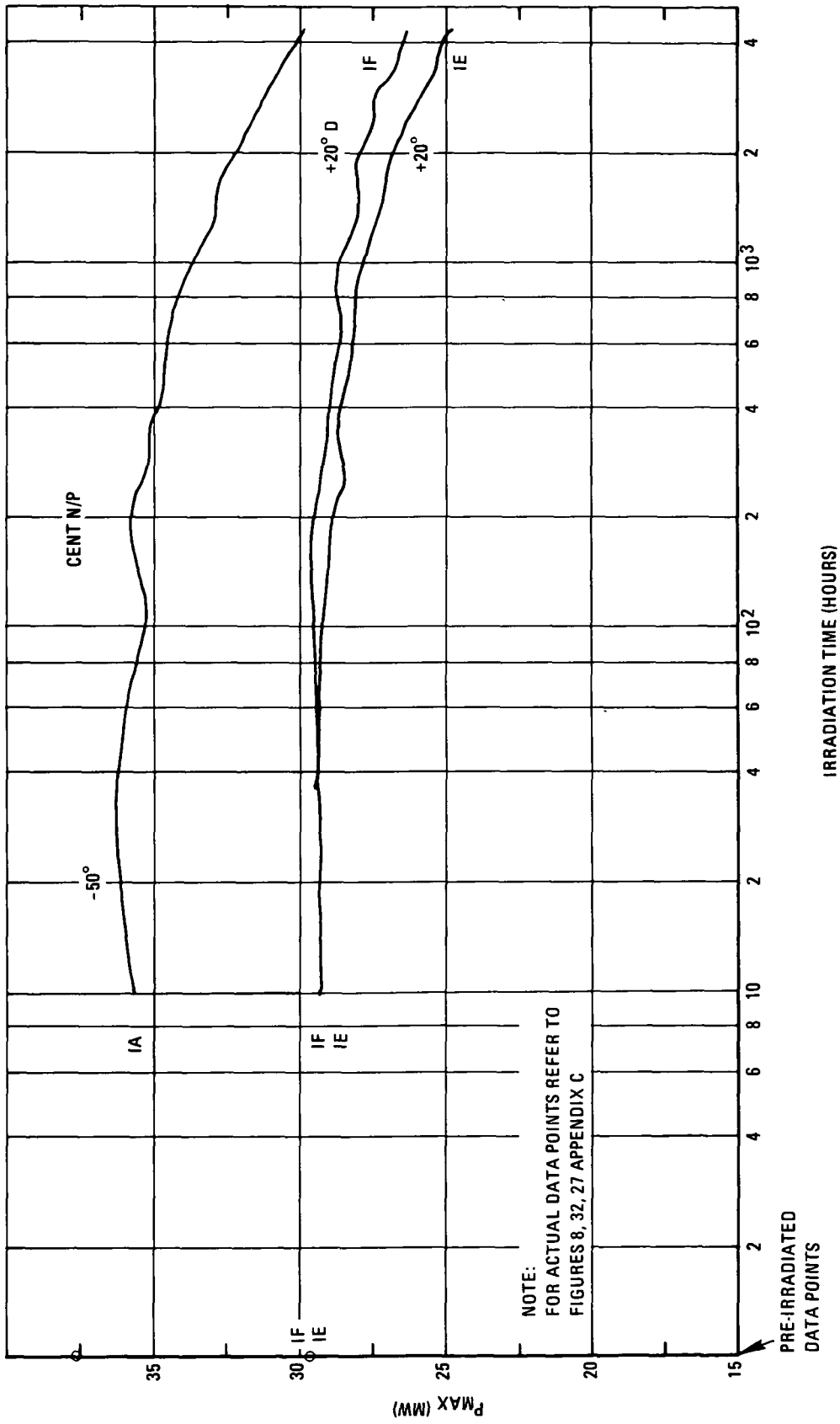

Figure 5-8 Centralab N/P Cell Comparisons at -50° and +20°C

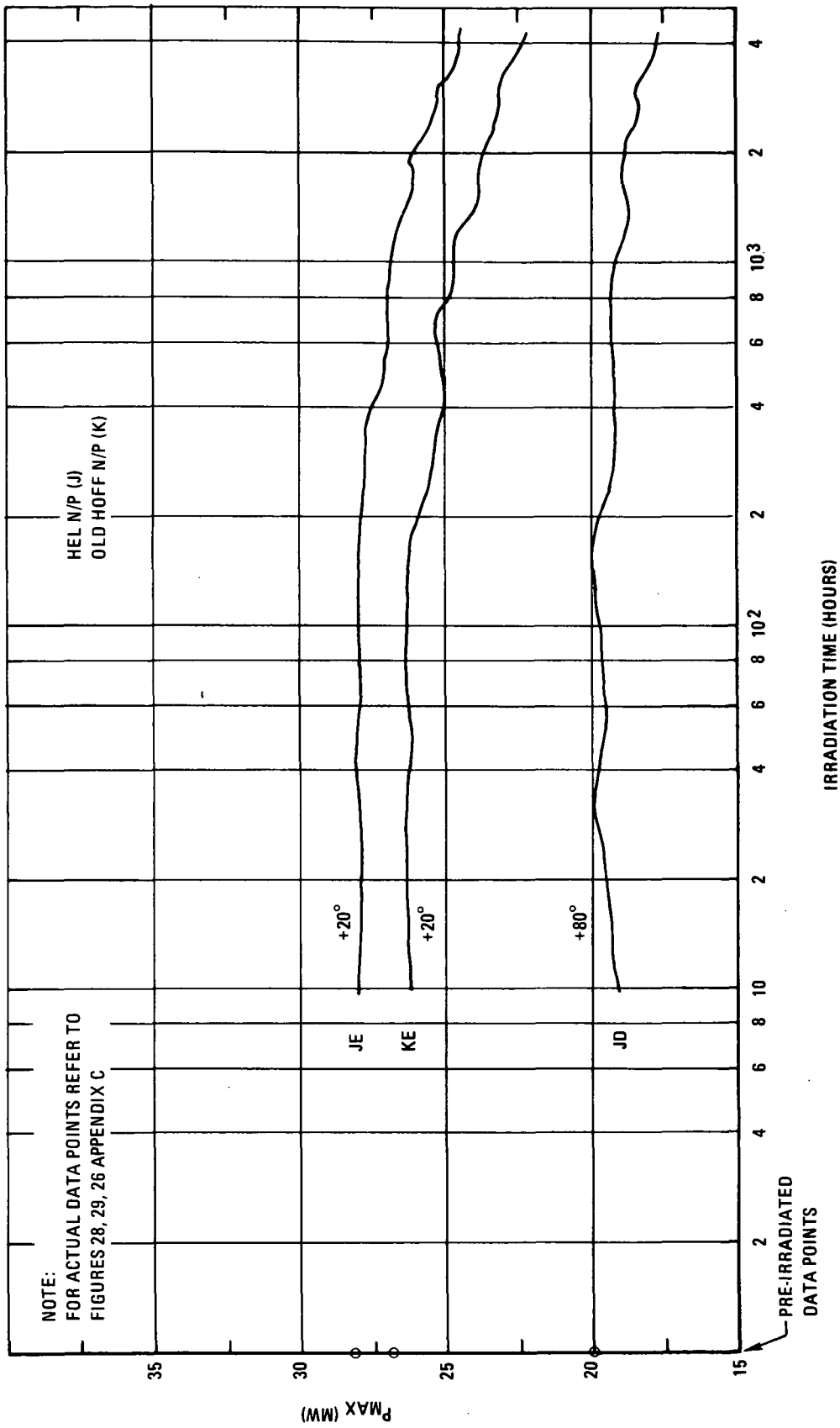

Figure 5-9 Heliotek and Hoffman N/P Cell Comparisons at +20° and +80°C

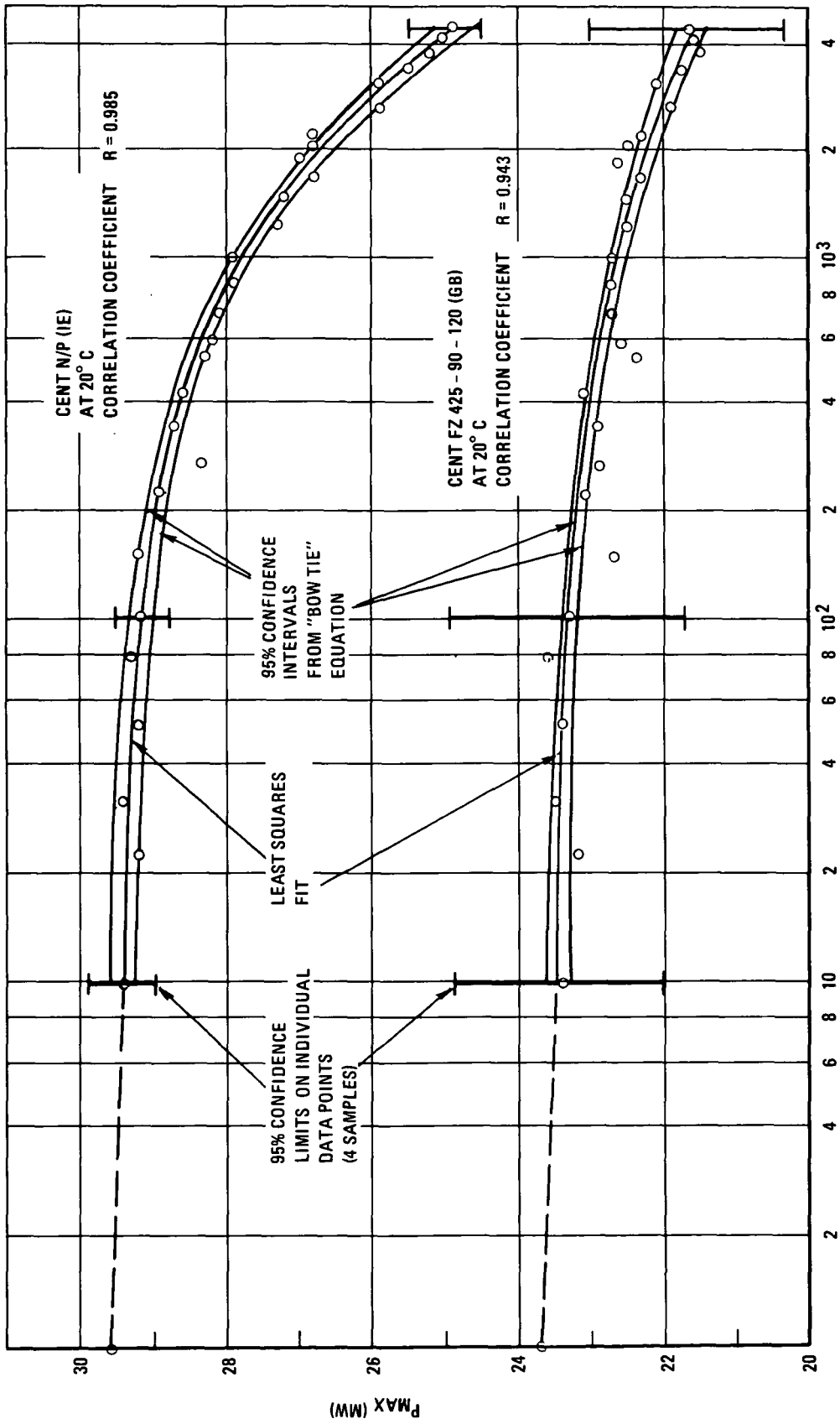

Figure 5-10 Correlation Characteristics for the Centralab N/P (IE) Cell and the Centralab Float Zone (GB) Cell

is concluded that the data scatter shown has little effect on the significance of the final fitted curve results because of the high number of data points taken (30 points through the course of the irradiation, four samples per group).

5.4 POST-IRRADIATION DATA

The cells were maintained at their irradiation temperature (and in vacuum) for a period of some 300 hours after the radioisotope source was removed from the chamber. Data were taken at three times during this period (45, 145, and 315 hours). Data for the 315-hour period are summarized in Table 5-3.

Analysis of these data showed little or no significant annealing trends except for the crucible cells at +20°C. It is thus felt that at these temperatures cell annealing was keeping pace with cell damage. It can be therefore argued that more lithium atoms were available for annealing reactions than were necessary. The effect of excess lithium atom availability on net degradation rate is not yet clearly understood. One cannot therefore conclude that these particular cell types were "optimized" for this environment, only that the particular combination of temperature and lithium atom availability appeared stable at the 6-month fluence.

It is interesting to compare the post-irradiation annealing characteristics of these cells with those of the 1967 cells irradiated in the earlier contractual effort performed for GSFC. Such a typical comparison is presented in Figure 5-11. The 1967 cells exhibit considerably higher post-irradiation recovery. It is thus concluded that the 1967 cells had insufficient lithium to permit annealing at the same rate as damage was being introduced. At the same flux ($\sim 10^{12}$ 1-MeV electrons/cm^2/day), however, the 1970 cells exhibit little or no further recovery, thus confirming lithium adequacy.

5.5 CELL COMPARISON DATA

In order to permit direct comparisons to be made, the maximum power degradation curves presented in Section 5.3 have been grouped together in Figures 5-12 through 5-15. These curves were hand-fitted so as to pass through all data point means.

TABLE 5-3

POST-IRRADIATION RECOVERY DATA

Cell Code	Cell Type	Irradiation Temperature (°C)	P_{max} % Recovery after 315 hr
AA	Hel Cruc	-50	0
AB	425-90-60	+20	+2.5
AC		+50	0
AD		+80	+0.5
AF		+20 Dark	+3.0
BA	Cen Cruc	-50	+1.0
BB	425-90-60	+20	+1.5
BD		+80	0
CA	Cen Cruc	-50	+2.0
CB	425-20-0	+20	+0.5
CD		+80	+0.5
DB	Type A, 1-mil cover	+20	+3.0
EA	Hel Float Zone	-50	+2.5
EB	425-90-120	+20	+0.5
EC		+50	-1.5
ED		+80	+0.5
EF		+20 Dark	+0.5
FA	Hel Float Zone	-50	+0.5
FB	350-90-60	+20	0
FD		+80	+1.5
GA	Cen Float Zone	-50	-3.0
GB	Boron 1	+20	0
GD		+80	0
HA	Cen Float Zone	-50	+3.5
HB	Boron 2	+20	0
HD		+80	0
IA	Cen 10 Ω-cm	-50	-1.5
IE	N/P	+20	-1.5
IF		+20 Dark	+0.5
JD	Hel 10 Ω-cm	+80	0
JE	N/P	+20	0
KE	Hof 10 Ω-cm N/P	+20	+0.5

Note: During post-irradiation period, cells were held at irradiation temperatures.

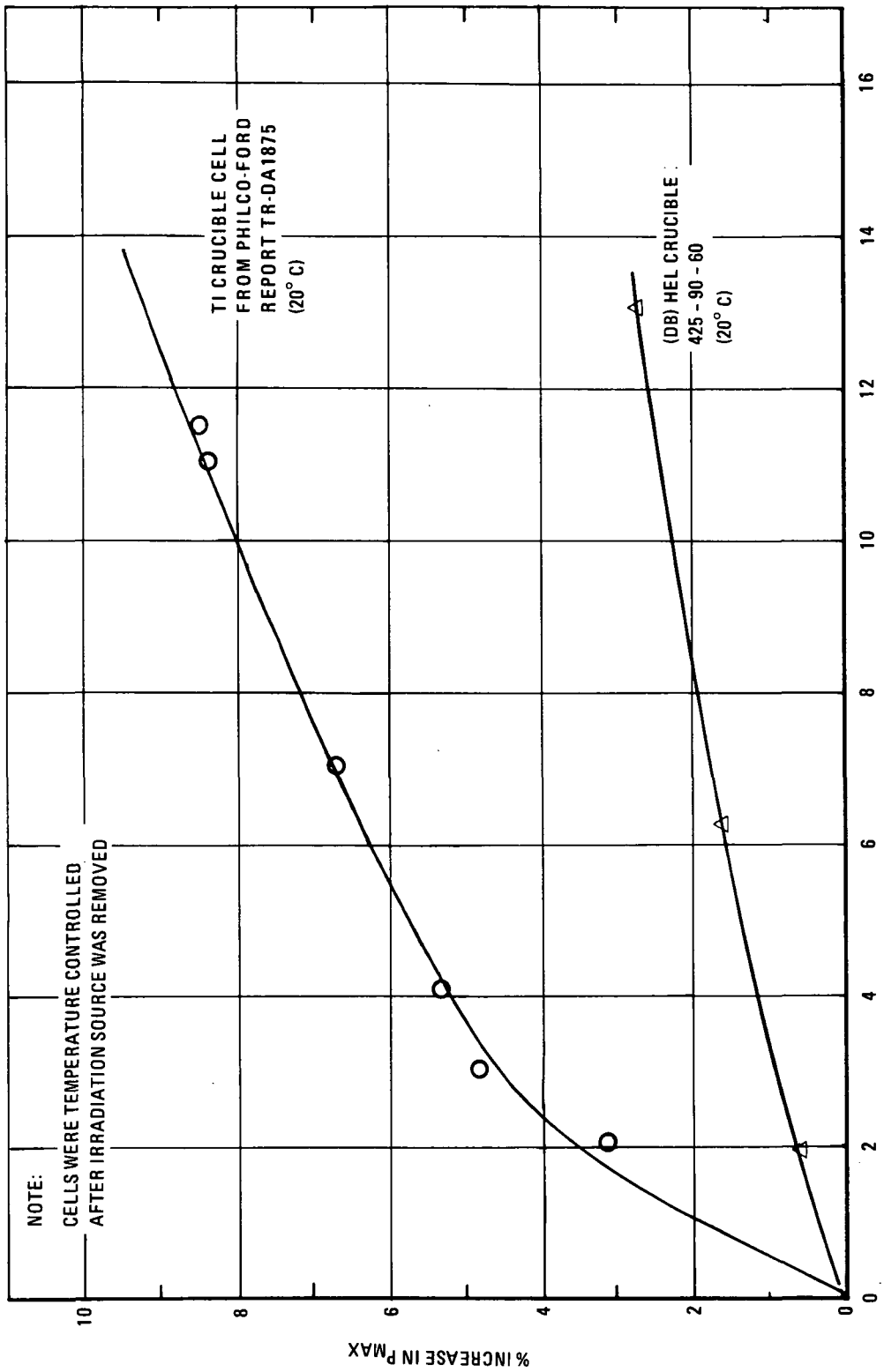

Figure 5-11 Comparison of Recovery Phenomena between Old (1967) and Present Day Lithium Solar Cells

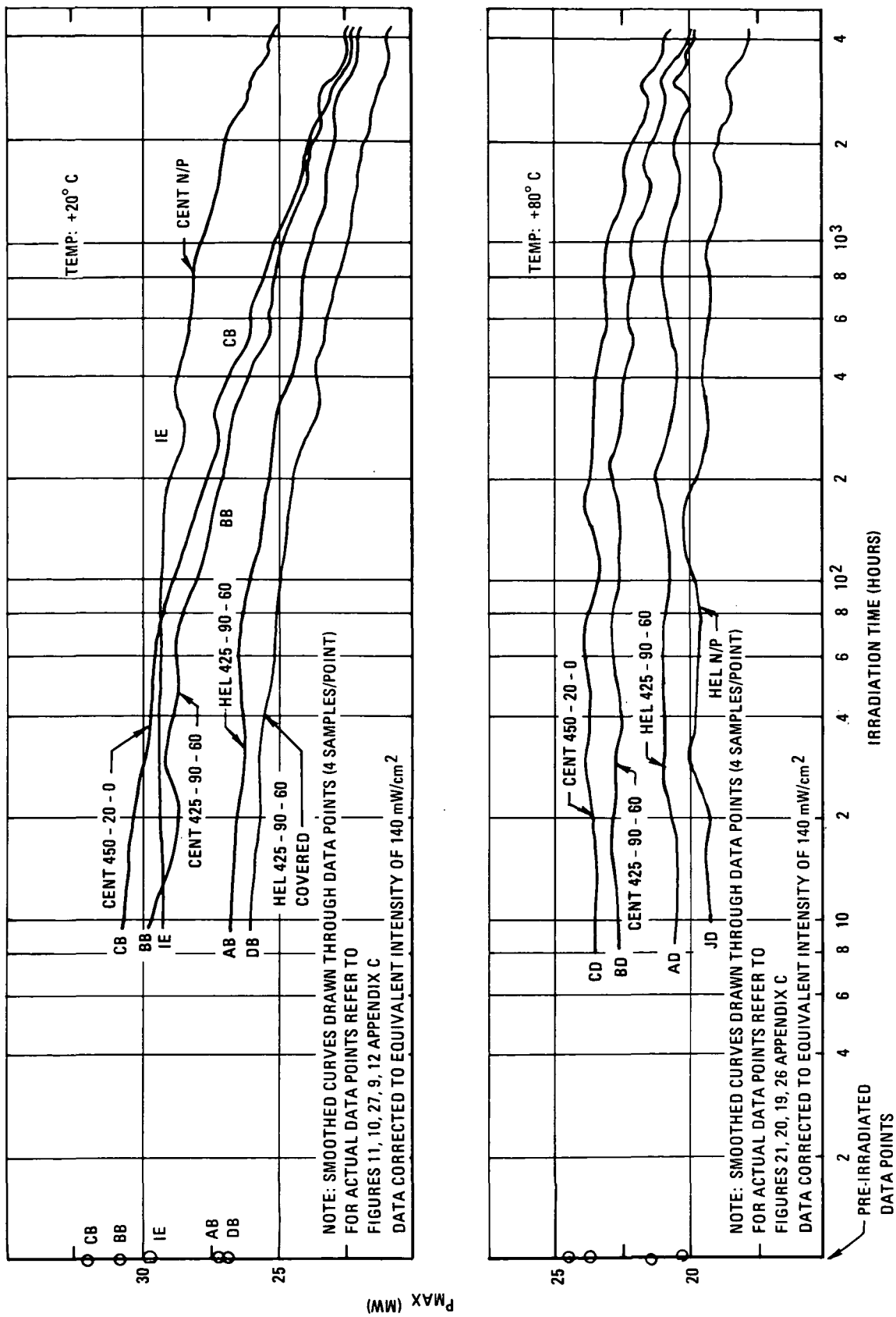

Figure 5-12 Crucible Cell Comparisons at +20° and 80°C

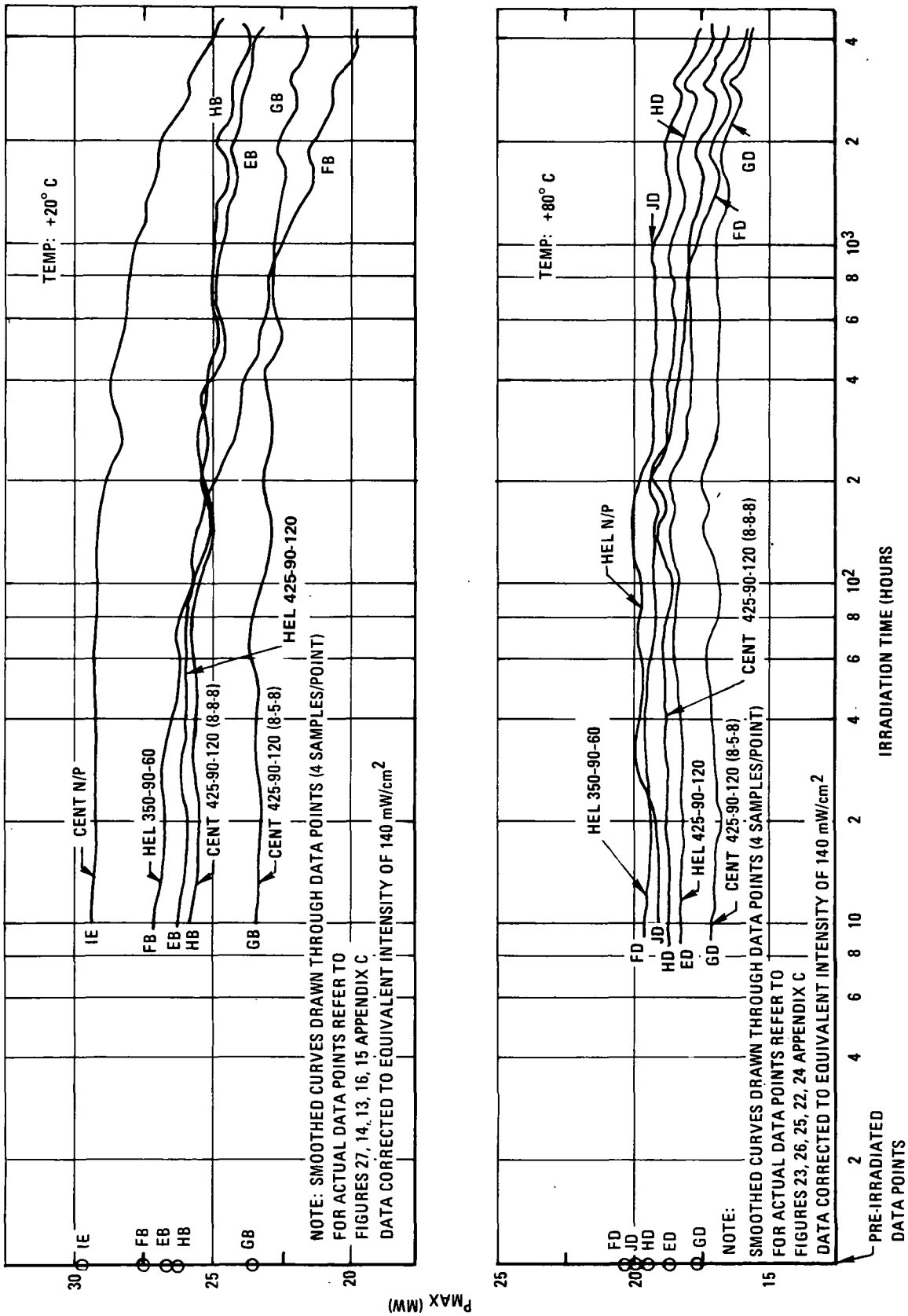

Figure 5-13 Float Zone Cell Comparisons at +20° and 80°C

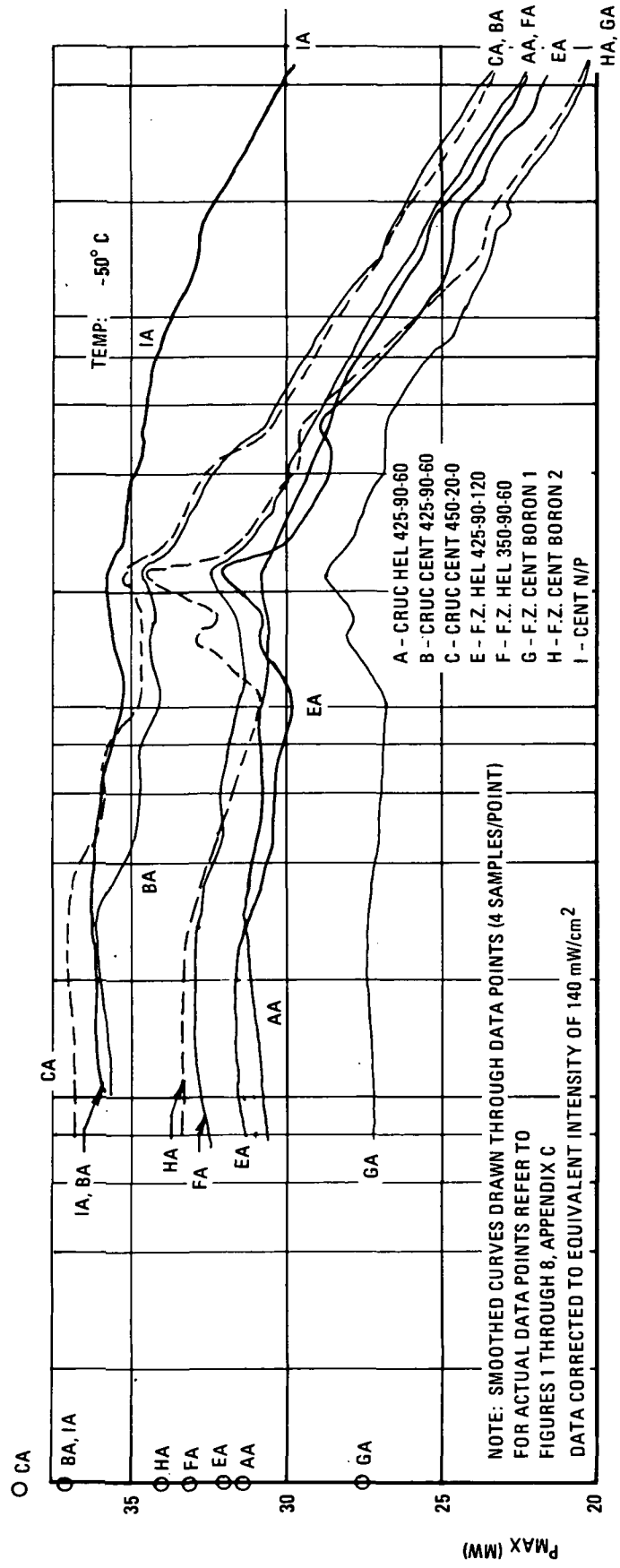

Figure 5-14 N/P, Crucible, Float Zone Comparisons at -50°C and +20°C

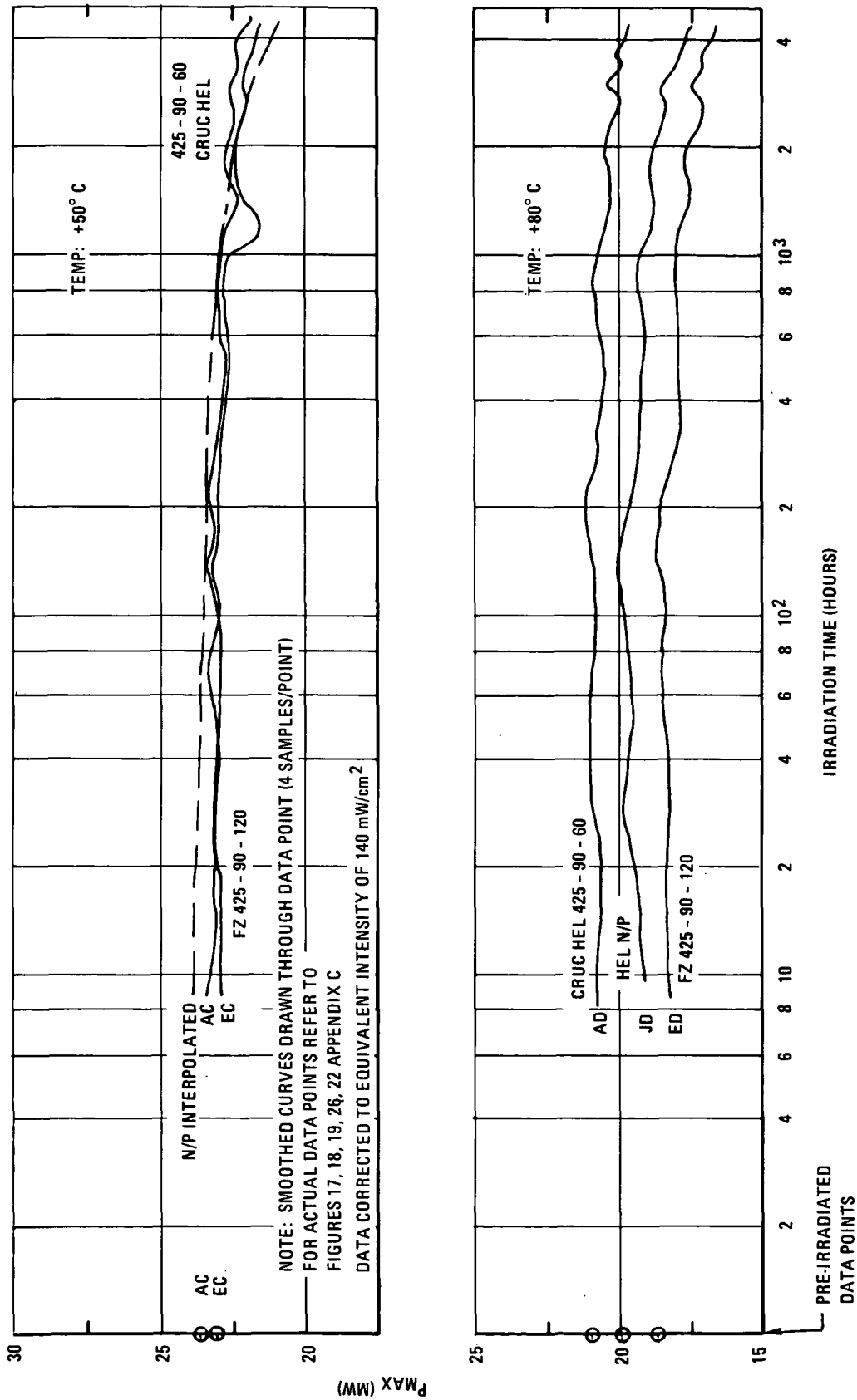

Figure 5-15 N/P, Crucible, Float Zone Cell Comparisons at +50° and 80°C

5.5.1 Crucible Lithium Cells

Figure 5-12 presents the curves for crucible cells separated into +20° and +80°C groups. In the +20°C group, it will be seen that the N/P cell outperforms all crucible lithium cells after 100 hours of irradiation. Note also that the three crucible types (CB, BB, AB), despite widely varying initial values (27.0 to 31.8 mW), converge toward a common value for power after 6 months irradiation (22.1 ± 0.2 mW).

The effect of a 1-mil integral cover can also be noted in these data. Cell type DB is identical with type AB (Hel Cruc 425-90-60) except that a 1-mil integral cover was applied to DB cells. The apparent effect of the covering was a slight (~2%) reduction of initial maximum power and no significant difference in degradation rate. It thus appears that the presence of an integral cover in no way influences the cell degradation characteristics. Further, it appears that this cover material (Corning 1720 aluminosilicate glass) suffered little or no noticeable darkening from the irradiation.

At 80°C, the relative performance of N/P and crucible lithium cells is quite different from that at +20°C. The lithium cells clearly outperform the N/P cells, primarily as a result of a higher initial maximum power. As noted earlier, this effect is primarily due to a more favorable temperature coefficient for maximum power for P/N cells. The tendency for the different crucible cells to converge after irradiation is also present at +80°C.

5.5.2 Float Zone Lithium Cells

Float zone lithium cell comparisons are made in Figure 5-13. Here, at +20°C, the lithium cell types demonstrate no convergence tendency and appear to behave quite independently. Type FB (Hel FZ 350-90-60) starts with a high output but degrades much more rapidly than the others. Types EB (Hel FZ 425-90-120), HB (Cen FZ 425-90-120,8-8-8), and GB (Cen FZ 425-90-120,8-5-8) appear to have equivalent relative degradation characteristics. The N/P cell, type IE, has a much higher initial output but appears to be degrading more rapidly than the float zone lithium cells at the 6-month point. Thus, at higher fluences (at +20°C), one might expect a crossover with float zone cells outperforming N/P cells.

At +80°C, the cells appear to be behaving quite similarly to the +20°C case, except for type FD (Hel FZ 350-90-60) which (as at +20°C) degrades at a much more rapid rate. The N/P cell, type JD, again outperforms the lithium cells, although with less margin than at 20°C.

5.5.3 Comparison of Best Cell Types at Various Temperatures

Figures 5-14 and 5-15 present the results of the best crucible and float zone cells compared with N/P cells at each of the irradiation temperatures. Referring to Figure 5-14, at -50°C the lithium cells behave like a standard (nonlithium) P/N cell compared to the N/P cells. The convergence tendency among lithium cells is very apparent at -50°C. The effect of sample warming (due to cooling system temporary failures) is seen, particularly with the float zone samples, as temporary periods of power improvement.

At +20°C (Figure 5-14), it is seen that although the crucible lithium cell (AB) started higher than the float zone cell (EB), it degrades more rapidly. At 6 months, N/P cells still appear superior to the lithium cells. It appears that the N/P and float zone curves are converging, however, and that at some higher fluence (at 2 years or so), a crossover might occur.

At +50°C (Figure 5-15), no N/P data were directly available. A curve was therefore constructed from interpolated data points at various times (assuming a linear P_{max}-temperature relationship over the range of +20° to +80°C). This curve is compared with lithium cell data at +50°C as shown in Figure 5-14. At this temperature, lithium and N/P cells appear roughly equivalent. It appears that lithium cells (of both types) might become superior to the N/P cell at higher fluences.

At +80°C the crucible cell is superior (13% higher P_{max}) to both N/P and float zone lithium cells. This superiority appears to be increasing at 6 months irradiation and presumably would continue increasing at higher fluences.

5.6 EFFECT OF ILLUMINATION

Cells of three types, crucible lithium (type A), float zone lithium (E), and N/P (I), were irradiated under two different sets of illumination/loading conditions. One group of each type was illuminated to a one-sun equivalent during the irradiation period and was loaded near the maximum power point. Another group of each type was shadowed by a movable foil shield during the irradiation and was left open-circuited. The foil shield was 0.00025-inch-thick aluminized mylar. This material and thickness were chosen so that the light would be reflected but the electron spectrum would pass through essentially unaltered.

The results of this comparative experiment are shown in Figure 5-16. In each case, the cells that were illuminated and loaded degraded more than those that were not illuminated (and left open-circuited). These differences were tested for significance using statistical methods. The results are presented in Table 5-4. The relative degradation data is more appropriate to consider when studying this effect than is absolute power since initial values were not controlled to be equal.

The important conclusion to be drawn from these data is that there is an apparent difference (at the 6% significance level or lower) in degradation experienced under the two conditions. The difference in relative degradation is low for crucible cells (0.3%) but is high enough to be highly significant for float zone and N/P cells. The reason for this apparent difference in degree of response to the effect has not yet been investigated.

As for the effect itself, it is given a high degree of prominence in at least one important reference (Ref. 17). The author suggests that injection level effects are of significance in solar cell degradation experiments and that past experimenters may have been deluding themselves with invalid data because of erroneous irradiation procedures (not properly accounting for injection level effects).

By virtue of the present data, it appears that the effect indeed exists and that it should be somehow accounted for in future experimental efforts and in spacecraft lifetime predictions. Further analysis of these results and continued experimentation with the effect will help to qualify its significance and provide a more sound understanding of its physical basis.

5.7 RELATIVE DEGRADATION AS A FUNCTION OF TEMPERATURE

In order to assess and compare the degradation characteristics of the various cell types over the range of irradiation temperatures, a plot of relative maximum power as a function of temperature was prepared and is presented in Figure 5-17. The plots presented are not really fitted curves, but are line-connected data points. Despite the inadequacy of temperature points, the information contained in this figure is of some importance in evaluating comparative degradation characteristics.

The relative maximum power characteristics of the N/P cells appear to be linear with temperature as shown in Figure 5-17. It is of great interest to note that the float zone cells (E, G, and H) appear to somewhat peak in relative performance at +20°C, falling off

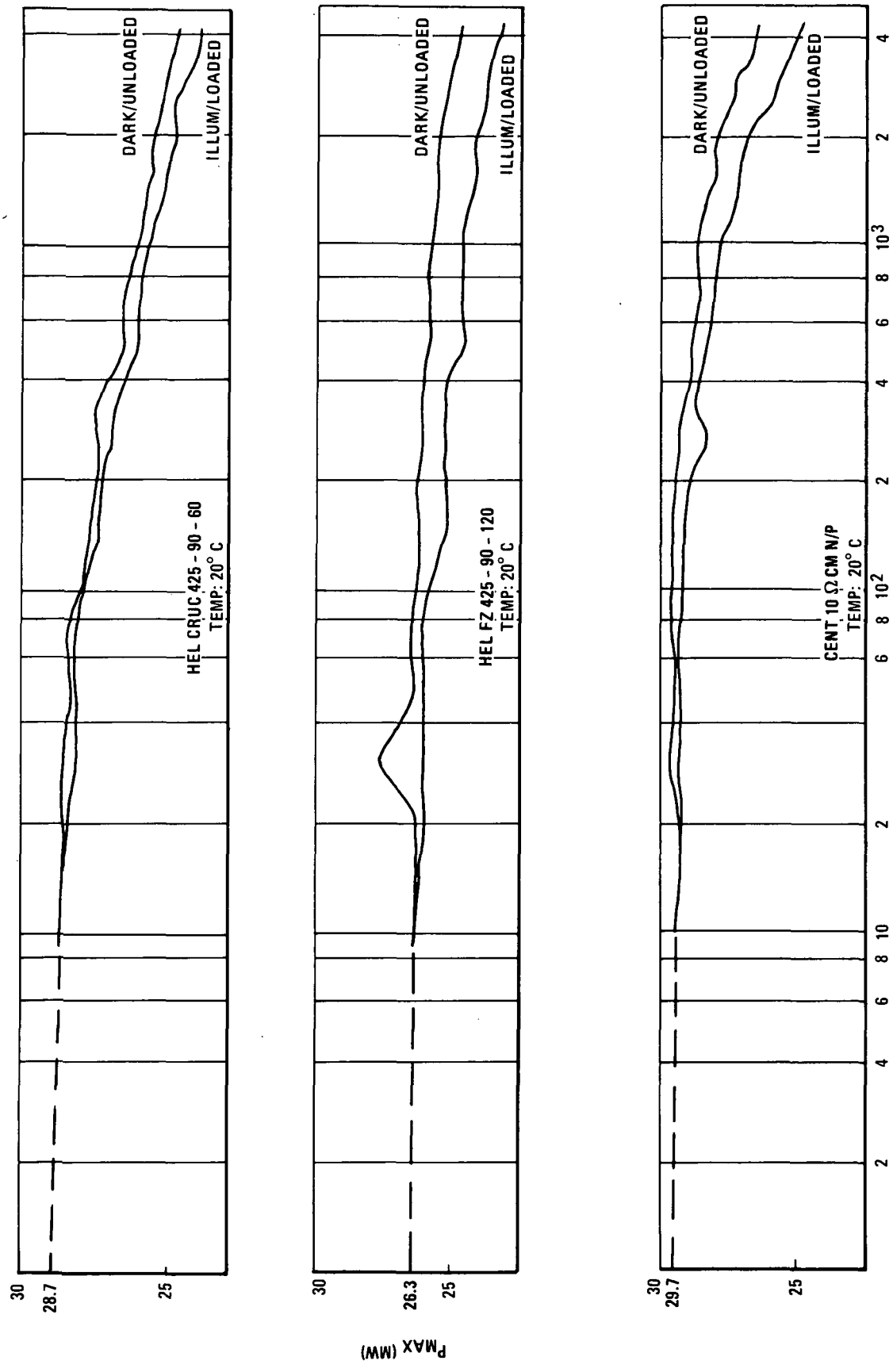

Figure 5-16 Effect of Illumination Loading

TABLE 5-4

RESULTS OF STATISTICAL ANALYSIS OF
DARK/OPEN VS ILLUMINATED/LOADED CELLS

Comparison	Degradation	Test for Difference ($\delta = 0$)		Magnitude of Difference at 2.5% Significance Level (% δ)
		Level (α)	$\bar{x}_1 \neq \bar{x}_2$	
AB-AF Crucible Lithium Cells	Absolute	<0.005	Yes	7.6
	Relative	0.06	Yes	0.3
EB-EF Float Zone Lithium Cells	Absolute	0.015	Yes	1.7
	Relative	<0.005	Yes	3.8
IE-IF N/P Cells	Absolute	0.006	Yes	1.7
	Relative	<0.005	Yes	4.3

Note: Refer to Appendix D for explanation of $\delta \cdot \%\ \delta = \frac{2\delta}{\bar{x}_1 - \bar{x}_2} \cdot 100.$

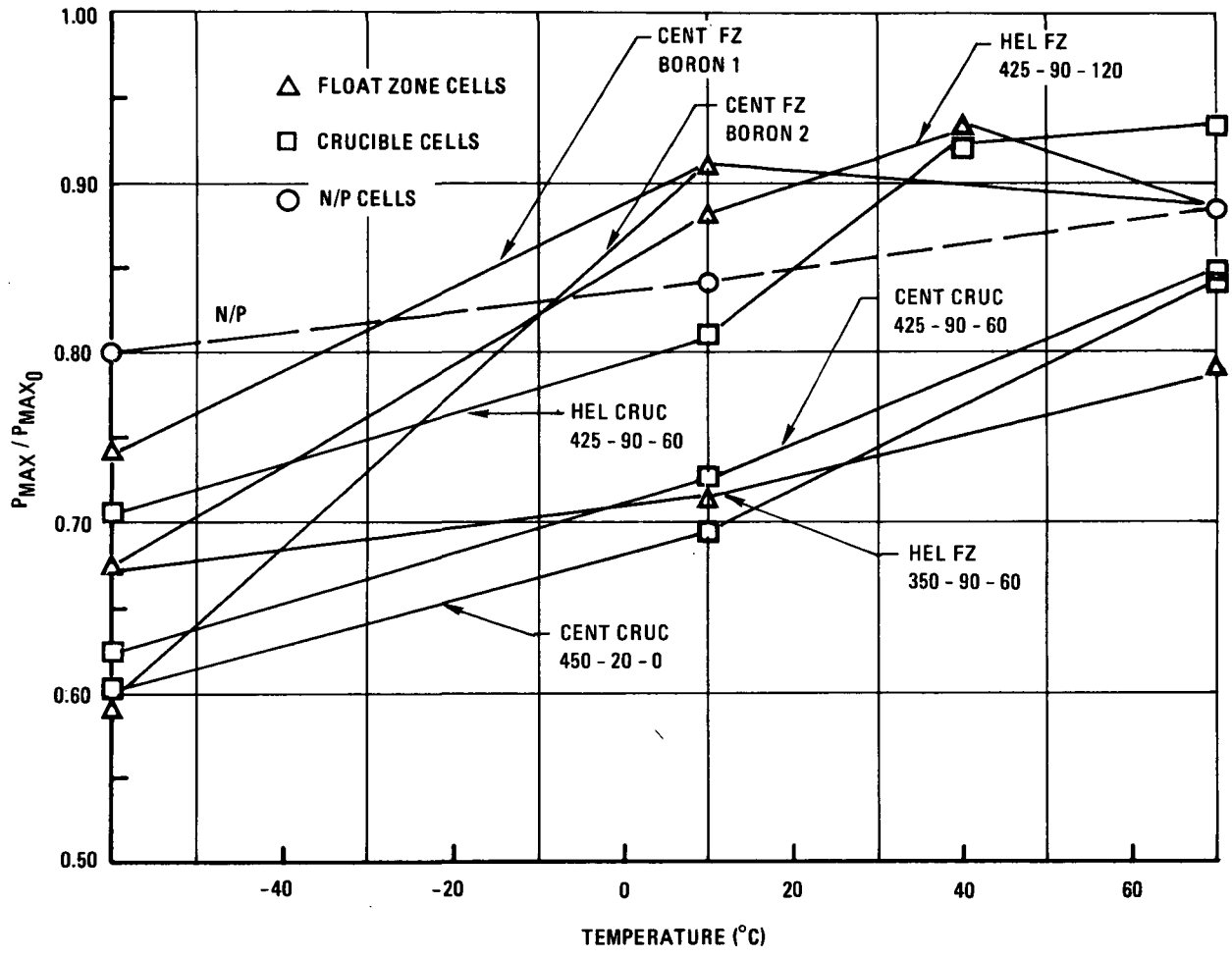

Figure 5-17 Relative Maximum Power as a Function of Irradiation Temperature

somewhat at higher temperatures. On the other hand, the crucible cells (A, B, and C) perform poorly at +20°C relative to N/P cells and type A improves at 80°C.

It is also interested to note the somewhat anomalous behavior of cell types A and F. Type A (Hel Cruc 425-90-60) clearly outperforms the other crucible cell types at all temperatures. Type F (Hel FZ 350-90-60) performs very poorly relative to the other cells at all temperatures except -50°C.

These data seem to suggest that if one were selecting a cell type to be further developed for a +20°C mission, he might select a float zone such as type G or H. On the other hand, a crucible cell (presumably a lower cost cell) would be appropriate, if not superior, for +50° or +80°C. At any rate, it appears clear that operating temperature would be of great importance in selecting a particular lithium cell type for a particular mission. This principle becomes more complex when one considers that all spacecraft solar cell array temperatures vary in some cyclic fashion, due either to eclipse shadowing effects or to other heat transfer characteristics. It appears that a considerable amount of additional experimental effort would be required to develop effective design optimization criteria for lithium cells because of the observed sensitivity of net degradation as a function of temperature.

5.8 STORAGE CELL DATA

Samples of each cell type, as available from the original groups of cells delivered to Philco-Ford, were stored in vacuum at +20° and +80°C for the duration of the 6-month irradiation. The I-V characteristics of these cells were measured 3 months after storage and again after 7 months. There was little apparent difference in cell characteristics measured at the two times. The 7-month storage data are presented in Table 5-5.

The data presented in the table have not been subjected to statistical significance testing, and therefore it is not possible to comment on their significance. It will be noted, however, that the +20°C storage data indicate a relatively small change with apparent consistency in the positive direction. The cells at +80°C indicate a tendency toward a greater increase during storage than those at +20°C.

It is difficult to assess the impact of the cell storage data on an interpretation of the irradiation results. The only pertinent observation appears to be that of short-circuit current and open-circuit voltage improvement of the float zone cells during storage. One could assume that the same relative effect occurred within the 80°C cells being irradiated. It can

therefore be argued that the effect (performance increasing approximately 4% in float zone cells) would be significant in interpreting the 6-month irradiation data.

TABLE 5-5

STORAGE CELL DATA
(7 Months Storage)

Cell Type	+20°C Storage			+80°C Storage		
	Number of Cells	I_{sc} % Change	V_{oc} % Change	Number of Cells	I_{sc} % Change	V_{oc} % Change
A Crucible Hel 425-90-60	4	+1.21	+0.45	4	+1.09	+1.54
B Crucible Cen 425-90-60	4	+0.52	+0.29	0	-	-
C Crucible Cen 425-20-0	4	+0.47	+0.89	4	+2.27	+1.45
D Crucible Hel (Int. Cover)	4	+0.98	+0.17	4	+1.87	+0.88
E FZ Hel 425-90-120	4	+1.43	+1.15	4	+2.83	+5.67
F FZ Hel 350-90-60	4	+2.17	+1.18	4	+4.10	+3.24
G FZ Cen 425-90-120(8-8-8)	4	+1.57	+1.18	3	+0.76	+4.54
H FZ Cen 425-90-120(8-5-8)	4	+2.66	+0.92	0	-	-
I Cen 10 Ω-cm N/P	4	+0.58	+0.05	4	+0.42	+0.23
J Hel 10 Ω-cm N/P	2	-0.53	0	0	-	-
K Hof 10 Ω-cm N/P	4	+1.12	0	0	-	-

Note: 1) "425-90-60", etc refers to lithium diffusion characteristics; eg, 425°C diffusion temperature, 90 minutes diffusion time, and 60 minutes redistribution time.

2) "8-5-8" refers to boron diffusion characteristics; eg, 8 minutes preheat, 5 minutes boron "tack-on", and 8 minutes boron diffusion.

5.9 IMPLIED PROTON/NEUTRON DEGRADATION CHARACTERISTICS

It has been shown in other irradiation efforts (using accelerators with monoenergetic particles) that P/N lithium cells demonstrate greater advantage over conventional N/P cells under proton and/or neutron irradiation (Reference 18). The results of this experiment demonstrate comparable-to-marginally-superior performance of lithium cells as compared to N/P cells. Coupling the results of this irradiation with those of the accelerator irradiations mentioned above indicates that lithium cells will have significantly superior performance when operating in a radiation environment where proton or neutron damage outshadows electron damage.

SECTION 6

CONCLUSIONS AND RECOMMENDATIONS

6.1 CONCLUSIONS

This experimental effort yielded data which are supported by a statistically significant experiment design and by statistical treatment of the data. Under the environmental conditions indicated, the following conclusions are made:

a. The experiment produced conclusive data with sufficiently high quality to significantly increase confidence in evaluating and comparing the various lithium and N/P cell types.

b. In general, the lithium cells tested compared favorably with N/P cells in the electron environment.

c. With a slight improvement in initial characteristics, the use of lithium cells is feasible for 5 to 10 year missions at synchronous altitude.

d. Lithium cells would appear to be clearly superior to N/P cells in proton- or neutron-dominant situations, based on comparative irradiation data and subsequent interpretation of the results presented in this report.

e. Float zone lithium cells have an apparent optimum operating temperature at +20°C. Crucible lithium cells appear optimum at +50°C and +80°C. Cell design optimization is extremely sensitive to changes in operating temperature.

f. No advantage was observed with respect to the incorporation of a 1-mil integral cover with crucible lithium cells.

g. A significant difference was observed in the degradation experienced in illuminated/loaded cells from those not illuminated and open-circuited. Subject to further substantiation, future calculations and experiments should account for this effect.

h. Lithium cells produced in 1970 are vastly superior to those produced in 1967. This was observed with regard to mean maximum power, variance of typical production lots, relative degradation, and post-irradiation recovery characteristics.

These conclusions led to a series of questions yet to be answered regarding the future usefulness of lithium cells. These questions and related comments are:

a. Can the intial (absolute) performance of lithium cells be improved without sacrificing relative degradation characteristics? If so, lithium cells could show a considerable advantage over N/P cells for most missions.

b. Can lithium cells be produced in large quantities with the same degradation characteristics as observed in this experiment? The transition from laboratory to production line must necessarily be accomplished without changes in cell degradation characteristics.

c. Would the apparent optimization of float zone cells at 20°C be better defined if more temperature points had been taken? Degradation sensitivity as a function of temperature indicates the need for data with greater resolution.

d. What quantitative superiority would be required to make a clear-cut decision in favor of using lithium cells over N/P cells? A designer must weigh the lithium cell advantages against the risk of using a new product.

e. Should future cell irradiations be performed under conditions of illumination and loading? It is possible that all array degradation predictions based on past (nonilluminated, nonloaded) experimental data should account for this apparent effect.

6.2 RECOMMENDATIONS

As a result of this effort, the following recommendations are made:

a. Perform further analysis of the data produced in this effort. Investigate short-circuit current and open-circuit voltage degradation characteristics. Investigate forward/reverse, dark/light diode characteristics. Expand statistical significance tests of results.

b. Consult further with cell manufacturers regarding interpretation of these results. Evaluate future production potentialities of the better lithium cells.

c. Consult with other contractors performing more basic physical research regarding significance and interpretation of these results.

d. Conduct a follow-on irradiation emphasizing verification of significant effects observed in this effort and increased resolution of observed temperature effects.

e. Conduct analysis relating actual orbital environmental characteristics to these results, thereby increasing their usefulness for specific missions. Develop preliminary models for optimizing lithium cell performance as a function of mission parameters.

f. Relate these results with those from the other real-time irradiation program (Lockheed Georgia Division) and with those from the 1-MeV acceleration irradiations performed by JPL.

SECTION 7

NEW TECHNOLOGY

No reportable items of new technology have been developed as a result of performing this contract.

SECTION 8

REFERENCES

1. J. J. Wysocki: "Self-Healing Radiation Resistant Silicon Solar Cells," Conference Record of the Sixth Photovoltaic Specialists Conference, IEEE, Cocoa Beach, Florida, 28-30 March 1967.

2. P. H. Fang: "Present Status of Lithium-Diffused Silicon Solar Cells," Conference Record of the Sixth Photovoltaic Specialists Conference, IEEE, Cocoa Beach, Florida, 28-30 March 1967.

3. R. G. Downing, J. R. Carter, and W. K. Van Atta: "Study and Determination of an Optimum Design for Space Utilized Lithium Doped Solar Cells," Report No. 13154-6009-RO-00, TRW Systems Group, Redondo Beach, Calif., 15 April 1970.

4. G. Brucker, T. Faith, J. Corra, and A. Holmes-Siedle: "Study to Determine and Improve Design for Lithium Doped Solar Cells," Report No. AEC R-3562F, RCA Corporation, Astro Electronics Division, Princeton, N.J., 10 April 1970.

5. D. M. Newell: Investigation of the Use of a Radioisotope for Space Environment Simulation, Report No. SRS-TR150, Philco-Ford Corporation, Space and Re-entry Systems Division, Palo Alto, Calif., 19 March 1967.

6. "Evaluation of the Effect of Space Radiation on Lithium P-on-N Solar Cells," Report No. TR-DA1875 (First Irradiation Run Report), Philco-Ford Corporation, Space and Re-entry Systems Division, Palo Alto, Calif., August 1968.

7. "Radiation Effects on Lithium P-on-N Solar Cells," Report No. ER 9357, Lockheed Georgia Company, Dawsonville, Georgia.

8. D. L. Reynard, and D. B. Orvis, "Beta Irradiation of Lithium Doped Solar Cells," Conference Record of the Seventh Photovoltaic Specialists Conference, IEEE, Pasadena, Calif. 19-21 November 1968.

9. "Engineering Experimental Program on the Effects of Near-Space Radiation on Lithium-Doped Solar Cells," WDL-TR4213, Philco-Ford Corporation, Palo Alto, Calif., 1 June 1970.

10. P. Iles: Private communication, July 1969.

11. E. C. de Wys: Private communication, December 1968.

12. P. H. Fang: Private communication, December 1967.

13. "Experimental Study of Solar Cell Performance at High Solar Intensities," Report No. TR-DA1636, Philco-Ford Corporation, Space and Re-entry Systems Division, Palo Alto, Calif., 25 November 1967.

14. J. I. Vette: "A Survey of the Trapped Radiation Environment," Conference Record of the Sixth IEEE Photovoltaic Specialists Conference, Cocoa Beach, Florida, 28-30 March 1967.

15. D. Curtin: Private communication, April 1971.

16. E. Ralph: Private communication, April 1971.

17. F. Larin: Radiation Effects in Semiconductor Devices, John Wiley & Sons, New York, 1968.

18. M. Wolf and G. J. Brucker: "Recent Developments in Radiation Hardening Silicon Solar Cells," 1970 Intersociety Energy Conversion Engineering Conference, Las Vegas, Nevada, September 1970.

APPENDIX A

SOLAR SIMULATOR STANDARDIZATION PROCEDURE AND RESULTS

APPENDIX A

SOLAR SIMULATOR STANDARDIZATION PROCEDURE AND RESULTS

Prior to each data acquistion period, the following procedure was initiated:

a. Move X-25 solar simulator to calibration position (illuminating standardization fixture).

b. Turn on X-25 solar simulator and allow a minimum of 10 minutes warmup.

c. Assure proper operation of X-25 system; verify tolerance limits on lamp current, lamp voltage, and lamp operating time.

d. Adjust intensity of X-25 output to give the Standard Cell output of 129.9 mA short-circuit current, and record results.

e. Record Standard Cell short-circuit current with red and blue filters.

f. Record the values of the five uniformity test cells.

g. Before proceeding, verify that the calibration data is within allowable limits.

h. Center the X-25 beam to the experiment chamber.

i. Record short-circuit current of the chamber monitor cell and verify adequacy.

j. Begin the data acquisition procedure.

The results of the standardization procedure for each data acquisition period are presented in Figures A-1 through A-5. The short-circuit currents for the five uniformity cells

(refer to Figure 3-8 for layout) are presented in Figure A-1. A general upward trend of approximately 1% is noted for all cells except cell 5.

The red-blue ratio, calculated from measurements using Wratten red and blue filters, rose steadily as a result of lamp and filter aging as shown in Figure A-2. The effect of this change has not been evaluated.

Figure A-3 presents the data taken using the wide bandpass filter spectral monitor cells. Again a slight upward trend is noted. Figure A-4 presents the filter transmission characteristics.

Figure A-5 presents data from the Chamber Monitor Cell mounted to the rear of the chamber. The cell responded to light passing through both front and rear chamber windows. This cell also indicated an approximately 1% rise during the 6-month irradiation period.

A uniformity plot was made of the X-25 beam at the end of the 6-month period using a traversing sensor. The traverse direction was rotated about the beam center and the beam found to be radially symmetric within ±1%. The cell locations are in the area where uniformity is within a total range of 3.5% as shown in Figure A-6.

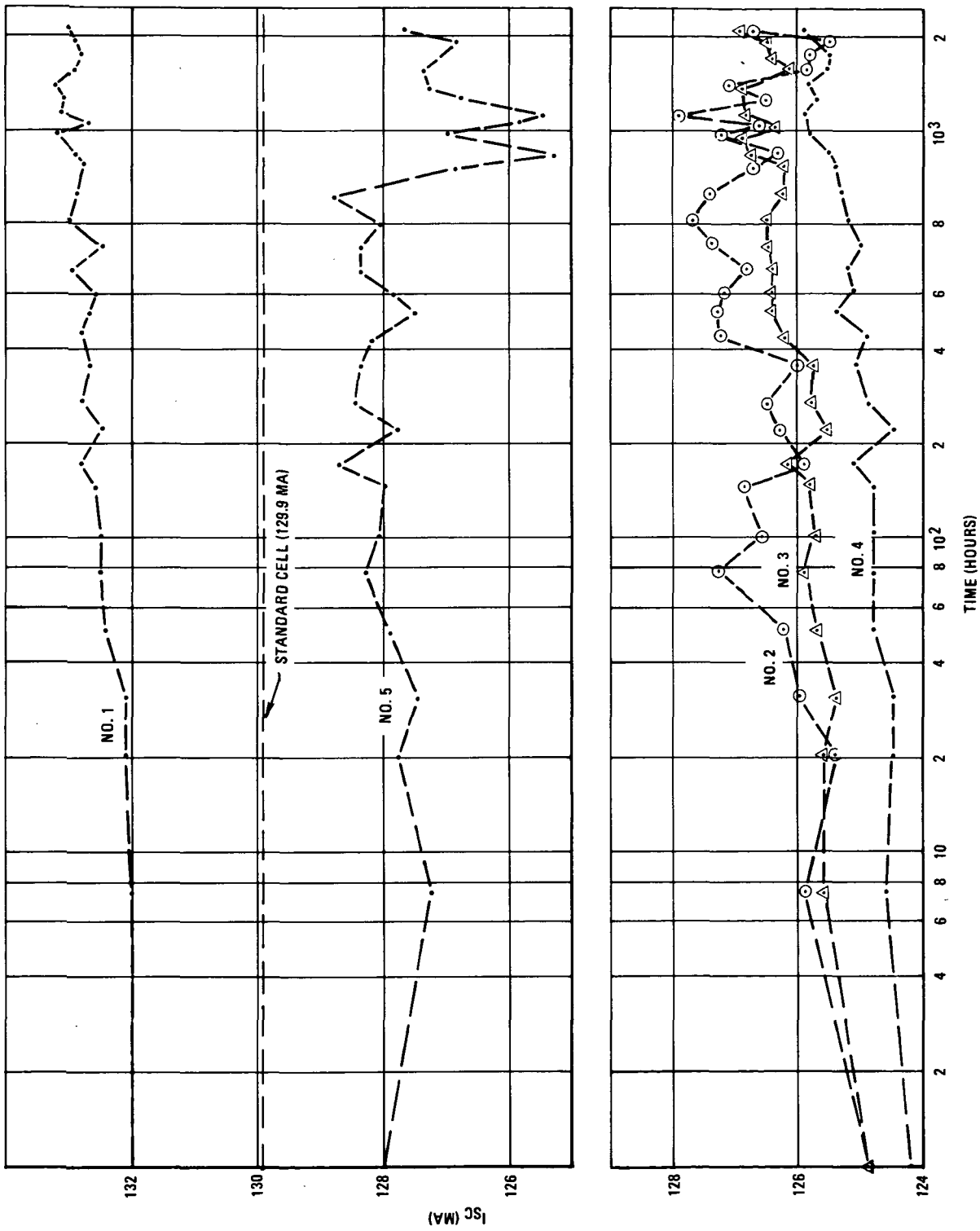

Figure A-1 JPL Test Calibration Uniformity Data

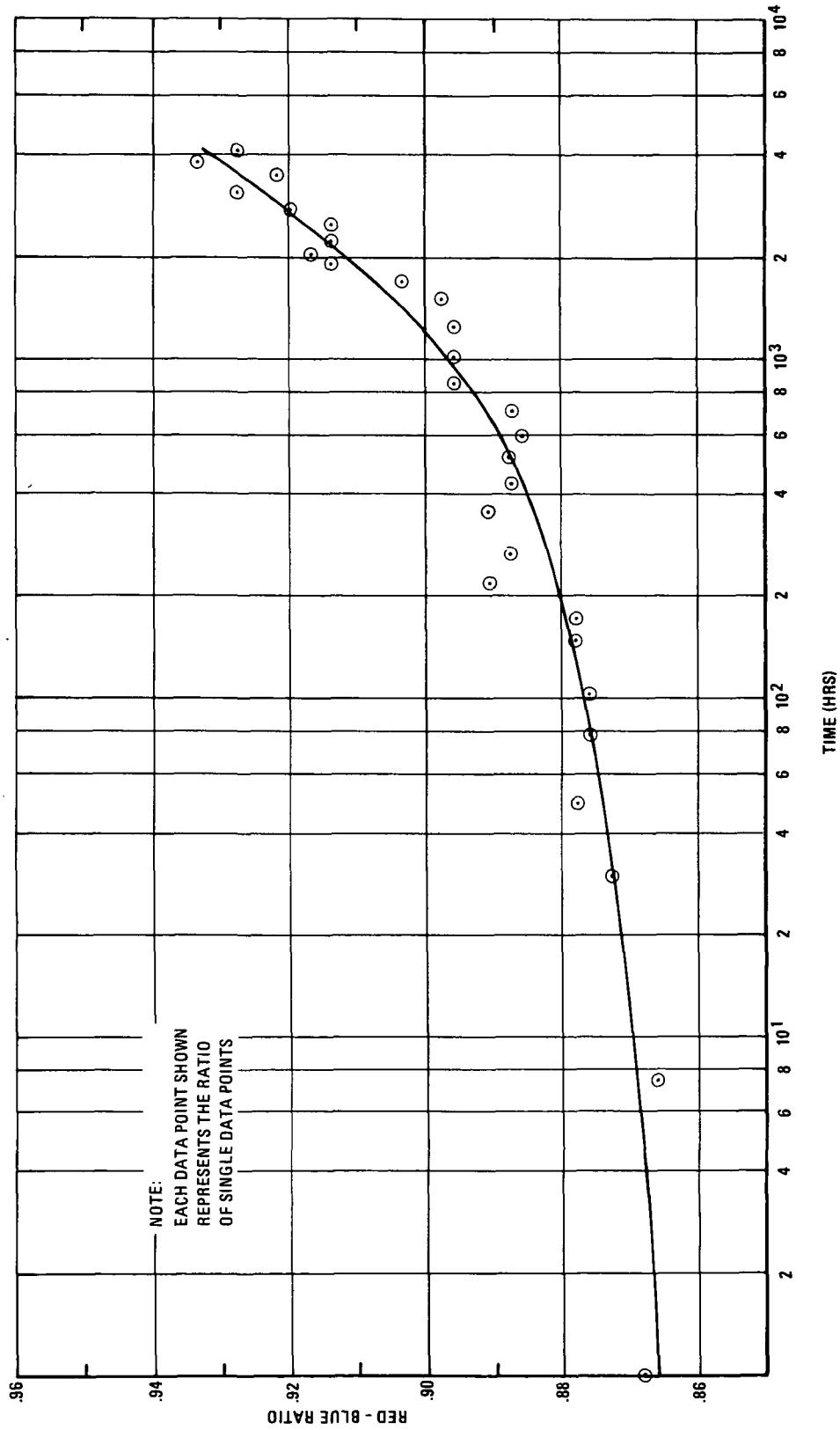

Figure A-2 JPL Test Calibration Red-Blue Ratio

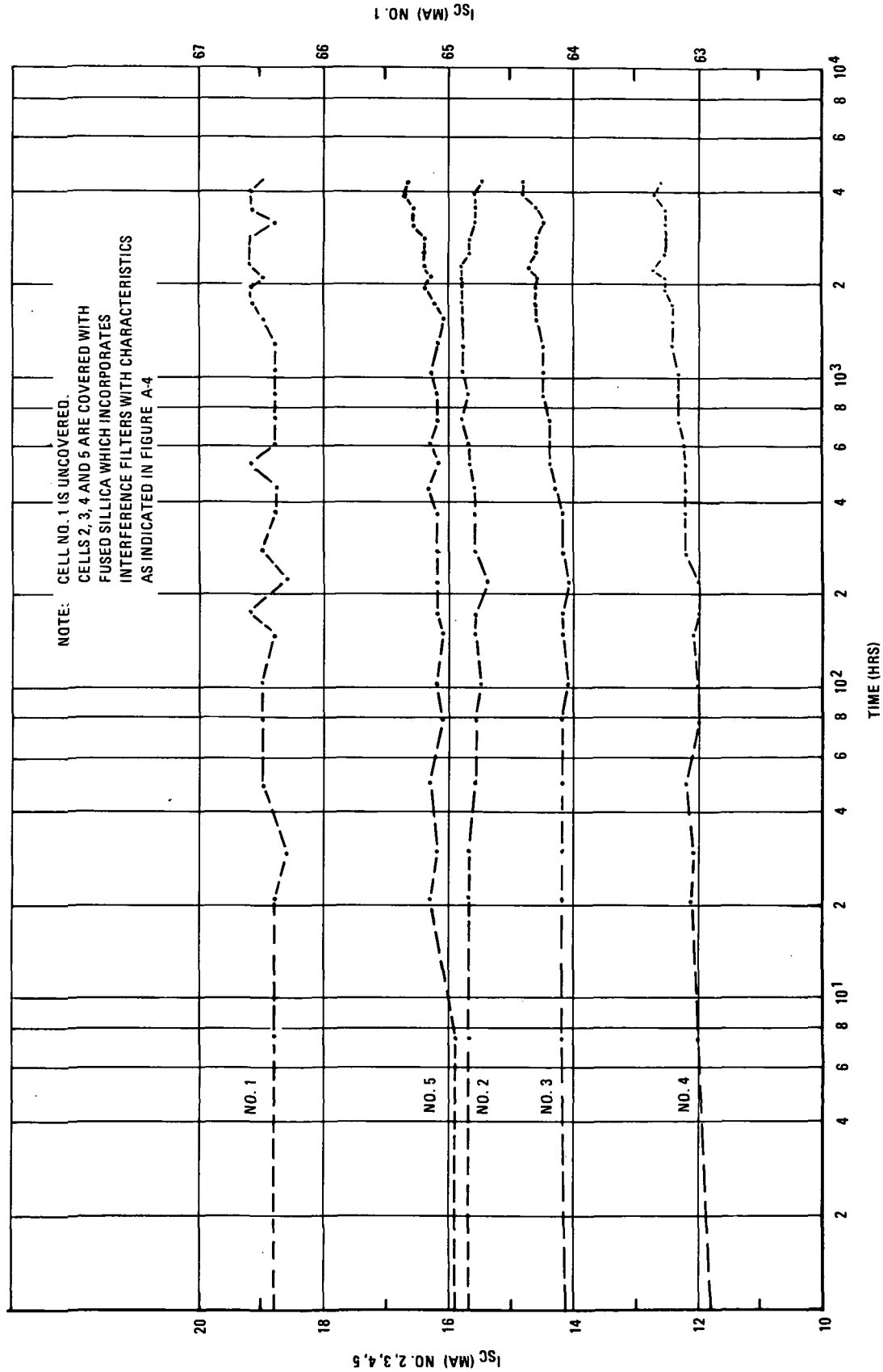

Figure A-3 JPL Test Calibration Spectral Measurement Data

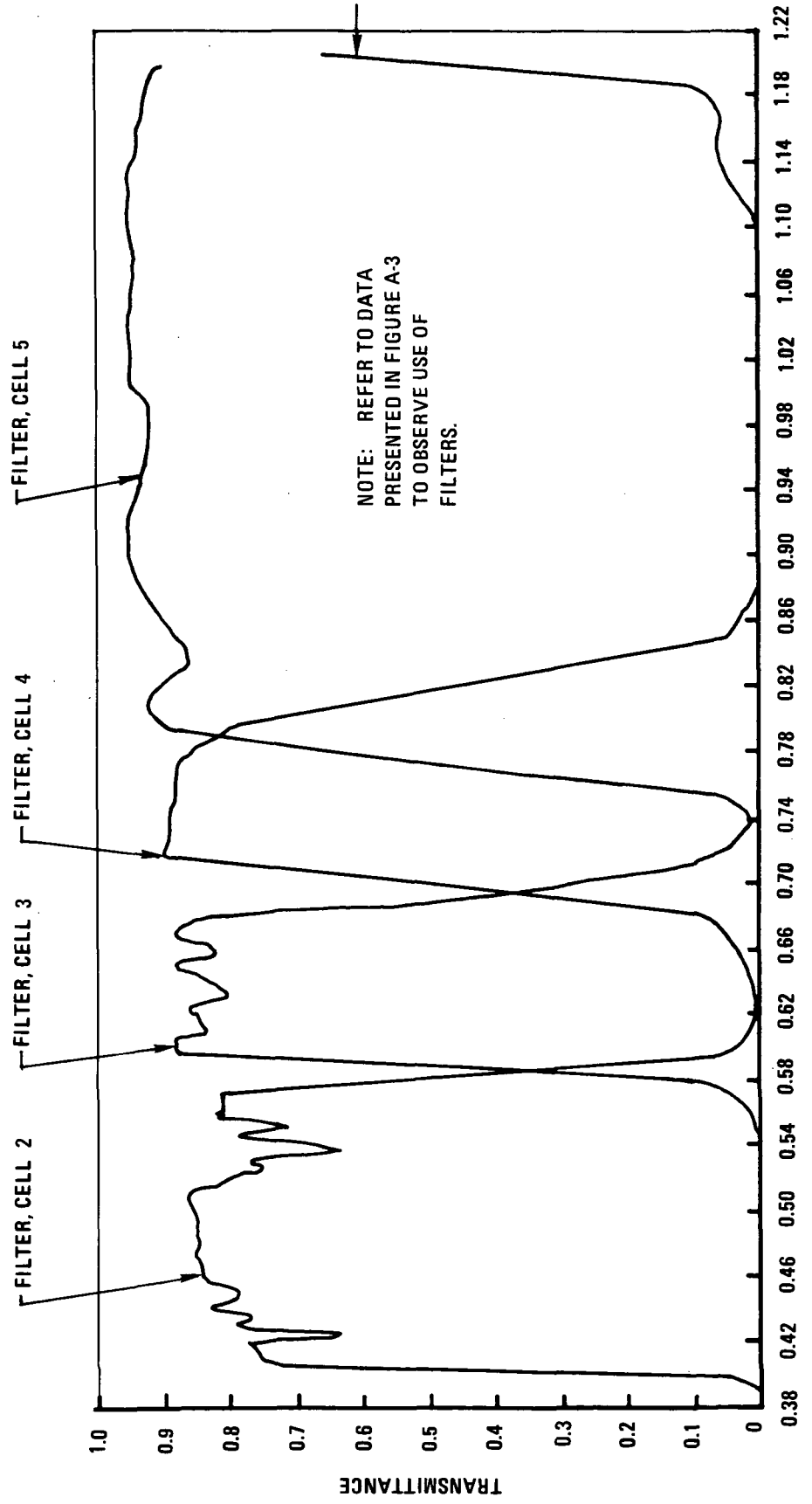

Figure A-4 Transmittance of Filters Used for Spectral Measurements

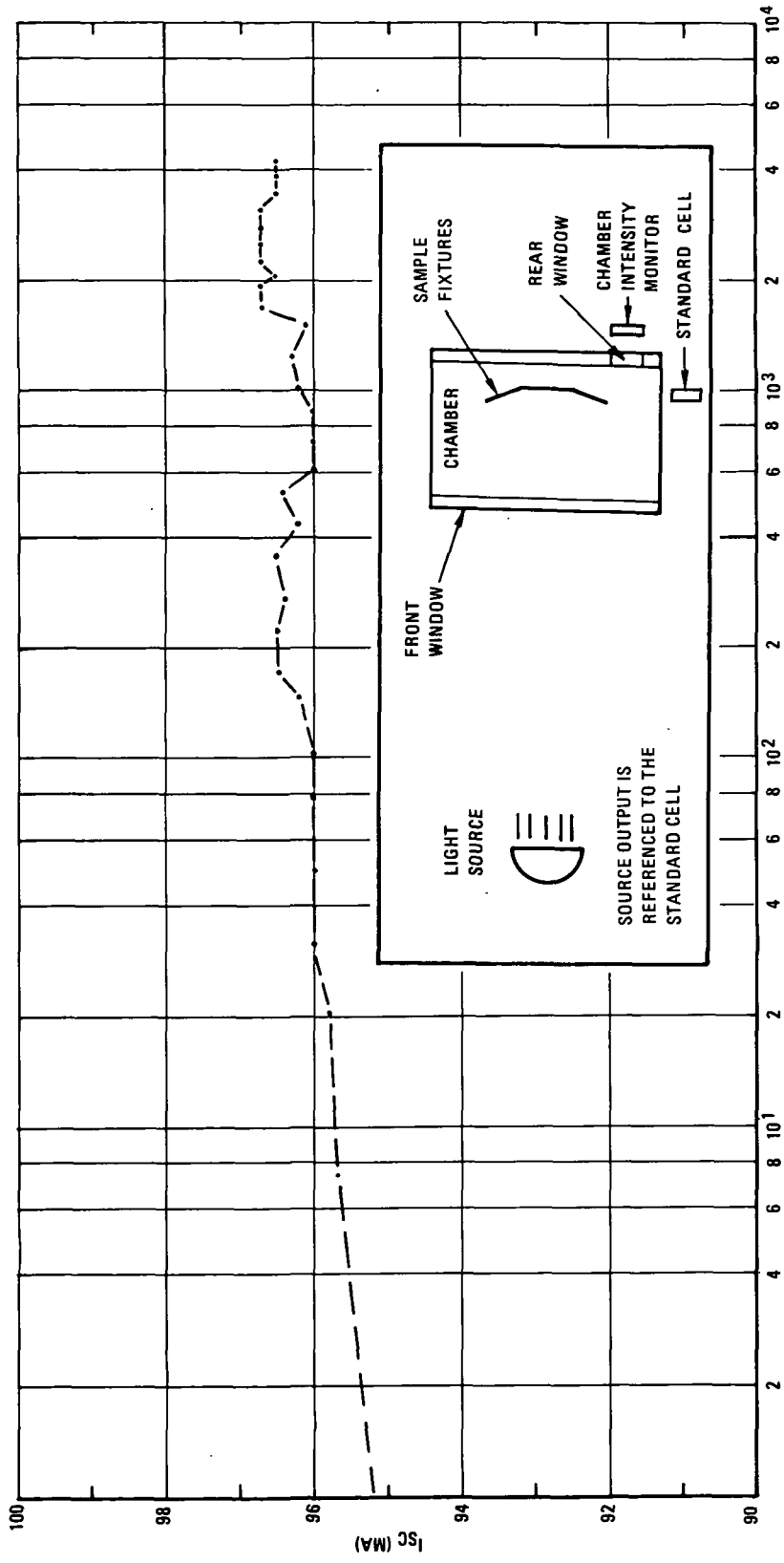

Figure A-5 JPL Test Calibration Chamber Intensity Monitor

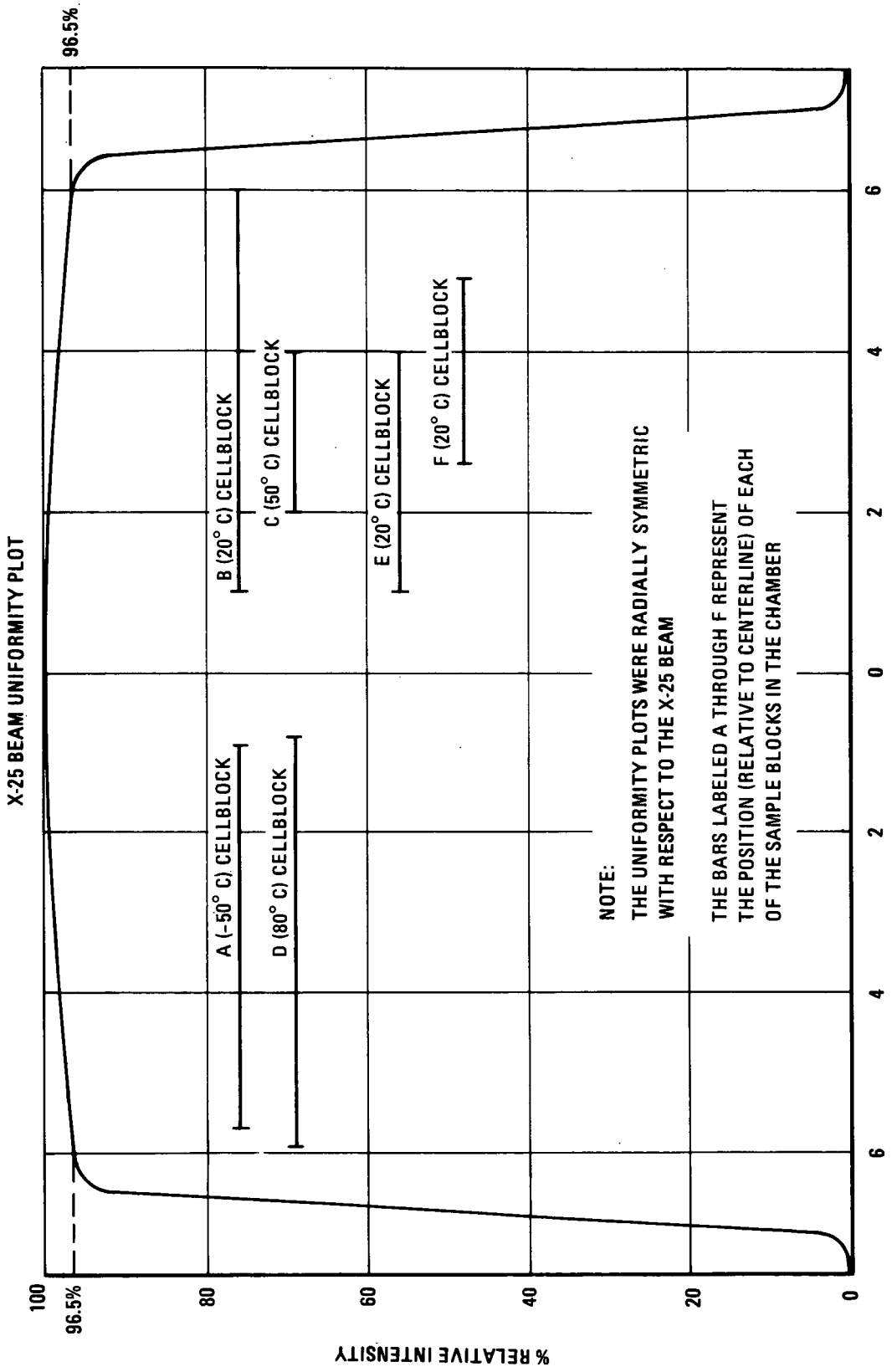

Figure A-6 X-25 Beam Uniformity Plot

APPENDIX B

PERFORMANCE MEASUREMENT PROCEDURE

APPENDIX B

PERFORMANCE MEASUREMENT PROCEDURE

Each of the 128 cells in the experiment is connected through the cell switching unit to the Spectrolab D-550 electronic load as shown in Figure B-1. The electronic load provides an automatic variable load to each of the solar cells in succession and also provides open-circuit voltage and short-circuit current measurements. The open-circuit voltage is measured with a Digitec Digital Voltmeter and the short-circuit current is measured with a Weston Ammeter.

As each cell is being swept through its variable load, its current/voltage characteristics are plotted on the Mosley Model 7000A X-Y recorder.

The accuracy of the DVM and ammeter are periodically checked with a Fluke Model 883A differential voltmeter.

The coordinates of the graph paper on the X-Y recorder are checked against the meter readings and adjustments are made if necessary.

The data acquistion procedure involves the following steps:

a. Go to first cell to be tested and measure short-circuit current and open-circuit voltage with calibrated DVM and ammeter and record on data sheet.

b. Plot I-V curve on Mosley X-Y plotter. Check open-circuit voltage and short-circuit current against instrument values and adjust plotter if necessary.

c. Continue plotting curves for each cell in the experiment.

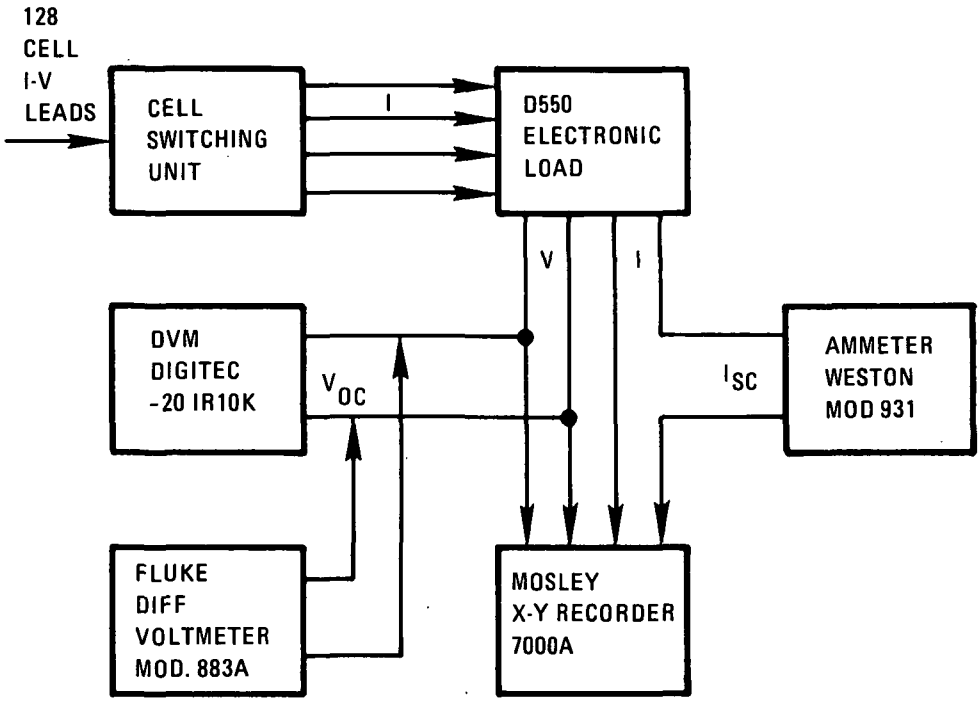

Figure B-1 Data Acquisition Equipment Block Diagram

APPENDIX C

CORRECTED DATA POINTS FOR EACH CELL TYPE AND TEST CONDITION

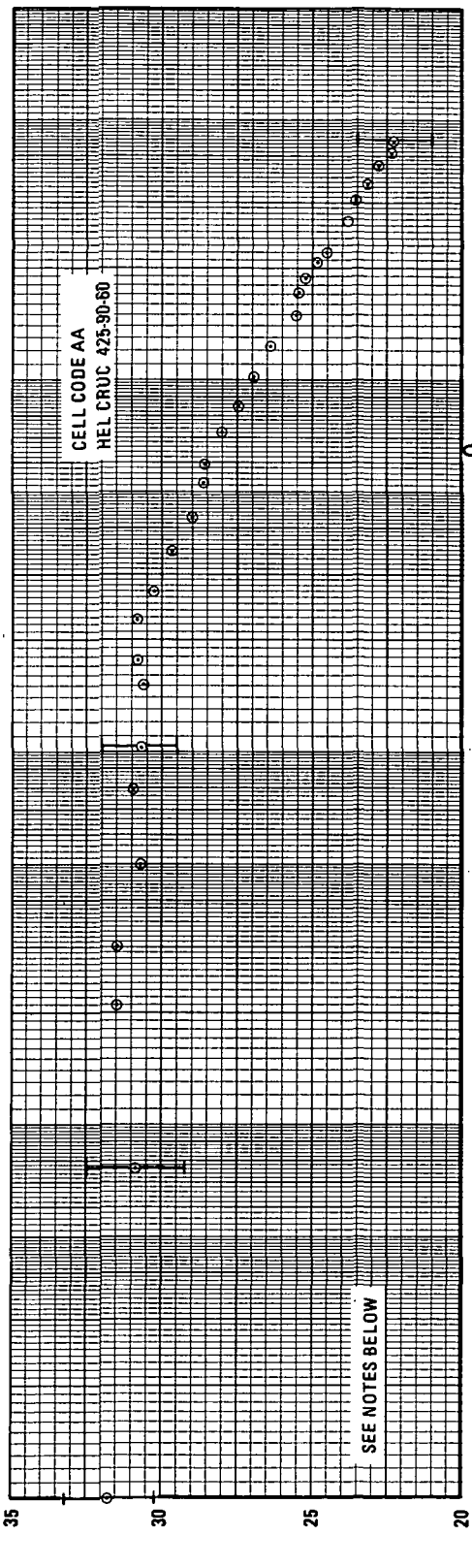

Figure C-1 P_{max} Data for Cell Type A at -50°C

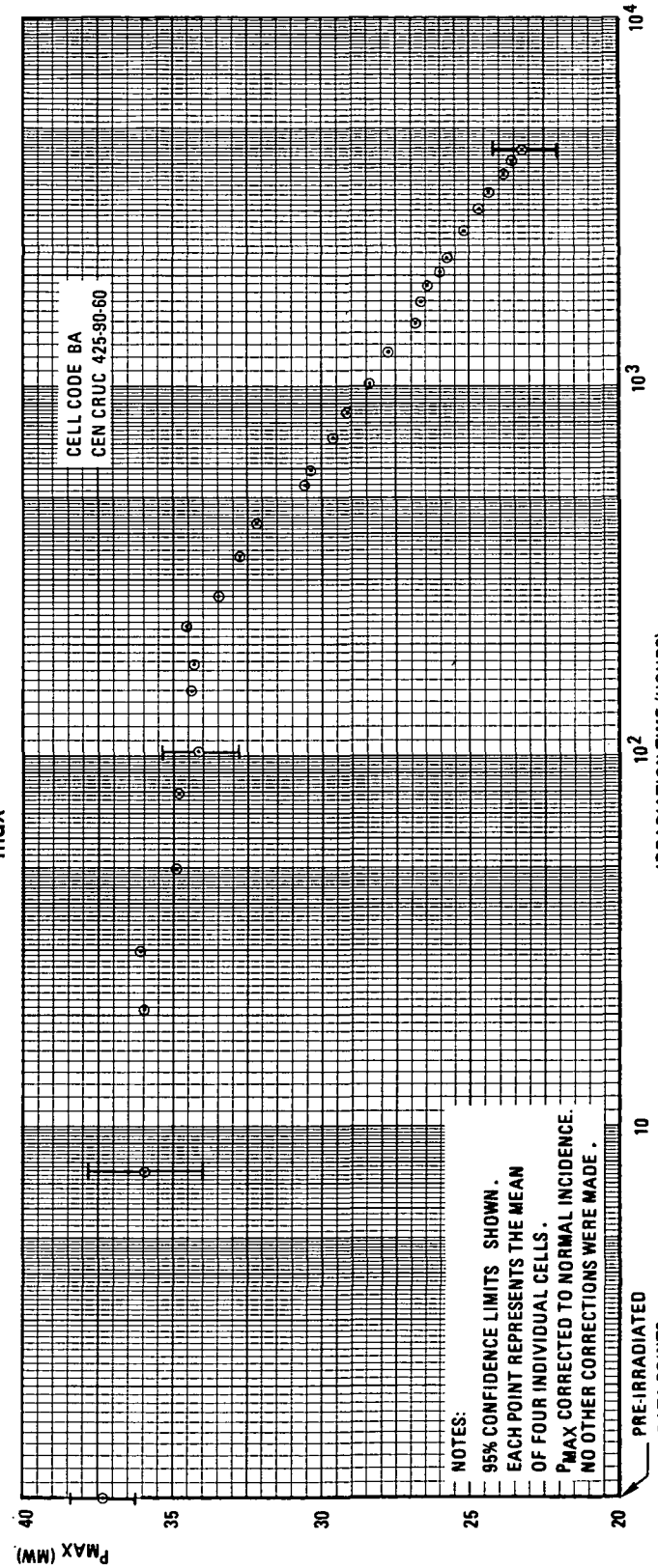

Figure C-2 P_{max} Data for Cell Type B at -50°C

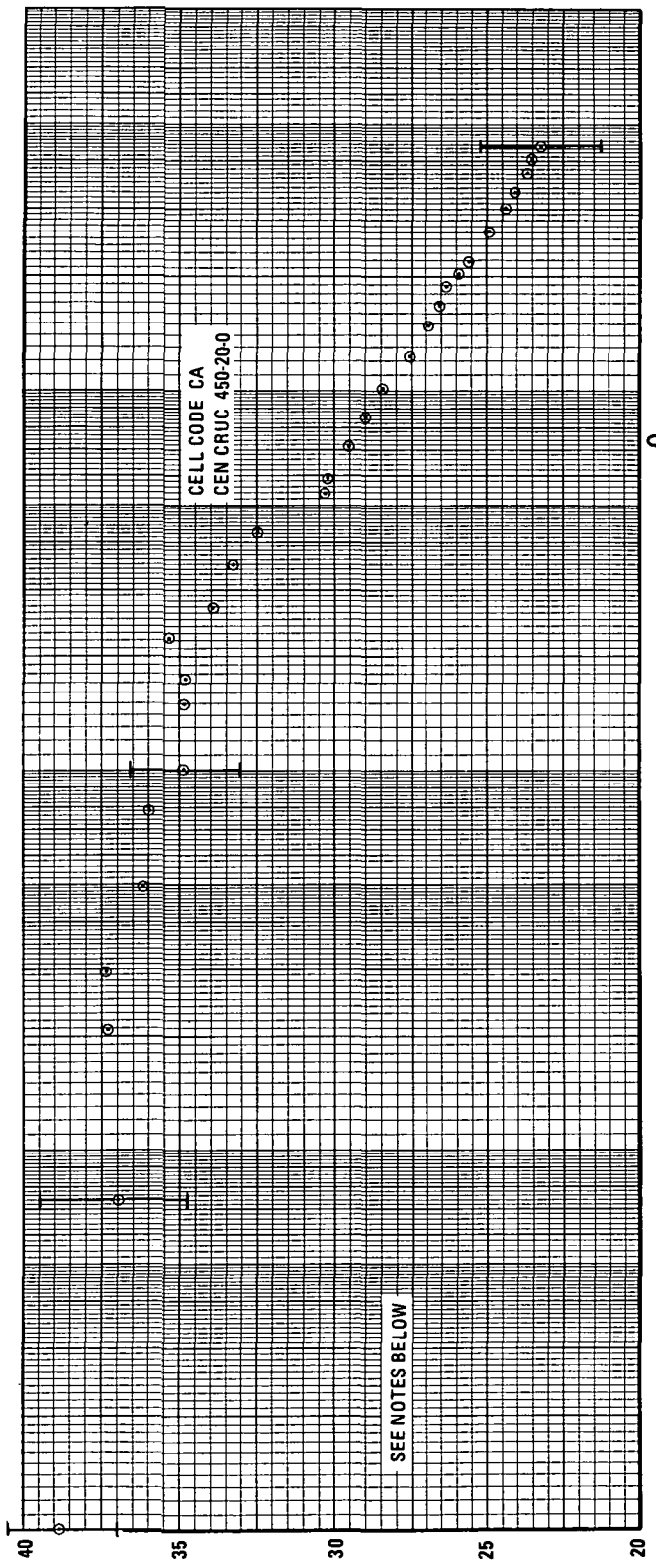

Figure C-3 P_{max} Data for Cell Type C at -50°C

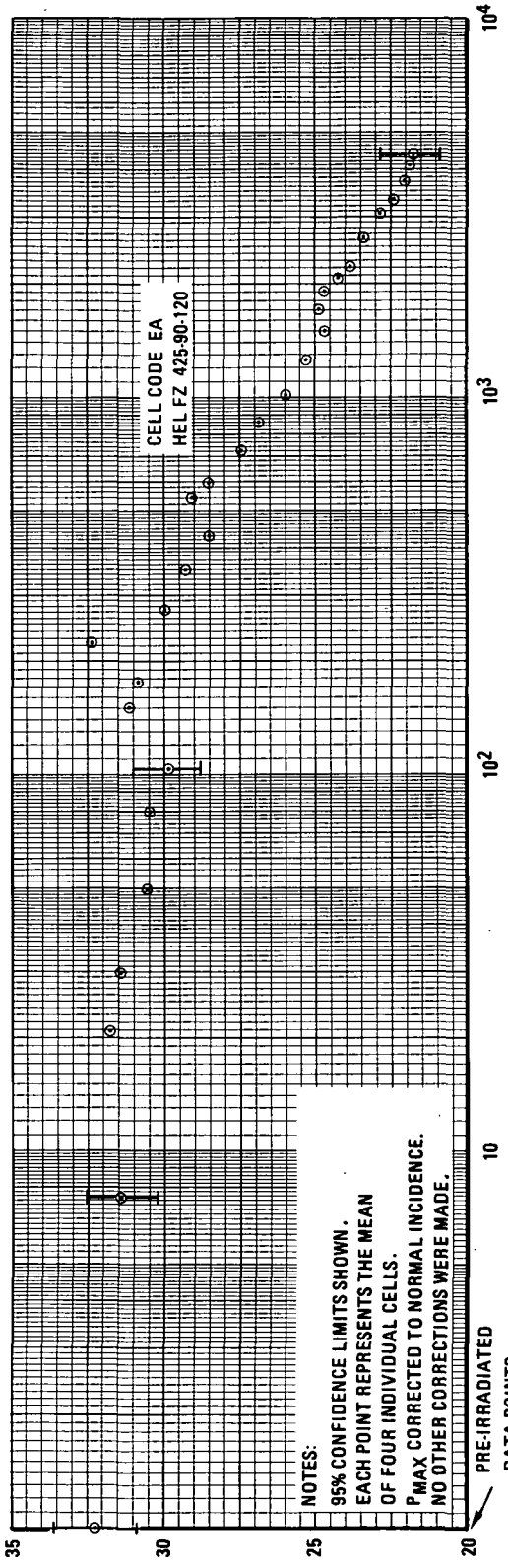

Figure C-4 P_{max} Data for Cell Type E at -50°C

P_{MAX} (MW)

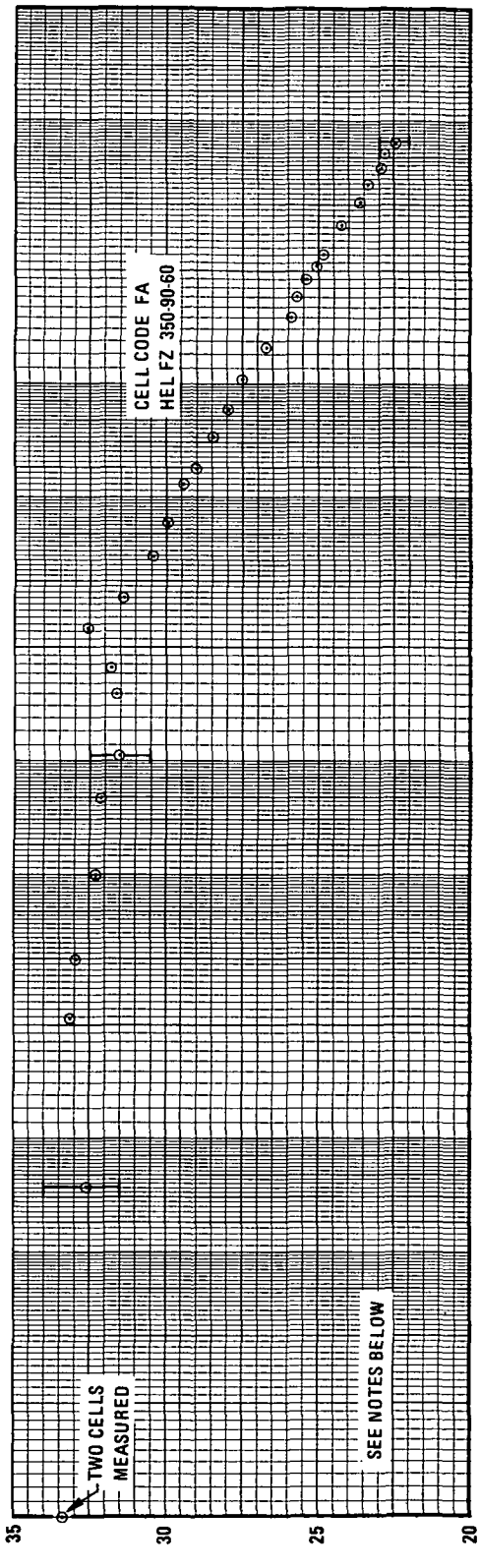

Figure C-5 P_{max} Data for Cell Type F at -50°C

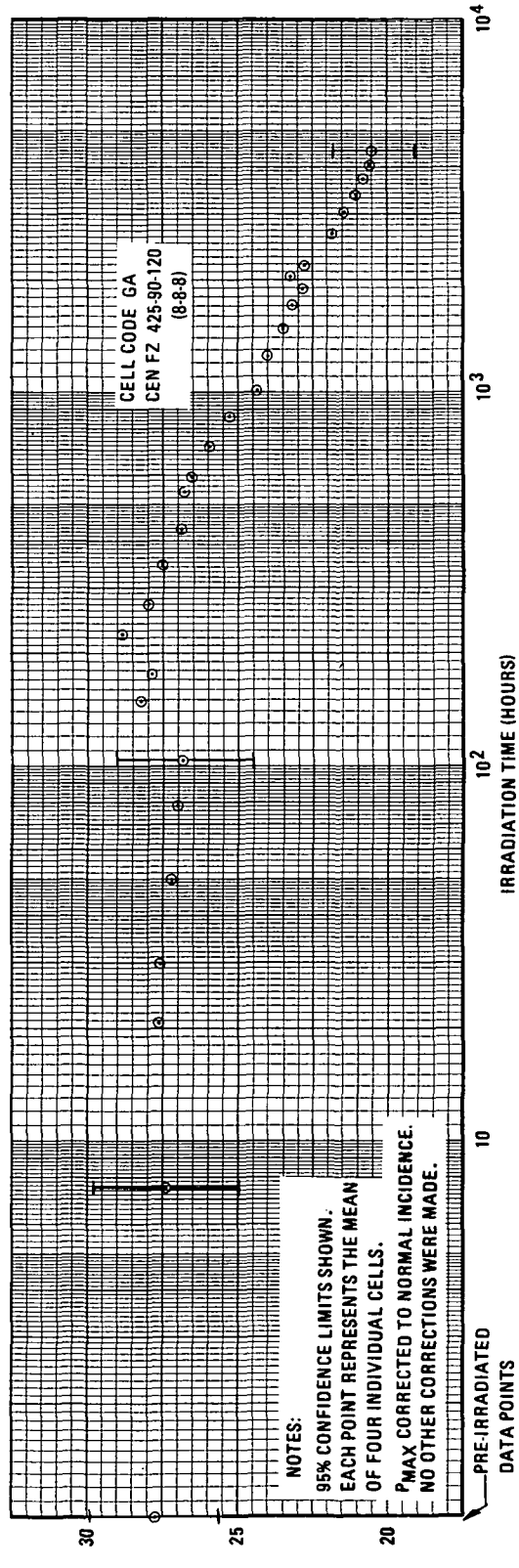

Figure C-6 P_{max} Data for Cell Type G at -50°C

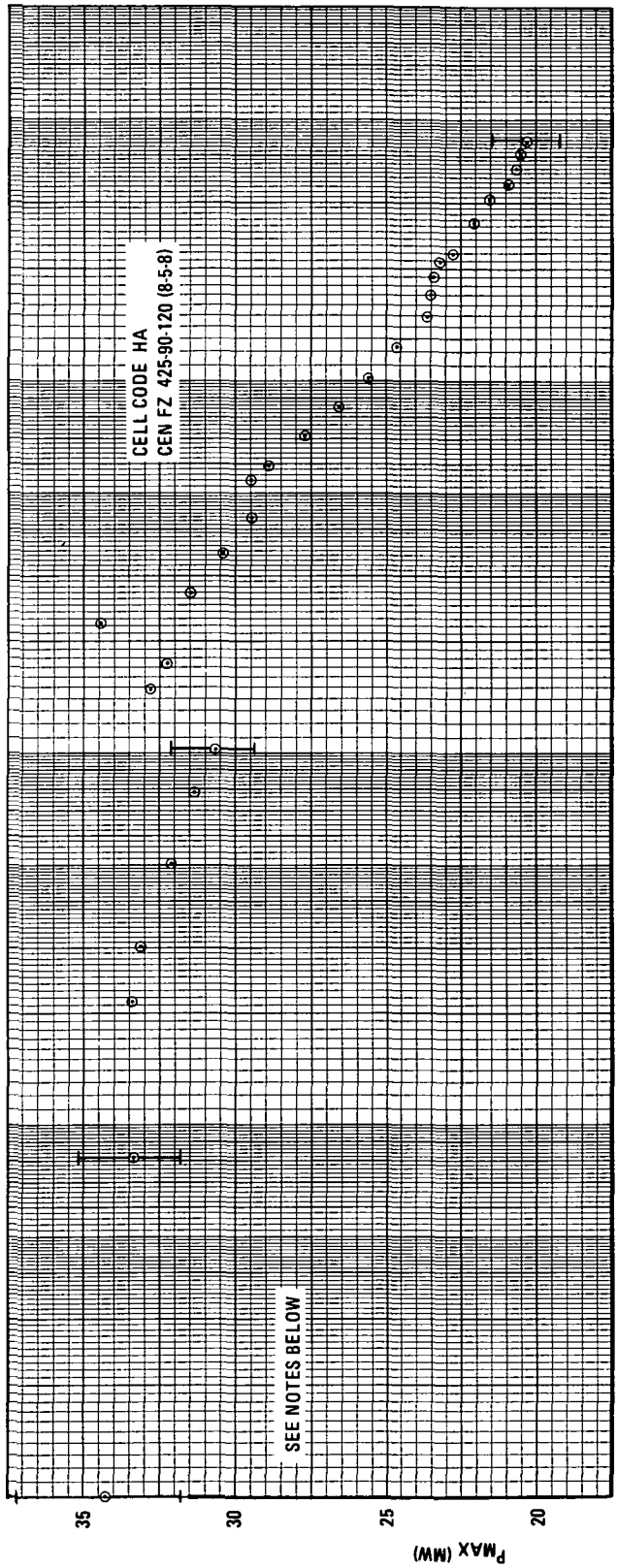

Figure C-7 P_{max} Data for Cell Type H at -50°C

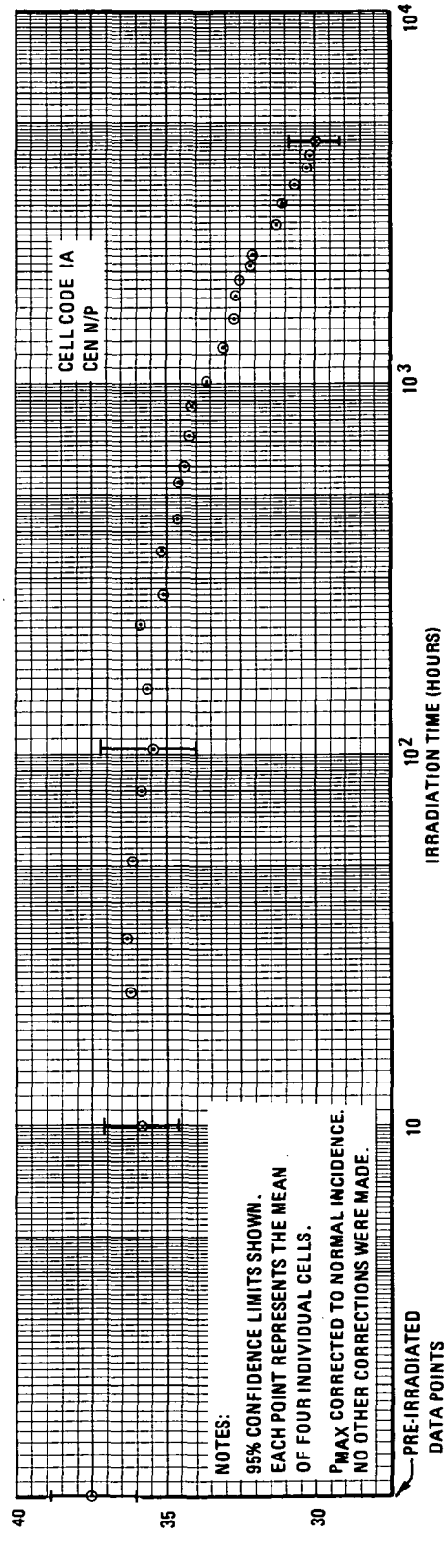

Figure C-8 P_{max} Data for Cell Type I at -50°C

PHILCO Ford
Philco-Ford Corporation
Western Development Laboratories Division

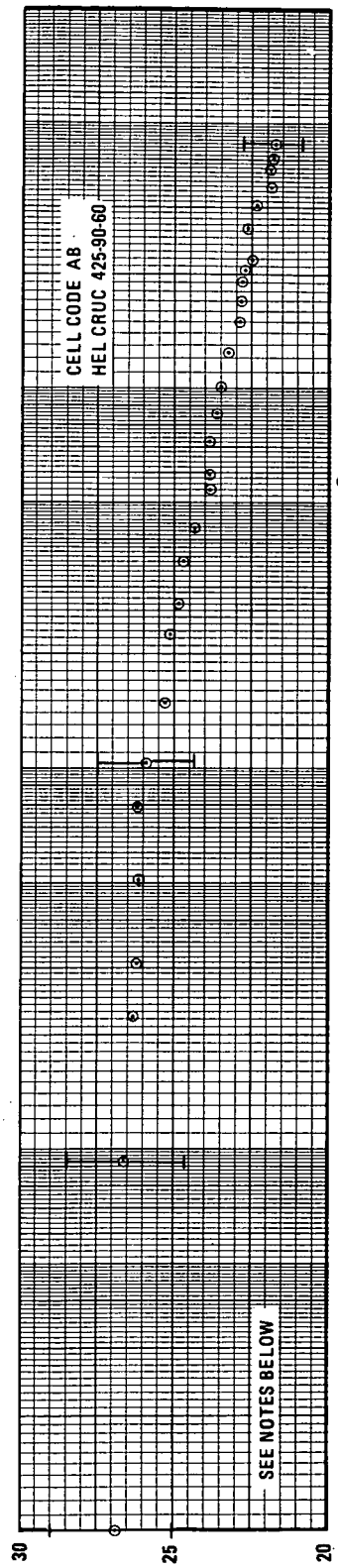

Figure C-9 P_{max} Data for Cell Type A at 20°C

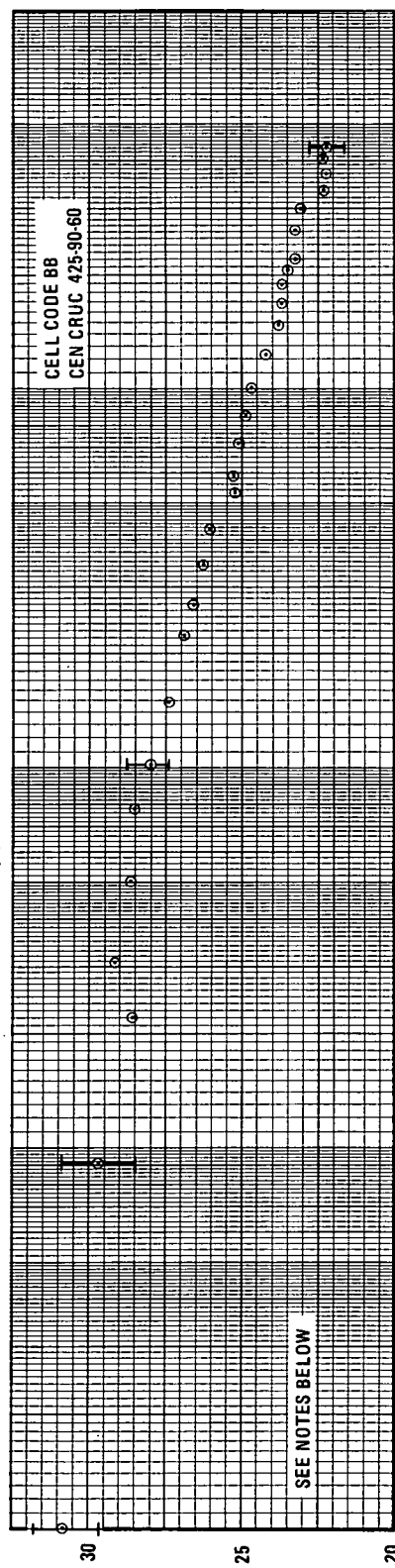

Figure C-10 P_{max} Data for Cell Type B at 20°C

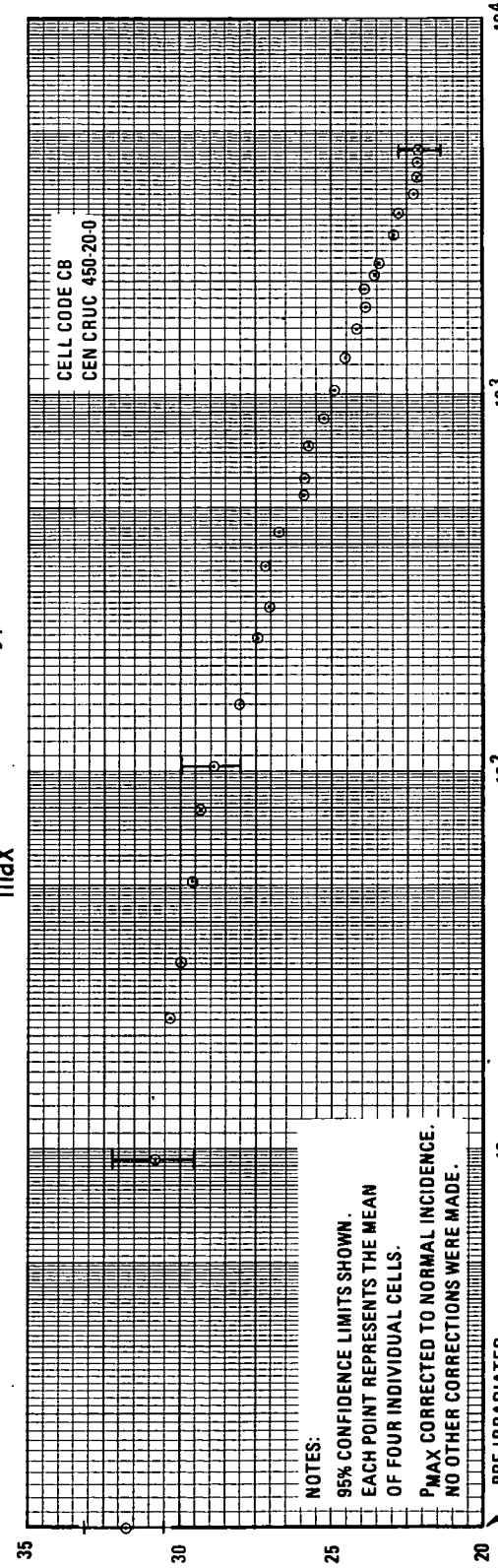

Figure C-11 P_{max} Data for Cell Type C at 20°C

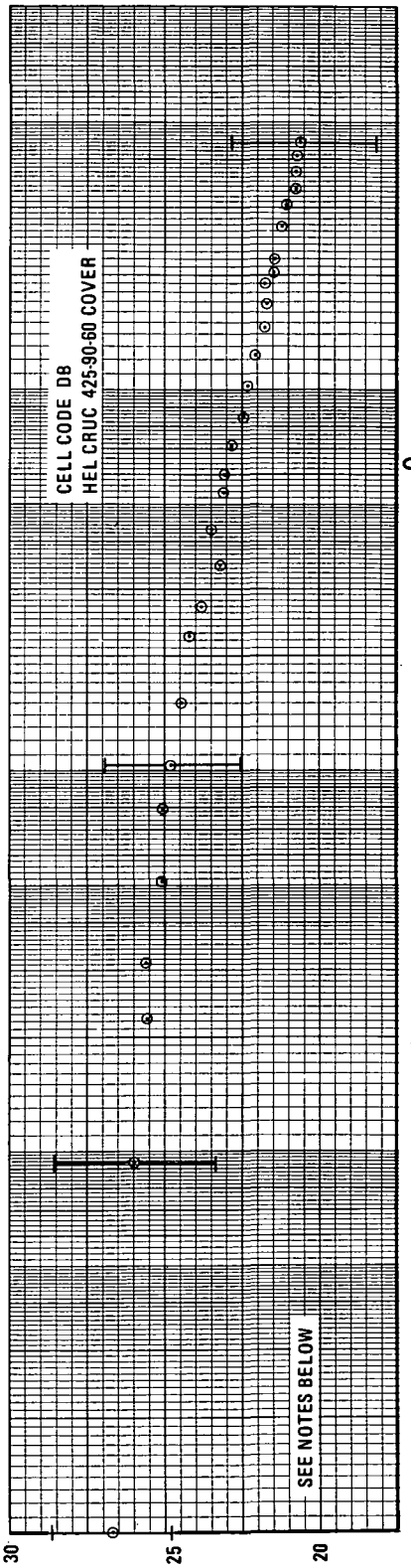

Figure C-12 P_{max} Data for Cell Type D at 20°C

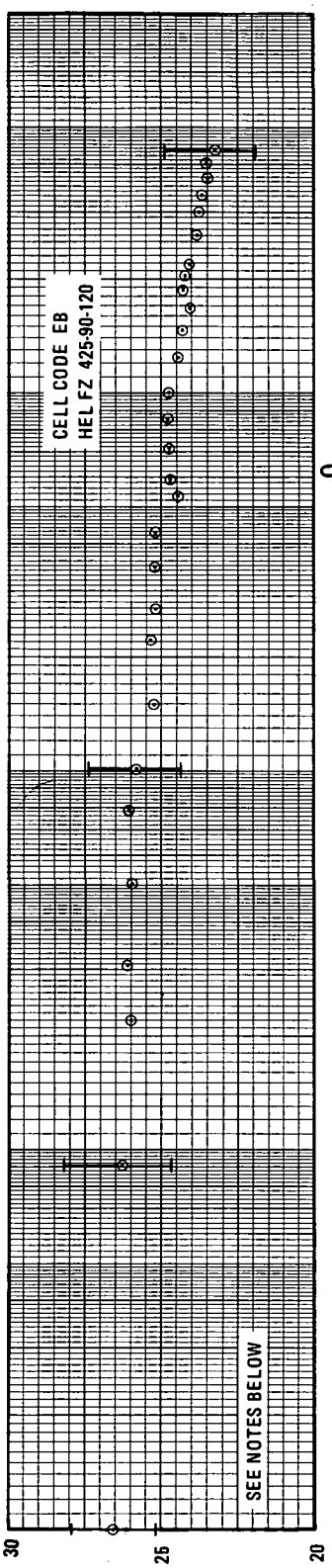

Figure C-13 P_{max} Data for Cell Type E at 20°C

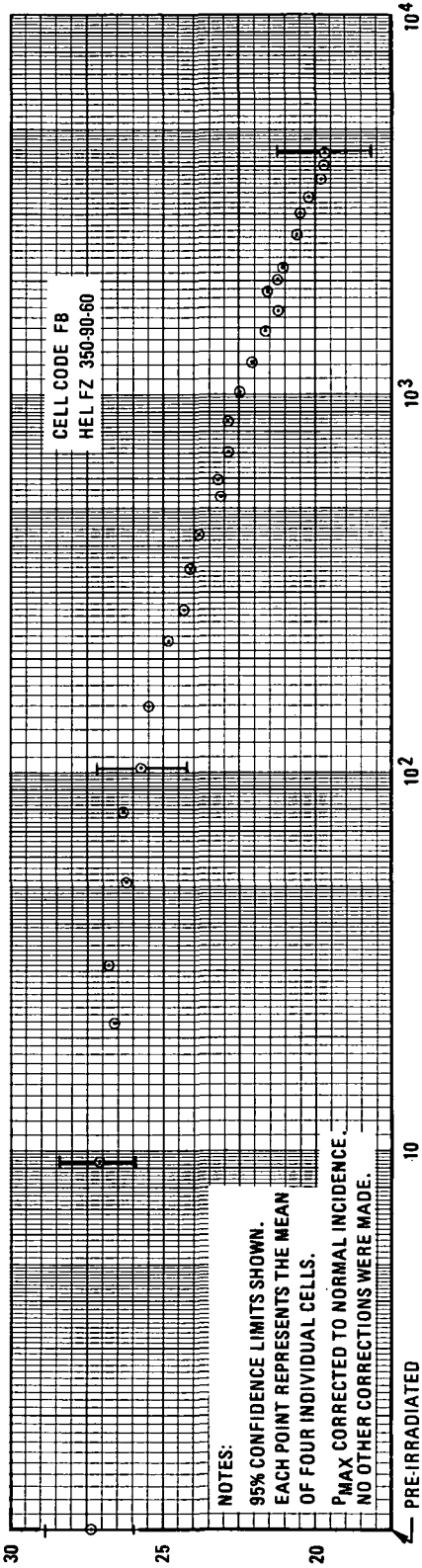

Figure C-14 P_{max} Data for Cell Type F at 20°C

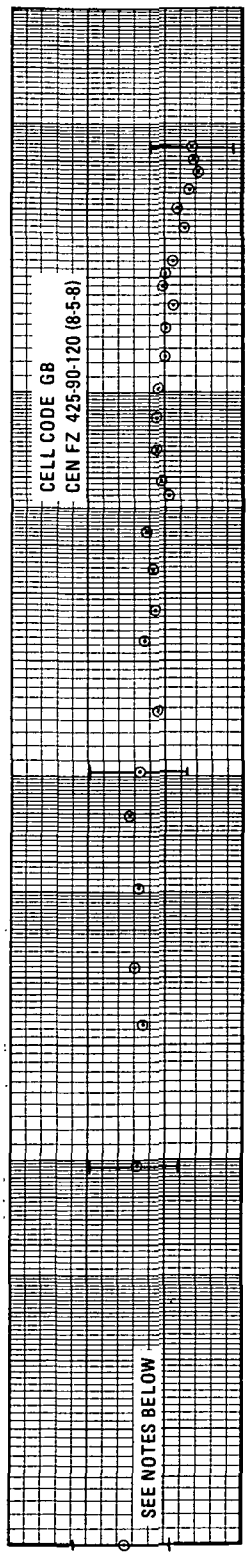

Figure C-15 P_{max} Data for Cell Type G at 20°C

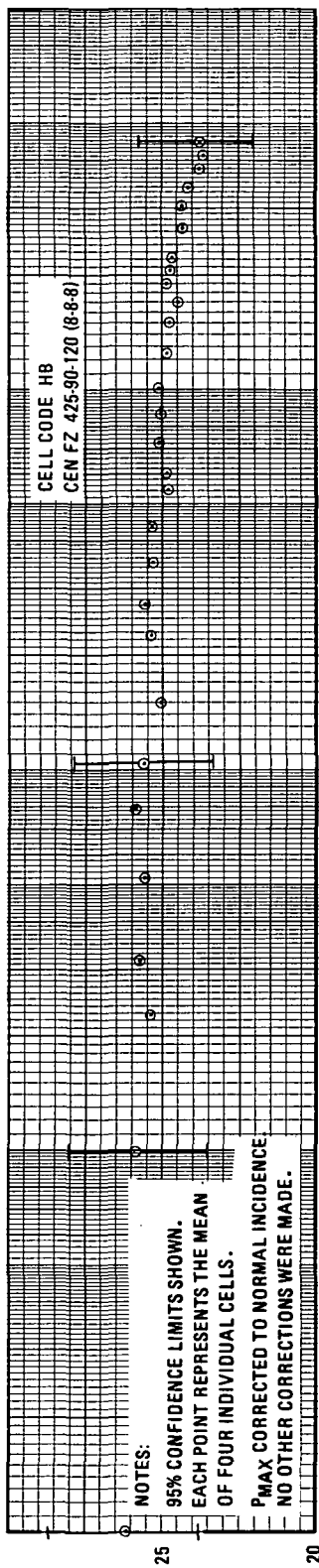

Figure C-16 P_{max} Data for Cell Type H at 20°C

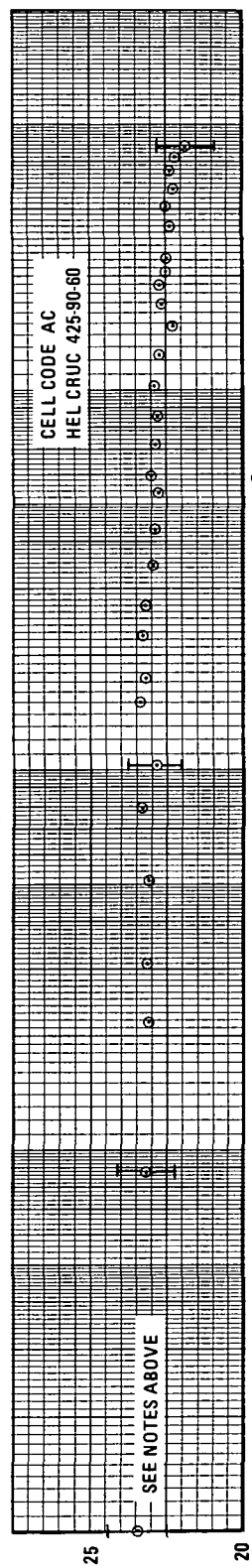

Figure C-17 P_{max} Data for Cell Type A at 50°C

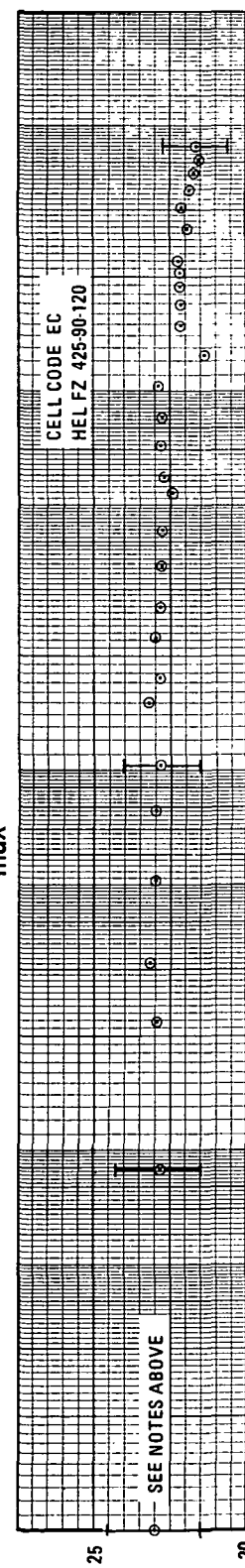

Figure C-18 P_{max} Data for Cell Type E at 50°C

P_{MAX} (MW)

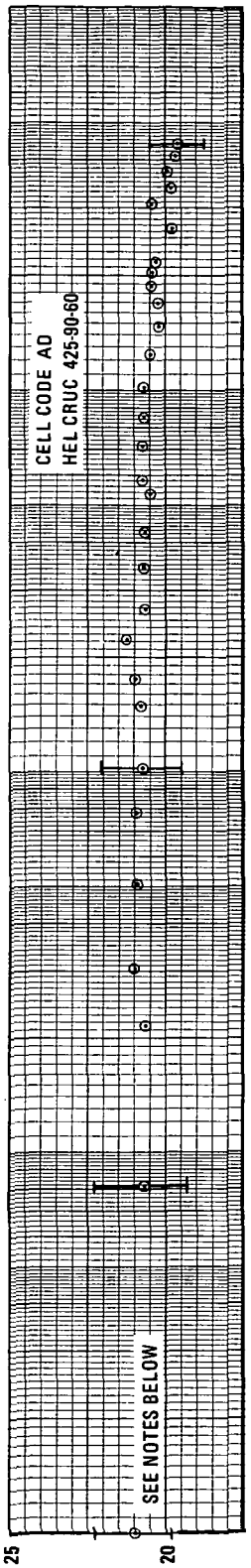

Figure C-19 P_{max} Data for Cell Type A at +80°C

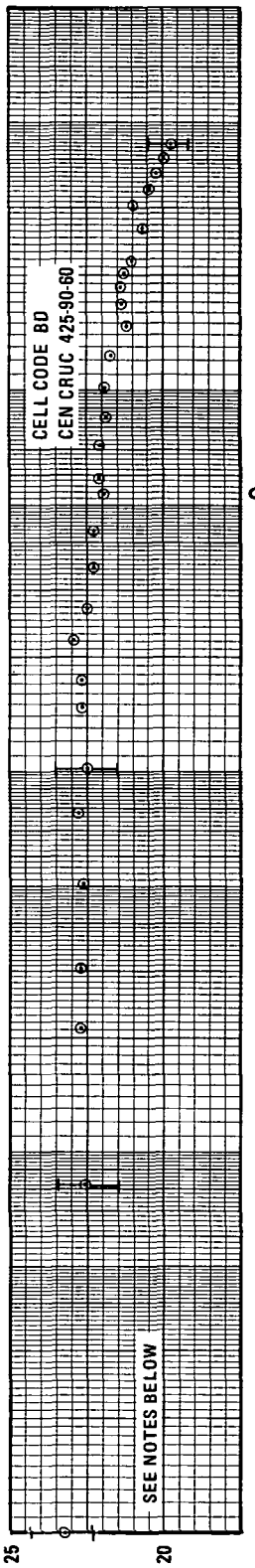

Figure C-20 P_{max} Data for Cell Type B at +80°C

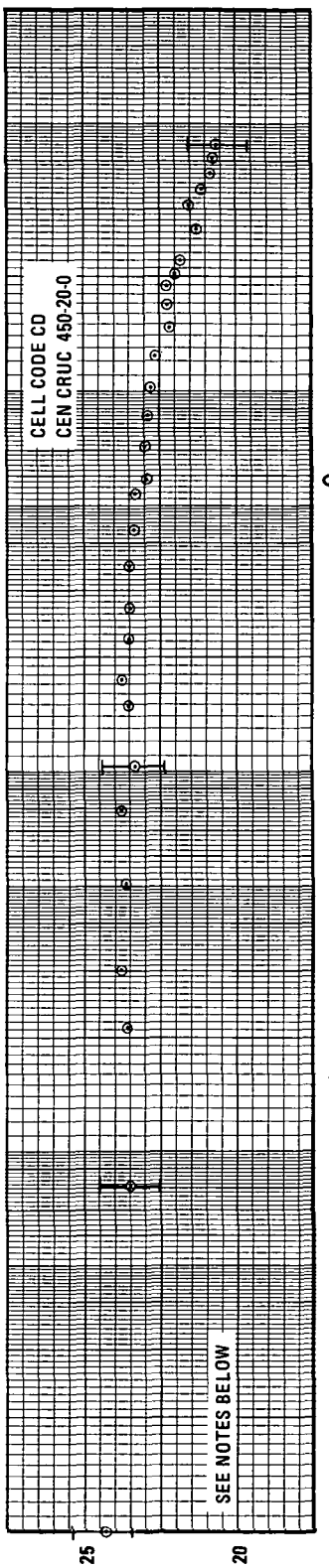

Figure C-21 P_{max} Data for Cell Type C at +80°C

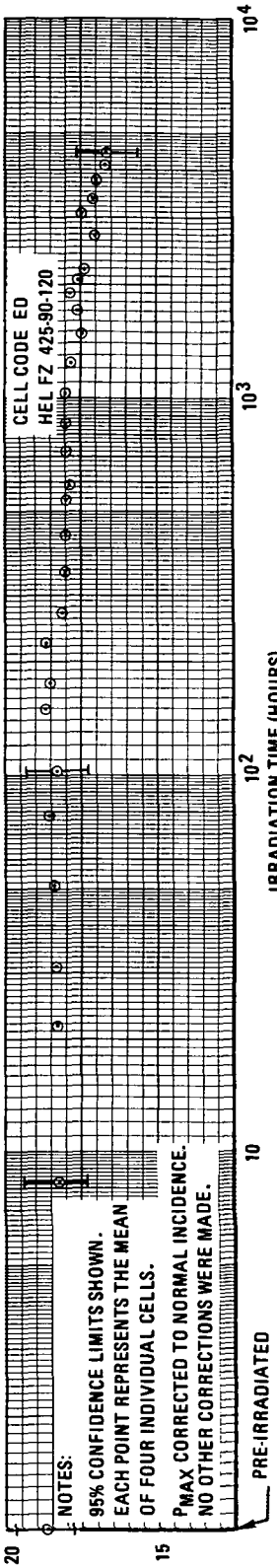

Figure C-22 P_{max} Data for Cell Type E at +80°C

P_{MAX} (MW)

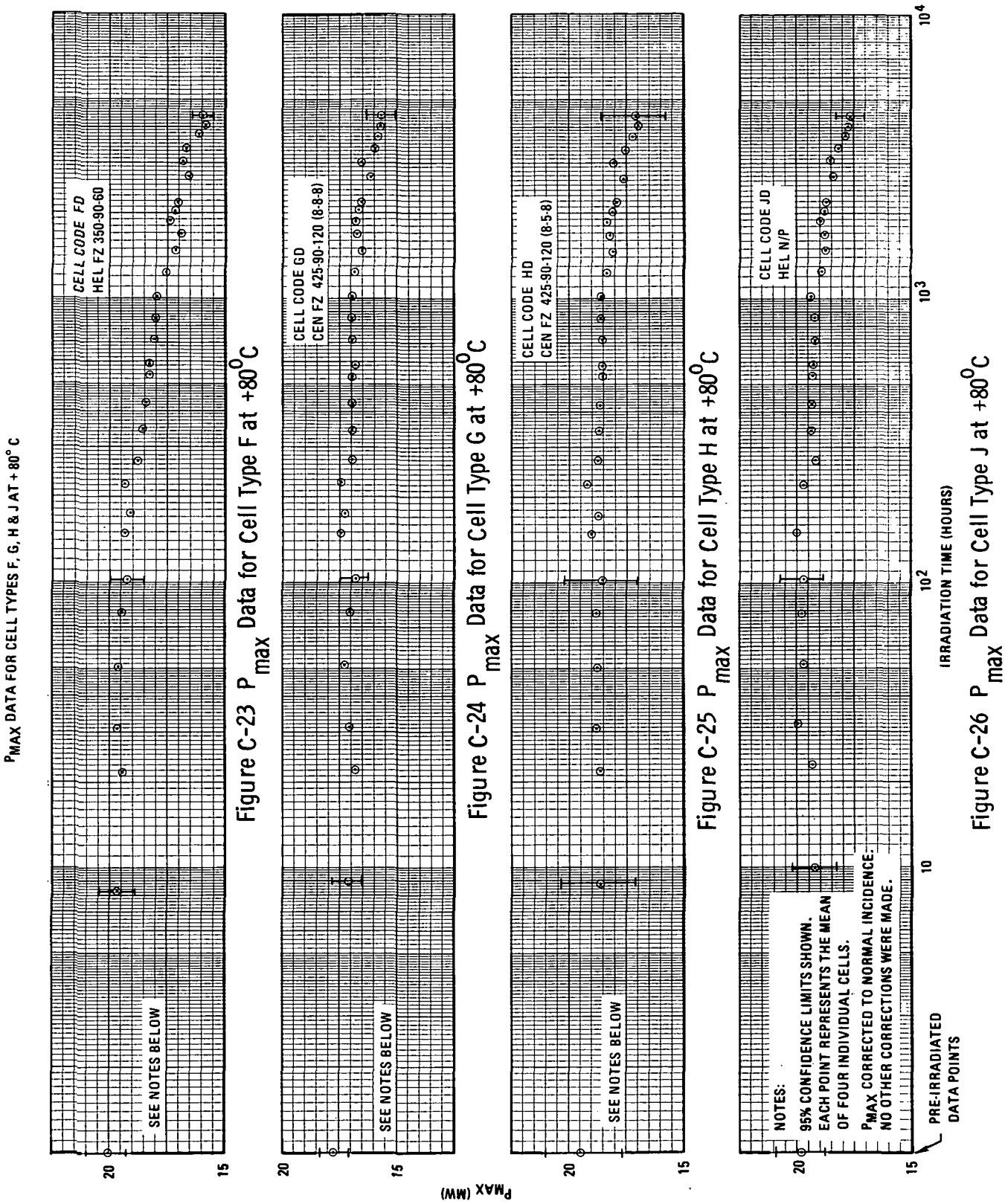

Figure C-23 P_{max} Data for Cell Type F at +80°C

Figure C-24 P_{max} Data for Cell Type G at +80°C

Figure C-25 P_{max} Data for Cell Type H at +80°C

Figure C-26 P_{max} Data for Cell Type J at +80°C

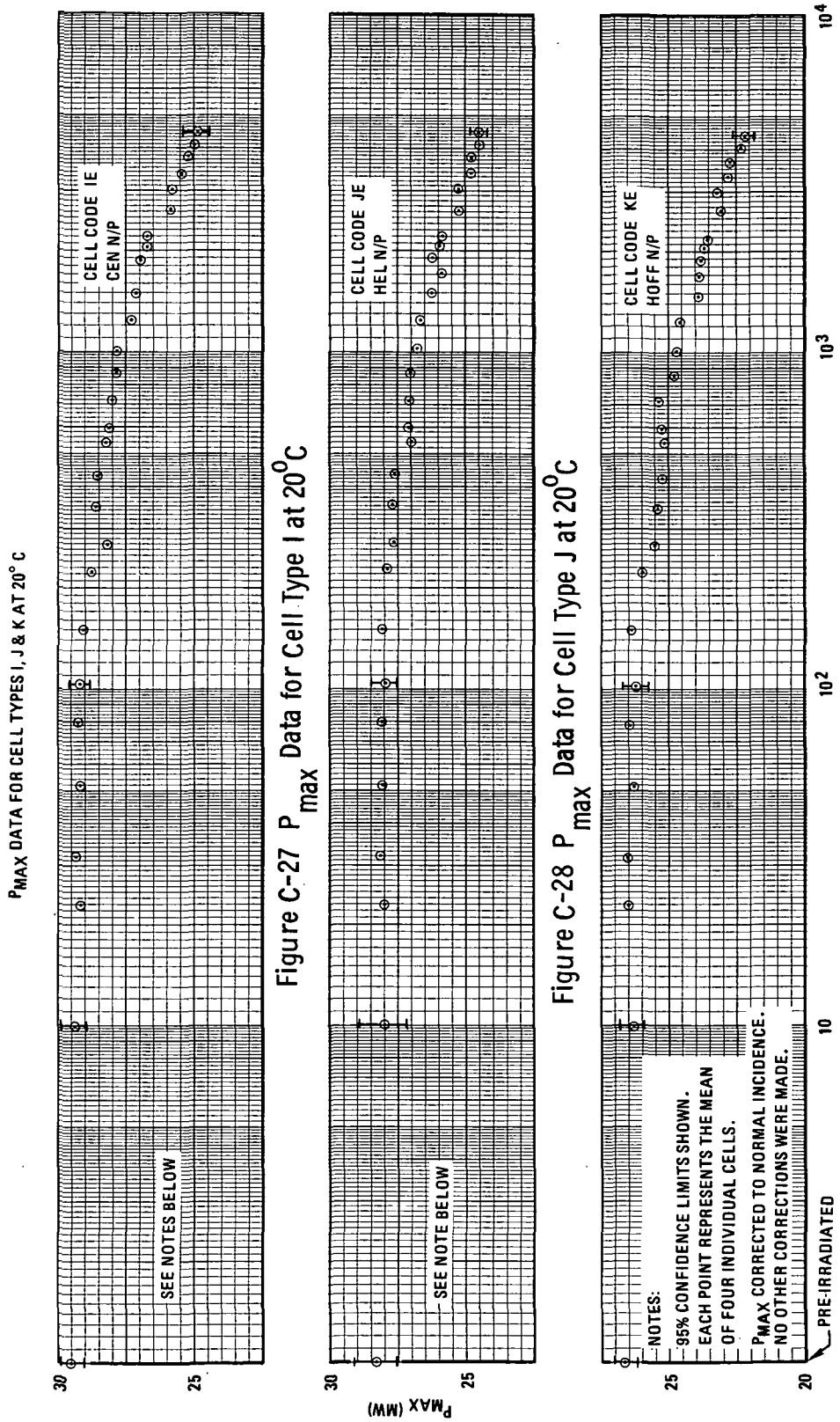

Figure C-27 P_{max} Data for Cell Type I at 20°C

Figure C-28 P_{max} Data for Cell Type J at 20°C

Figure C-29 P_{max} Data for Cell Type K at 20°C

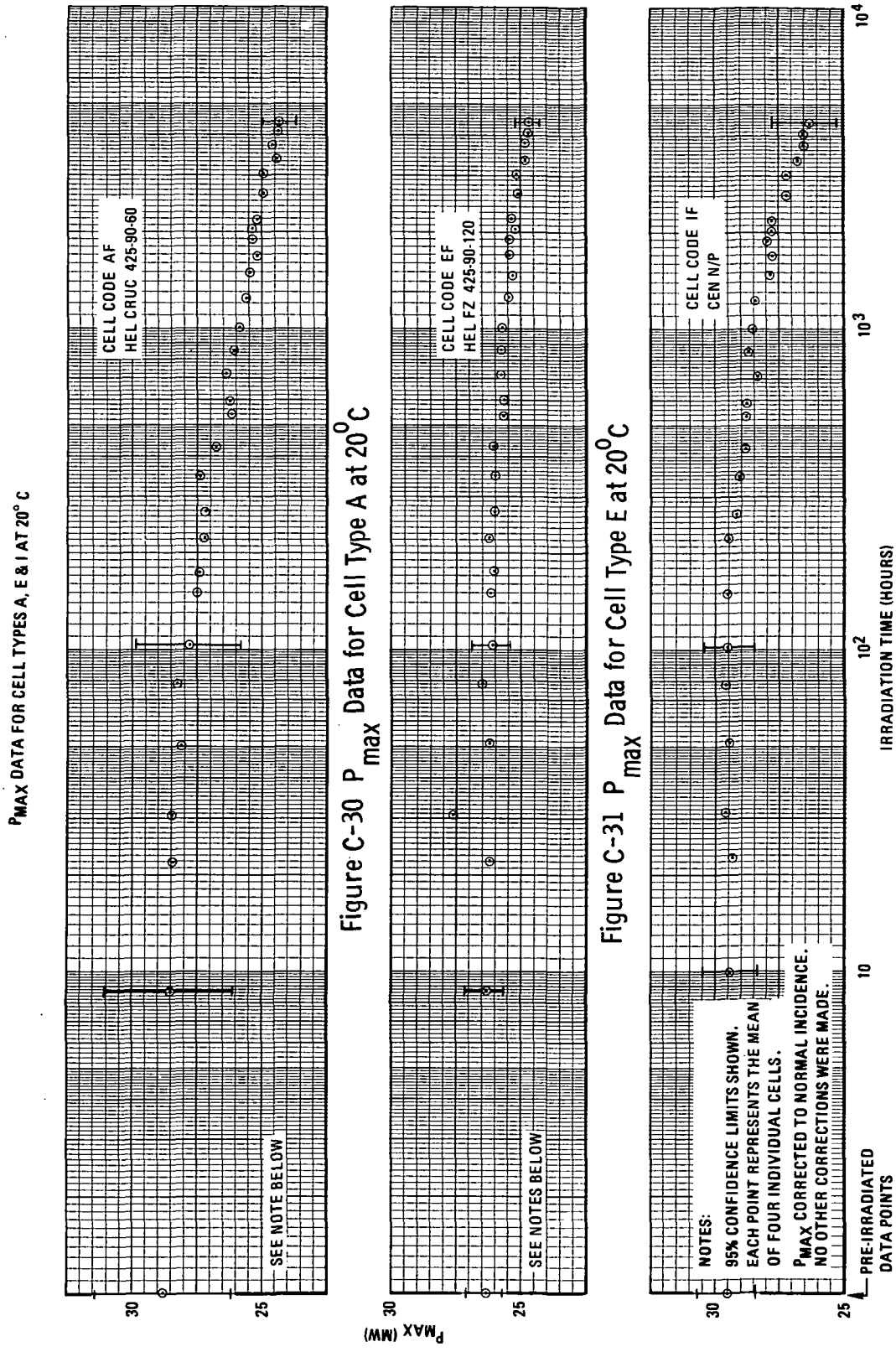

Figure C-30 P_{max} Data for Cell Type A at 20°C

Figure C-31 P_{max} Data for Cell Type E at 20°C

Figure C-32 P_{max} Data for Cell Type I at 20°C

APPENDIX D

DESCRIPTION OF STATISTICAL METHODS EMPLOYED

APPENDIX D

DESCRIPTION OF STATISTICAL METHODS EMPLOYED

D.1 F-Test

It is important to determine whether two samples being compared come from populations having equal variances. In the t-test, which is described in the following section, it is assumed that the two samples do come from populations with equal variances. The F statistic, which is used to evaluate the validity of this assumption, is defined as follows:

> "If s_1^2 and s_2^2 are the variances of independent random samples of size n_1 and n_2, respectively, taken from two normal populations having the same variance, then
>
> $$F = \frac{s_1^2}{s_2^2} \qquad \text{(D-1)}$$
>
> is a value of a random variable having the F distribution with the parameters $\nu_1 = n_1 - 1$ and $\nu_2 = n_2 - 1$." (Reference: Probability and Statistics, Miller and Freund, Prentice-Hall, 1965.)

The F statistic is calculated for the two samples from the experimental data. The F statistic for a given level of significance (eg, 5%) is found in a standard statistical table. If the calculated value is higher than that indicated from the table, the assumption of equal variances is invalid. If the calculated value is less than the table value, the assumption is valid.

D.2 t-Test

The t-test is used in this instance to test the validity of a hypothesis concerning two means. If either (or both) samples are small and the population variances are unknown, tests of the null hypothesis ($H_o: \mu_1 - \mu_2 = \delta$) can be based on a suitable t statistic, provided it is

reasonable to assume that both populations are normal and have equal variances. Under these conditions it can be shown that the sampling distribution of the statistic

$$t = \frac{(\bar{x}_1 - \bar{x}_2) - \delta}{s_{\bar{x}_1 - \bar{x}_2}} \qquad \text{(D-2)}$$

is the t distribution with $(n_1 + n_2 - 2)$ degrees of freedom. The denominator involves a "pooled estimate" of the population variance. Using appropriate estimates of the population variance, the following version of the t statistic is obtained:

$$t = \frac{(\bar{x}_1 - \bar{x}_2) - \delta}{\sqrt{(n_1 - 1)\, s_1^2 + (n_2 - 1) s_2^2}} \quad \sqrt{\frac{n_1 n_2 (n_1 + n_2 - 2)}{n_1 + n_2}} \qquad \text{(D-3)}$$

The parameter δ is used to determine "how different" two means are. When δ is set to zero, the null hypothesis is $\mu_1 = \mu_2$ with the alternative hypothesis being $\mu_1 \neq \mu_2$. If $t < -t_{a/2}$ or $t > t_{a/2}$ the null hypothesis is rejected and a difference between μ_1 and μ_2 is assumed. One may then take the analysis one step further and get an estimate of the difference between μ_1 and μ_2 at a particular level of significance. The null hypothesis is $|\mu_1 - \mu_2| = \delta$ with the one-sided alternative $|\mu_1 - \mu_2| > \delta$. If $t > t_a$, then one must reject the null hypothesis at the α level of significance and assume that μ_1 differs from μ_2 by at least as much as δ. If one sets $t_\alpha = t$ in equation (D-3) and solves for δ, δ_{crit} assures the following significance:

> μ_1 cannot be assumed to be different from μ_2 by any more than δ at the α level of significance.

D.3 "Bow-Tie" Formula

Referring to Figure 5-10, the confidence intervals for the fitted (least squares fit) curves result from application of the following equation:

$$y_{limits} = \bar{y}_{x_o} \pm 1.96 \sqrt{\left[\frac{1}{n} + \frac{(x_o - \bar{x})^2}{\sum_{i=1}^{n} (x_i - \bar{x})^2}\right] \frac{\sum_{i=1}^{n} (y_i - \bar{y}_i)^2}{n-2}}$$

The resulting confidence limits account for the increased confidence in data which form a regression curve over that in the individual data points from which that curve was drawn. This concept is developed in the book Introduction to Statistical Reasoning, P. J. McCarthy, McGraw-Hill, 1957, pp. 358-360 .

PHILCO Ford

Philco-Ford Corporation
Western Development Laboratories Division
Palo Alto, California 94303